GENE-ENVIRONMENT INTERACTIONS BETWEEN MUTANT *HUNTINGTIN* AND MANGANESE EXPOSURE ALTER STRIATAL NEUROCHEMISTRY AND MEDIUM SPINY NEURON MORPHOLOGY

By

Jennifer Lea Madison

Dissertation

Submitted to the Faculty of the

Graduate School of Vanderbilt University

in partial fulfillment of the requirements

for the degree of

DOCTOR OF PHILOSOPHY

in

Pharmacology

August, 2011

Nashville, Tennessee

Approved:

Professor Michael Aschner

Professor Aaron B. Bowman

Professor Gregg D. Stanwood

Professor Eugenia V. Gurevich

Professor Malcolm J. Avison

ABSTRACT

Huntington's disease is a fatal autosomal dominant neurodegenerative disease caused by an expansion of CAG repeats in the DNA of the *Huntingtin* gene. The length of the repeat is inversely related to the age of disease onset, however it only accounts for 60% of the variability in the age of onset. Therefore, other genetic and environmental effects contribute to the remaining 40% in the variability in age of onset. Multiple neurodegenerative diseases exhibit alterations in metal ion homeostasis. Research in our laboratories has demonstrated a disease-toxicant interaction between mutant *Huntingtin* and manganese exposure *in vitro*. Manganese is an essential trace metal that is necessary for many physiological processes, including neurotransmitter synthesis. In high levels, manganese can be damaging to the brain. Exposure that leads to this damage is typically encountered in an occupational setting such as when welding, smelting or mining manganese.

The research described in this dissertation is the first to describe the complex gene-environment interactions between mutant *Huntingtin* and manganese exposure *in vivo*. The neurochemical and morphological changes identified herein are complex and exhibit both positive and negative effects. My research also identified the earliest evidence for striatal dendritic pathology in YAC128 mice that occur between 13 and 16 weeks postnatal. Additionally, this is the first research to show gender-specific changes in MSN morphology following manganese exposure. These alterations in neuron morphology were most

prevalent when manganese levels were elevated and were not due to differential striatal manganese accumulation.

Taken together, these data lay the groundwork for understanding the gene-environment interaction between mutant *Huntingtin* and Mn exposure. Future studies will further our understanding of this interaction that may one day lead to therapeutic intervention. These studies also reinforce the need to include animals of both genders in experimentation to further our understanding of disease across both genders.

For my parents Leroy and Rhonda who provided me with the perfect gene-environment interaction to achieve my dreams.

"Individual destiny is determined by gene expression, which is always influenced by interactions with and triggers by the environment. No organism, including humans, has a destiny independent of its environment."

– Dan Agin, Ph.D. in *More Than Genes*

ACKNOWLEDGEMENTS

First and foremost, I would like to thank Drs. Michael Aschner and Aaron B. Bowman for taking me into their laboratories where I conducted my dissertation research. I learned what it means to be a successful scientist from both of them. I learned how to find the positive side of an experiment that produced unexpected results. Both Aaron and Miki are unendingly optimistic and that helped keep me going when I could not see how my data would ever make it to publication. From Aaron's unmatched enthusiasm to Miki's endless kindness, I could not ask for better mentors. Being a member of these two laboratories has enriched my life, both in and out of the laboratory. I cannot thank them enough for the opportunity you gave me to do my dissertation work with them.

I would also like to thank my dissertation committee for all of their professional and personal guidance. Drs. Eugenia V. Gurevich (Chair), Malcolm J. Avison, and Gregg D. Stanwood made my committee meetings a comfortable place to discuss data and ideas. They supported me in my scientific and career goals. I could not have navigated graduate school without them. I want to give an additional thanks to Dr. Gregg D. Stanwood for his ability to tell me what I was not able to see and advise me on how to deal with difficult situations. I cannot thank him enough for his advice, without which I would not be where I am today.

I came into graduate school at Vanderbilt University specifically to join the Department of Pharmacology. Not only did I get a fantastic education in Pharmacology, I learned how to think like a scientist. I cannot say enough great

things about A. Karen Gieg and the rest of the department administrators. They have saved me many times and help to keep this great department running.

My research would not be possible without the financial support by NIH grants ES10563 (MA) and ES016931 (ABB). I would like to thank Ms. Rosanne Delapp and Dr. David Kosson in the Department of Civil and Environmental Engineering at Vanderbilt University for performing the ICP-MS analysis of striatal Mn levels and Mr. Christopher Jetter for technical assistance. I am grateful for instruction and advice on the Golgi staining technique from Dr. Ariel Deutch and members of his laboratory. HPLC determinations were performed by the Center for Molecular Neuroscience/Kennedy Center Neurochemistry Core Lab at Vanderbilt University. The CMN/KC Neurochemistry Core Lab is supported by Vanderbilt Kennedy Center for Research on Human Development, Vanderbilt Conte Center for Neuroscience Research and The Vanderbilt Center for Molecular Neuroscience.

My labmates have always made life in and out of lab enjoyable. From those who have trained me and taught me all of the laboratory techniques I know to those whose work was the basis for my dissertation research, I cannot thank them enough for their contribution directly and indirectly to my successful dissertation research. Dr. Michael Bubser taught me most of the scientific techniques that were integral to my dissertation research. He is a fantastic and dedicated scientist who can scare the living daylights out of me on a quiet weekend in the lab and then blow me away on the dance floor. Dr. M. Diana Neely has always been supportive and asked tough questions but always in the

most constructive manner. Drs. Brian N. Mathur, Bonnie G. Coffa and Sheila V. Kusnoor were wonderful labmates and I am thankful for our time together. Dr. B. Blairanne Williams laid the scientific groundwork for my dissertation research. She also provided me with a wealth of knowledge about anything I could ask her about and continuous support. Dr. Michał Węgrzynowicz was indispensible in my dissertation research. Without his help, none of these experiments would have been possible. I also need to thank Gunnar Kwakye for his uplifting and enlightening conversations about science and life in general. Margaret Adams was one of my closest lab friends in the Aschner lab. We came up with outrageous hypotheses together and I will miss those times. Dr. Ebany Martinez-Finley has become a fantastic friend over the past year. We bonded over our shared love of Hatch green chile.

I could not have made it through graduate school without the help and support of my friends and family. My classmates in the Department of Pharmacology were true friends. Our friendship was solidified during our first department retreat and they have been an unending source of support since then. Special thanks to Drs. Sheila V. Kusnoor, Kirsten J. Helmcke and Daniel Balasubramanian for friendship throughout grad school. I could not have gotten through the difficult times without your friendship. I would also like to thank Drs. Ashley Brady, Abigail M. Brown, Kimberly A. Petrie and Jana K. Shirey-Rice who always empathized with me and provided me unconditional support and positive words of encouragement.

András Nadás has been nothing but a blessing to me. He came into my life through mutual friends and we immediately clicked. He has been my local source of unending support through my most difficult times in graduate school. András also played a critical role in my analysis of the Golgi data. Without the macros that he spent a couple of hours writing and teaching me to use, I would still be copying and pasting data in Excel. András was always willing to listen to me talk about my experiments, results and discuss my data. Not only did he listen, he wanted to understand. András shares my love of photography and dancing. He introduced me to his Hungarian culture and (amazing) food during a difficult time in my life. During my first trip to Hungary, I learned how little it takes to make people happy and that the most important ingredients for a happy life are wonderful friends and family. I cannot imagine my life without my perfect match.

I would not be where I am today without my family. I was lucky to grow up close to my grandparents, aunts, uncles and cousins; all of whom have helped to make me the person I am today. My parents always told me that I could do anything that I wanted to when I grew up and they meant it. They always pushed me to do the best that I could do and not regret the results because I gave it my all. I cannot thank my parents or my brothers enough for their unending support from near and far, positivity, friendship and love.

TABLE OF CONTENTS

LIST OF TABLES

LIST OF FIGURES

LIST OF ABBREVIATIONS

3-MT 3-methoxytyramine

3-NP ..... 3-nitropropionic acid

6-OHDA 6-hydroxydopamine

ANOVA ..... analysis of variance

Cd ..... cadmium

Cit ..... citrulline

DA ..... dopamine

DOAPC ..... 3,4-dihydroxyphenylacetic acid

GABA ..... γ-aminobutryic acid

Glu ..... glutamate

Gly ..... glycine

GP ..... globus pallidus

HD ..... Huntington's disease

Hg ..... mercury

HTT ..... *Huntingtin*

HVA ..... homovanillic acid

MeHg ..... methyl mercury

Mn ..... manganese

Ni ..... nickel

NMDAR ..... N-methyl-D-aspartate receptor

Pb ..... lead

Ser ..... serine

SN ..... substantia nigra

SNpc..... substantia nigra pars compacta

SNpr ..... substantia nigra pars reticulata

Veh ..... vehicle

WT ..... wild-type

WT-Mn..... wild-type mangaenese

WT-Mn-F ..... wild-type manganese female

WT-Mn-M..... wild-type manganese male

WT-Veh ..... wild-type vehicle

WT-Veh-F ..... wild-type vehicle female

WT-Veh-M ..... wild-type vehicle male

YAC128-Mn ..... YAC128 manganese

YAC128-Mn-F..... YAC128 manganese female

YAC128-Mn-M ..... YAC128 manganese male

YAC128-Veh..... YAC128 vehicle

YAC128-Veh-F ..... YAC128 vehicle female

YAC128-Veh-M ..... YAC128 vehicle male

Zn ..... zinc

CHAPTER I

INTRODUCTION

Huntington's disease

Human Disease

Huntington's disease (HD) is a fatal autosomal dominant neurodegenerative disease with onset occurring in mid-life. Prevalence of HD in populations of European descent is approximately 4-10 per 100,000 people; whereas prevalence in non-European populations is reduced by more than 10-fold and mutations in genes other than *Huntingtin* (*HTT*) are commonly found (Harper, 1992; Margolis et al., 2005; Wild et al., 2008; Wild and Tabrizi, 2007). Duration of the disease is approximately 15 years from symptom onset to death (Harper, 1992; Hayden et al., 1981). Diagnostic criteria include a family history of the disease, progressive motor dysfunction with chorea or rigidity not due to another cause, and psychiatric disturbances with progressive dementia of no other cause (Vonsattel and DiFiglia, 1998). To date, tetrabenazine is the only drug that has been FDA approved to treat HD chorea, but is only palliative, not a disease modifying drug.

Genetics

HD is the most common genetic neurodegenerative disease. It is caused by an expansion of CAG codon repeats in exon 1 of the *HTT* gene located on the

short arm of chromosome 4 (4p16.3) (Huntington's Disease Collaborative Research, 1993). The function of wild-type (WT) *HTT* is unknown, although it is known to play a role in many cellular processes including cell signaling, gene transcription, vesicle transport, apoptosis and clathrin-mediated endocytosis (Harjes and Wanker, 2003). HD is autosomal dominant; therefore children of affected persons have a 50% chance of inheriting the disease. HD does not affect reproduction because typical age of disease onset is 40-50 years of age, thus the disease can be propagated across generations. Age of disease onset is inversely correlated with the number of CAG repeats (Andrew et al., 1993; Brinkman et al., 1997; Duyao et al., 1995; Wexler et al., 2004a). The Huntington Disease Collaborative Research Group defined a normal range of CAG repeats in the *HTT* gene to be fewer than 30 repeats (Huntington's Disease Collaborative Research, 1993). Full penetrance of the disease occurs when CAG repeat length is greater than 39 and incomplete penetrance occurs when CAG repeat length is between 35 and 39 (Wexler et al., 2004). Juvenile-onset HD accounts for 5-10% of HD cases and occurs when CAG repeats exceeds 60 (Huntington's Disease Collaborative Research, 1993).

Although there is a strong inverse correlation between CAG repeat length and age of disease onset, it only accounts for approximately 60% of the variation in disease onset (Andrew et al., 1993; Brinkman et al., 1997; Duyao et al., 1995; Stine et al., 1993; Wexler et al., 2004a). This allows the possibility of other genetic or environmental factors to modify the age of disease onset and progression of symptoms.

Symptoms

HD is characterized by cognitive, motor and psychiatric symptoms. Cognitive dysfunction includes impaired executive function (required for organizational and planning behavior), delayed acquisition of new motor skills and language function (Folstein, 1989). Depression is a common symptom and risk of suicide is ten times greater than the general population (Paulsen et al., 2005). Mania and other psychotic symptoms can also manifest. Fine motor skills deteriorate early on and are useful in establishing the diagnosis of HD (Walker, 2007). Chorea is the most common motor symptom of adult onset HD, but severity and duration of this symptom is not correlated with length of disease. Juvenile-onset HD is characterized by rigidity without chorea (Huntington's Disease Collaborative Research, 1993). Gait and postural instability are altered later in the course of disease.

Pathology

The primary pathology of HD is degeneration and loss of neurons in the caudate and putamen. Although *HTT* is ubiquitously expressed throughout the entire body, medium spiny neurons (MSN) in the striatum (caudate and putamen in humans) are especially susceptible to degeneration. The striatum is not the only brain region affected by HD. Studies have shown degeneration and/or dysfunction in other subcortical regions such as the substantia nigra (SN), thalamus and hypothalamus (Heinsen et al., 1999; Kassubek et al., 2005; Kipps et al., 2005; Kloppel et al., 2009; Petersen and Bjorkqvist, 2006; Politis et al., 2008; van den Bogaard et al., 2011; Wild et al., 2010) and multiple cortical brain

regions (Thu et al., 2010). White matter pathways throughout the brain are also altered in HD, thereby affecting connectivity throughout the brain (Dumas et al., 2011; Hobbs et al., 2010). Evidence of changes in volume of multiple brain regions is evident in prodromal HD and accelerates the closer a patient gets to estimated age of motor symptom onset (Aylward et al., 2000; Aylward et al., 2011; Aylward et al., 2004; Hobbs et al., 2010; Majid et al., 2011; Tabrizi et al., 2011).

Post-mortem studies of neurons in the striatum revealed that MSN are specifically damaged in HD. Graveland et al. (1985a) and Ferrante et al. (1991) described MSNs in post-mortem striatum of mid- and late-stage HD subjects as having either proliferative or degenerative changes. Proliferative changes occurred more frequently in mid-stage HD specimens. These changes were characterized by an increase in spine density at the ends of dendritic trees, an increase in size of dendritic spines and a re-curving of the dendritic tree toward the soma. Degenerative changes were more frequent during later stages of HD. MSNs exhibiting degenerative changes showed a decrease in spine density, a reduced dendritic arbor and focal swellings along the dendrite. Changes in MSN morphology precede gross striatal neuron loss (Ferrante et al., 1991).

Animal Models

Chemical models

Chemical models of HD were used before the *HTT* gene was identified in human HD patients. The first chemical model consisted of injecting glutamatergic

excitotoxins into the brain. These included substances such as kainic acid and quinolinic acid, which are both agonists at ionotropic Glu receptors (Coyle and Schwarcz, 1976; McGeer and McGeer, 1976). Quinolinic acid lesions of the striatum have been shown to closely reproduce neuropathology, neurochemistry and symptomatology that are characteristic of HD (Beal et al., 1991; Ferrante et al., 1993; Sun et al., 2003).

A second type of chemical lesion has been used to mimic HD. These toxicants impair mitochondrial function and deplete the cell of the energy source ATP. The electron transport chain generates the energy to produces the majority of ATP in the cell through a series of enzyme complexes that reduce oxygen to water. Dysfunction of complex II, III and IV has been associated with HD (Brennan et al., 1985; Browne et al., 1997; Browne and Beal, 1994; Mann et al., 1990). 3-nitropropionic acid (3-NP) is a suicide inhibitor of Complex II. Accidental ingestion of 3-NP occurred in China through contaminated sugar cane and produced an irreversible non-progressive dystonia. Subsequent brain imaging showed that exposure to 3-NP caused bilateral damage to the putamen (Ferrante, 2009). 3-NP has been used to study the effects of inhibiting Complex II on many aspects of striatal biology. These studies have shown that mitochondrial dysfunction of this type causes excitotoxicity, oxidative stress, MSN death and motor dysfunction (AC et al., 1992; Beal et al., 1993; Brouillet et al., 1993; Sun et al., 2002). Interestingly, decortication of animals prior to 3-NP exposure prevents striatal lesions, suggesting that Glu excitotoxicity plays a large role in the

mechanism of striatal degeneration by 3-NP and potentially in HD (Beal et al., 1993).

Exon 1 fragment mouse models

After the discovery of the mutated gene that causes HD, a variety of mouse models were developed. The first mouse models of HD were published in 1996 (Mangiarini et al., 1996). They express exon 1 of the human *HTT* gene, with an expansion of CAG repeats, under the control of the human promoter in addition to the endogenous mouse huntingtin gene. The R6/1 mouse line has an approximate 120 CAG repeat while the R6/2 mouse line has about 150 CAG repeats (Mangiarini et al., 1996). The R6/2 line is the most studied mouse model of HD. The R6/2 line has an earlier age of disease symptom onset and shorter lifespan than the R6/1 line that is likely due to the longer CAG expansion. The R6/2 line has phenotypic symptoms similar to HD patients with motor dysfunction, atrophy of the striatum, loss of body weight and inclusions of mutant *HTT* (Mangiarini et al., 1996). A comprehensive behavioral study found significant and progressive rotarod deficiencies, climbing activity and hypoactivity in R6/2 mice at 4 weeks old. R6/2 mice begin to lose weight around 7 weeks and gait abnormalities at 8 weeks. At 12 weeks R6/2 mice exhibit an increase in anxiety, a deficit in pre-pulse inhibition and a decrease in grip strength (Menalled et al., 2009). However, there are inconsistencies between mutant *HTT* aggregation and inclusions between the R6/2 model and HD. The R6/2 mice present with aggregates throughout the brain at postnatal day 1 that increase

with age. This is in contrast to HD patients who do not develop aggregates this aggressively.

The R6/1 mouse model is not as extensively studied as the R6/2 model. R6/1 mice develop less severe symptoms at a later age compared to R6/2 mice. In contrast to R6/2 mice, they have a normal lifespan aided by the slower progression of disease symptoms. Mutant *HTT* aggregates appear at 2 months of age, much later than R6/2 mice. R6/1 mice exhibit no striatal neuron loss; however there are abnormalities in MSN morphology consistent with a degenerative phenotype (Naver et al., 2003; Spires et al., 2004). Because of the prolonged progression of symptoms, the R6/1 mouse model may be more useful to study potential disease modifying therapeutics than the R6/2 mouse model.

Full length mouse models

A second type of HD mouse model expresses the full length *HTT* gene. The YAC128 mouse model expresses the full length human *HTT* gene containing 128 CAG repeats with the human promoter on a yeast artificial chromosome (YAC) in addition to the endogenous murine *HTT* gene (Slow et al., 2003). The first abnormality in YAC128 mice is a procedural learning deficit at 2 months of age (Van Raamsdonk et al., 2005b). Motor dysfunction sets in at 3 months with a hyperkinetic phenotype, a rotarod deficit at 4 months and a hypokinetic phenotype by 6 months (Menalled et al., 2009; Slow et al., 2003; Van Raamsdonk et al., 2005b). However, despite these motor symptoms changes in striatal volume are not detected until 9 months. Cortical volume is reduced, striatal neuron loss and *HTT* aggregates are present at 12 months (Slow et al.,

2003). This mouse model has a high fidelity of symptoms and pathology with HD, which is why we chose to use it for our experiments (Carroll et al., 2011).

A second full length *HTT* mouse model is the BACHD model. A bacterial artificial chromosome (BAC) expresses full length mutant human *HTT* with 97 repeats that contain both CAA and CAG repeats (Gray et al., 2008). At two months old, BACHD mice exhibit deficits on the rotarod that progressively worsen with age. There is no significant gross neuropathology at 6 months, but there is significant atrophy throughout the brain at 12 months. Electrophysiology studies of MSNs revealed a significant decrease in corticostriatal input to MSNs in BACHD mice (Gray et al., 2008).

Exon 1 fragment versus full length *huntingtin*

The full length and exon 1 mouse models of HD show similar motor and pathological phenotypes; however there are distinct differences in the rate, severity and presence of symptoms between the different models. In general the full length mouse models show milder behavior and motor deficits than the R6/2 mouse model (Menalled et al., 2009; Menalled and Chesselet, 2002). The R6/2 mouse model has a significantly faster progression than the full length models. The R6/2 mice show gait abnormalities, anxiety and a significant decrease in survival that is unique to this model. The BACHD mouse model shows some behavioral phenotypes that only occur in the R6/2 model, but not other models of HD. These include a decrease in grip strength, climbing and a pre-pulse inhibition deficit. All models show deficits on the rotarod and open field behavior, but to different extents and at different ages.

The neuropathology of HD mouse models does not fully recapitulate the disease in humans. R6/2 mice show ubiquitinated mutant *HTT* aggregates in the nucleus and cytoplasm of neurons. However, the extent and distribution of these aggregates does not match human pathology. R6/2 mice show an abundance of *HTT* aggregates throughout the entire brain on an overwhelming scale (Vonsattel, 2008). BACHD mice, on the other hand, show mutant *HTT* aggregates that are more similar in distribution and number to HD patients (Ferrante, 2009). The genetic models are a much more accurate representation of HD than the chemical models of HD.

Striatal neurochemistry neuron morphology in HD

Post-mortem studies of neuron in the HD striatum showed that MSNs exhibit both proliferative and degenerative changes (Ferrante et al., 1991; Graveland et al., 1985b). Proliferative changes, characterized by an increase in spine density at the ends of dendritic trees, an increase in size of dendritic spines and a re-curving of the dendritic tree toward the soma occurred more frequently in mid-stage HD. Degenerative changes were more frequent during late stage HD and are characterized by a decrease in spine density, a reduced dendritic arbor and focal swellings along the dendrite. Neuron morphology studies in mouse models of HD consistently show degenerative changes in striatal MSN morphology. Morphological studies of striatal MSNs in R6/1(Spires et al., 2004), R6/2 (Klapstein et al., 2001), HD48 and HD89 (Guidetti et al., 2001) mice all

showed a decrease in spine density across branch order and was only evident in symptomatic mice (Klapstein et al., 2001).

Changes in striatal neurochemistry of HD patients may influence MSN morphology and are present in HD mouse models. GABA levels are decreased in the putamen, nucleus accumbens, subthalamic nucleus, substantia nigra, thalamus, globus pallidus and occipital cortex (Bonilla et al., 1988; Spokes et al., 1980; Urquhart et al., 1975). Activity of glutamic acid dehydrogenase (GAD), the enzyme required to synthetize GABA, is reduced in the putamen, caudate and globus pallidus (Urquhart et al., 1975; Wu et al., 1979). Alterations in GABA release and GAD expression are also present in mouse models of HD (Gourfinkel-An et al., 2003; Nicniocaill et al., 2001). Levels of striatal DA and DA receptors are reduced in the striatum and cortex in HD (Andre et al., 2010; Augood et al., 1997; Bernheimer et al., 1973; Kish et al., 1987; Pavese et al., 2010). Reduced striatal DA levels and disturbances in dopaminergic signaling have also been observed in the mouse models of HD (Bibb et al., 2000; Cha et al., 1998; Johnson et al., 2006). Post-mortem studies of HD and mouse models show changes in GABA and DA that may lead to changes in MSN morphology.

Manganese Toxicity

Sources of exposure

Manganese (Mn) is an essential trace mental that is present at 0.1% of the earth's crust and can be found in soil at concentrations from 40 to 900 mg/kg

(Cooper, 1984). It can be released into the environment in multitude of ways. Mn in the soil can leach into ground water, wells and aquifers thereby contaminating drinking water. Mn is also present in a number of common foods including nuts, whole grains, tea, leafy vegetables, pineapple, brown rice and beans (Pennington and Young, 1991). The daily intake requirement of Mn is approximately 2-5 mg Mn per day (Aschner and Aschner, 2005). Only 1-5% of orally ingested Mn is absorbed by the body (Davis et al., 1993). Mn is normally excreted in the bile with the exception of the small amount of absorption that occurs in the intestine. Neonates absorb a greater percentage of Mn which may be due to the fact that their biliary function is not yet fully established. Neonates who are critically ill or born prematurely are commonly fed through total parenteral nutrition (TPN). Mn concentrations in these solutions are not consistent and mineral supplements are commonly added with variable amounts of Mn. Neonatal absorption of Mn from milk is approximately 8% whereas absorption from TPN is 100% (Aschner and Aschner, 2005). This can pose a serious problem to neonates who are exposed to excessive Mn in TPN. Hepatic dysfunction and cholestasis are two risk factors for increased Mn accumulation (Butterworth, 2010; Butterworth et al., 1995; Krieger et al., 1995). Since at least 90% of Mn is removed by the liver and excreted in the bile, dysfunction of either system could lead to an increase in Mn absorption from the diet. Chronic hepatic encephalopathy and biliary atresia in adults can lead to an increase in Mn in the globus pallidus (Butterworth et al., 1995; Ikeda et al., 2000). Critically ill neonates are also at risk for Mn accumulation in the brain due to TPN containing Mn,

underdeveloped biliary function, and frequently develop hepatic dysfunction and cholestasis which increases Mn absorption (Aschner and Aschner, 2005).

Methylcyclopentadienyl manganese tricarbonyl (MMT) is a gasoline additive used as an antiknock agent (Cooper, 1984). This is a controversial source of airborne Mn exposure. MMT has been used in Canada for more than 20 years. In some cases elevated indoor and outdoor Mn levels have been found near high traffic urban areas compared to lower traffic rural areas (Bolte et al., 2004; Boudia et al., 2006; Zayed et al., 2003). However, in other cases airborne Mn levels have not exceeded the current reference concentration for inhaled Mn set by the United States Environmental Protection Agency and there is little evidence for soil contamination in high traffic areas (Dobson et al., 2004; Pfeifer et al., 2004). MMT is a controversial source of Mn exposure; however it continues to be studied in order to further elucidate the effects of its usage in gasoline.

Mn poisoning can occur though illicit drug use of methcathinone (or ephedrone). Methcathinone is a homemade drug that is derived from the combination of pseudoephedrine and potassium permanganate (Sikk et al., 2011; Sikk et al., 2010). Intravenous (i.v.) use of this drug in Eastern Europe and Russia was shown to cause symptoms similar to Mn poisoning (manganism) and Parkinsonism more than 20 years ago (de Bie et al., 2007; Sanotsky et al., 2007; Selikhova et al., 2008; Sikk et al., 2011; Sikk et al., 2010; Sikk et al., 2007; Stepens et al., 2008). However, only recently has interest in studying the effects of this drug grown. Onset of motor dysfunction associated with methcathinone

use can occur as early as months after beginning drug use and up to years later. Neuroimaging studies using T1-weighted magnetic resonance imaging (MRI) show hyper-intense globus pallidus (GP) and substantia nigra (SN) in current methcathinone users, consistent with Mn deposition in these brain regions (Sikk et al., 2010; Stepens et al., 2008). Motor symptoms are unresponsive to L-DOPA therapy, metal chelation, dopaminergic medications and anticholinergic drugs (Sikk et al., 2011). As of yet there is no treatment that improves motor symptoms.

The majority of Mn exposure occurs through occupational exposure. Mn is commonly used as an agent in welding material. Proper ventilation equipment is not always provided or used during welding, therefore exposing welders to Mn through inhalation. Not only can Mn be absorbed nasally and transported to the brain, it can also accumulate in the lungs and cause respiratory problems (Bowler et al., 2006; Bowler et al., 2007a; Bowler et al., 2007b). Ferroalloy smelting plants are another means of occupation and environmental Mn exposure (Huang et al., 1989; Jiang et al., 2007; Wang et al., 1989). Studies in Europe have found Mn contamination and elevated Mn levels in people living near ferroalloy plants (Lucchini et al., 2007; Lucchini et al., 2009; Squitti et al., 2009). Dry cell battery production, manufacturing glass and ceramic glazes are other occupational means of Mn exposure (Bader et al., 1999; Srivastava et al., 1991).

Manganism

Manganism is a progressive motor dysfunction that was first described in Mn ore workers by James Couper in 1837 (Couper, 1837; McMillan, 1999). Early stage manganism is characterized by behavioral, emotional and cognitive changes. Fine motor skills and speech may also be affected at this stage. At the intermediate stage, more severe motor symptoms appear. At this stage patients may present with ‘masque manganique’ or a loss of facial expression. Psychotic symptoms also progress and have been termed ‘locura manganica’ or manganese madness. The final stage of manganism produces symptoms such as limb rigidity, dystonia, tremors, gait abnormalities, a tendency to fall backward and a cock-like walk are present (Lucchini et al., 2009; Roth, 2009).

The motor symptoms of manganism are similar yet distinct from Parkinson’s disease (PD). Similarities in motor symptoms include rigidity and bradykinesia; however, manganism has a distinct cock-walk versus the festinating gait observed in PD (Lucchini et al., 2009). Patients with manganism rarely show a sustained response to L-3,4-dihydroxyphenylalanine (L-DOPA) or other dopamine (DA) replacement therapy and fail to show reduced striatal DA uptake (Calne et al., 1994; Huang et al., 2003). Recently, exposure to chronic low level Mn exposure has been shown to be a risk factor for PD as is living near industrial Mn operations (Gorell et al., 1997; Gorell et al., 1999; Lucchini et al., 2007; Lucchini et al., 2009; Perl and Olanow, 2007).

Pathology

Mn accumulates preferentially in the basal ganglia, specifically the striatum, globus pallidus (GP) and SN (Aschner et al., 2005; Dobson et al., 2004; Dodd et al., 2005; Erikson et al., 2002; Erikson et al., 2004b; Fitsanakis et al., 2008; Olanow et al., 1996; Williams et al., 2010b). Rodent, non-human primate and human post-mortem studies have found that the striatum shows damage following exposure to Mn (Aschner et al., 2007; Milatovic et al., 2009; Olanow, 2004; Perl and Olanow, 2007). Moreover, the nigrostriatal DA system is negatively impacted by Mn exposure (Guilarte et al., 2008; Guilarte et al., 2006; Huang et al., 2003; Kessler et al., 2003; Kim et al., 2002; Stanwood et al., 2009). In PD, the pigmented DA neurons of the SN degenerate resulting in damage to striatal medium spiny neurons (MSN) (Day et al., 2006; Garcia et al., 2010; Wright et al., 2009; Zaja-Milatovic et al., 2005). Therefore, overlapping, but not identical brain regions are involved in Mn neurotoxicity and PD, with striatal MSNs affected in both conditions (Garcia et al., 2010; Milatovic et al., 2009; Zaja-Milatovic et al., 2005).

Animal models

Animal models of Mn toxicity have shown to be reliable representations of human Mn poisoning. However, like all animal models of human disease there are limitations to disease fidelity. Due to structural differences in brain anatomy, rodents accumulate Mn in a slightly different pattern than non-human primates and humans. Non-human primates and rats were injected with the same dose of

Mn and measured accumulation 2 days later using MRI. Rodents accumulated less Mn than the non-human primates of approximately the same size and weight (Bock et al., 2008). Olfactory absorption of Mn is observed in animal models of inhalational Mn exposure; however it is unlikely to account for the large increase in Mn accumulation in the GP, which are thought to be due to systemic exposure (Bock et al., 2008; Dorman et al., 2006a; Dorman et al., 2006b).

Through the use of animal models, we have a better idea of how Mn is transported throughout the body and how it accumulates in the brain. Both astrocytes and neurons accumulate Mn, however astrocytes can accumulate as much as 50x as much Mn as neurons (Wedler et al., 1989). Mn can be taken up into cells via the divalent metal transporter 1 (DMT1), transferrin receptor (TfR), dopamine transporter (DAT) or other metal cation transporters (Anderson et al., 2007; Aschner and Gannon, 1994; Erikson and Aschner, 2006; Erikson et al., 2005). Mn tends to accumulate in non-heme iron (Fe) rich regions of the brain. This may be due in part to accumulation though transporters such as DMT1 and the TfR that are highly expressed in these brain regions (Dobson et al., 2004). Within cells, Mn has been shown to accumulate in the mitochondria and nucleus and cause dysfunction of these organelles (Gavin et al., 1999; Kalia et al., 2008).

Pathology

Mn toxicity at the molecular level has elucidated potential mechanisms of toxicity leading to pathology. Mn has been shown to accumulate in the mitochondria through the calcium uniporter (Gavin et al., 1999). This may disrupt calcium (Ca) levels in the mitochondria required for normal function (Tjalkens et

al., 2006). Mn can also inhibit Complex I of the mitochondrial electron transport chain (Chen et al., 2001). Mn has been shown to cause oxidative stress (Milatovic et al., 2007; Milatovic et al., 2009) and oxidize DA (Archibald and Tyree, 1987; Benedetto et al., 2010; Florence and Stauber, 1989).

Animal models of Mn toxicity show similar pathology to manganism, PD and animal models of PD. Rodents and non-human primates accumulate high levels of Mn in the basal ganglia and show motor deficits (Dodd et al., 2005; Golub et al., 2005; Guilarte et al., 2006; Vezer et al., 2007). These motor deficits may be due to dysfunction of the nigrostriatal DA pathway and damage to striatal MSNs (Burton and Guilarte, 2009; Burton et al., 2009; Guilarte et al., 2008; Guilarte et al., 2006; Milatovic et al., 2009; Stanwood et al., 2009). This is similar to neuropathology observed in animal models of PD (Day et al., 2006; Garcia et al., 2010).

Striatum

The striatum is the major input region of the basal ganglia. In humans the striatum consists of the caudate and putamen, but it is one structure in rodents. The basal ganglia consists of many subcortical nuclei that include the striatum, globus pallidus internal and external segments (GPi and GPe, respectively), subthalamic nucleus (STN) and substantia nigra pars compacta and pars reticulata (SNpc and SNpr, respectively) (Chakravarthy et al., 2010; Stocco et al., 2010).

The striatum is responsible for integrating information from multiple cortical and subcortical areas to regulate motor activity. Control of motor function was thought to be the only function of the striatum since movement disorders involve pathologies that include striatal dysfunction (Butterworth, 2010; Couper, 1837; Pfeiffer, 2007; Wilson, 1914). However, recently the striatum has also been implicated in cognitive functions such as procedural learning and spatial learning (Balleine et al., 2009; Voorn et al., 2004). The striatum receives topographical inputs from motor cortex, prefrontal cortex and thalamus, integrates this information and sends it back to the cortex through the thalamus.

Medium spiny neuron subtypes

Striatal MSNs compose approximately 95% of all neurons in the rodent striatum and 77% in primates (Graveland et al., 1985c; Rymar et al., 2004; Yelnik et al., 1991). In addition to MSNs, the striatum contains a small percentage of aspiny GABAergic interneurons and cholinergic interneurons. MSNs are GABAergic projection neurons with a medium sized soma and dendrites studded with dendritic spines. The striatum is composed of two main populations of MSNs defined based on their efferent projection, DA receptor and neuropeptide expression (Gerfen et al., 1990; Surmeier et al., 2007). MSNs also make inhibitory connections with other MSNs within the striatum through axon collaterals (Somogyi et al., 1981).

DA has opposing effects on the two subtypes of MSNs. There are two main categories of DA receptors; both are G-protein coupled receptors (GPCRs),

but they each couple to different effector proteins. D1 type DA receptors include D1 and D5 receptors (D1R and D5R). When stimulated by DA, these GPCRs couple to the Gαs effector which stimulates adenylate cyclase (AC) to stimulate the neuron. D2 type receptors include D2, D3, and D4 receptors (D2R, D3R and D4R). D2Rs couple to the Gαi subunit, which inhibits AC and decreases activity of these neurons.

Striatal MSNs receive a DA input from the SNpc and glutamatergic (Glu) inputs from the STN, thalamus and cortex. DA neurons form a synapse onto the neck of dendritic spines while cortical Glu inputs synapse onto the head of the spine. Corticostriatal presynaptic terminals express D2Rs that act to regulate corticostriatal Glu release (Bamford et al., 2004). Disruption of this synaptic triad has important consequences for motor function (Bamford et al., 2004; Day et al., 2006; Deutch et al., 2007; Garcia et al., 2010; Joshi et al., 2009).

Direct and indirect extrapyramidal pathways

There are two large pathways in the basal ganglia, the direct and indirect pathways. MSNs that express D1Rs co-express the neuropeptide substance P (SP) and project to the GPi/SNpr compose the direct or striatonigral pathway. The indirect, or striatopallidal, pathway is comprised of MSNs that express D2Rs and the neuropeptide enkephalin that project to the GPe. GABA neurons of the GPe project to the STN, where Glu neurons project to the GPi/SNpr. GABAergic neurons of the GPi/SNpr then project to the thalamus, and the thalamus projects to the cortex. At rest, the indirect pathway predominates to inhibit motor activity.

However, prior to onset of motor activity the direct pathway is activated and the indirect pathway is inhibited to allow motor activity to occur. This complicated integration of motor activity occurs in the striatum and is why its dysfunction plays a critical role in motor diseases such as HD, PD and manganism.

Medium spiny neuron morphology

Neuron morphology is characteristic of each major type of neuron. The dendritic arbor complexity, dendritic spine density and shape of the neuron determines how the neuron receives and propagates information that results in behavior such as movement or cognition (Alvarez and Sabatini, 2007). Dendritic spines and their morphology is importance for synaptic connections. Mature spines are mushroom shaped and have a large spine head and thin neck. These spines frequently receive glutamatergic inputs onto the head of the spine (Nimchinsky et al., 2002). In the case of MSNs, dendritic spines also receive a DA input onto the neck of the spine (Gerfen et al., 1990). Neuron morphology is labile, especially that of dendritic spines, and is influenced by exposure to toxicants, stress, neurochemistry, age, exercise and drugs (Alcantara-Gonzalez et al., 2010; Alfarez et al., 2009; Alvarez and Sabatini, 2007; Bindu et al., 2007; Eadie et al., 2005; Fischer et al., 2000; Gupta et al., 2007; Irwin et al., 2000; Johansson and Belichenko, 2002; Mervis et al., 1991; Milatovic et al., 2010; Solis et al., 2009; Stranahan et al., 2007; Yuste and Bonhoeffer, 2001).

Gene x Environment Interactions

Almost all diseases are the result of a combination of genetics and exposure to environment factors (Horowitz and Greenamyre, 2010; Hunter, 2005; Nabholz and von Overbeck, 2004). The genetic component can be causal (Mendelian) or susceptibility genes. A causal gene is a single gene in which a mutation, deletion, insertion or rearrangement directly causes a disease. These genes can be autosomal dominant, autosomal recessive or X-linked and follow well established inheritance patterns. Susceptibility genes have variations in the DNA sequence that occur normally throughout the human population. Each susceptibility gene only confers a small increase in risk of developing a specific disease. Multiple susceptibility genes or exposure to an environmental agent that can interact with such genes can initiate disease onset.

Exposure to environmental factors can alter gene expression (epigenetics) or cell signaling pathways to cause onset of disease or alter disease progression. Environmental exposure can occur at any point throughout life to alter susceptibility to disease. Prenatal exposure and postnatal exposure in young children are critical time periods because the brain is still developing. *In utero* toxicant exposure is an emerging field that will shed light on many factors that have the potential to influence disease later in life. Exposure to toxic environmental agents is not only a concern during development; it is a growing concern in adult populations especially because of an increasing lifespan.

Gene-environment interactions play a role in many diseases, from cancer to respiratory diseases and autoimmunity diseases to neurodegenerative

diseases (Bjorkman et al., 2000; Chia, 2008; Gualtierotti et al., 2010; Horowitz and Greenamyre, 2010; Laviola et al., 2008; Nabholz and von Overbeck, 2004; Schwartz, 2010; Vance et al., 2010). To illustrate gene-environment interaction involvement in disease, I will briefly discuss Parkinson's disease.

Parkinson's disease is a neurodegenerative disease with genetic and environmental risk factors. There are a few genes that have a strong link to development of familial or heritable PD. These genes include parkin, LRRK2, PINK1, α-synuclein and DJ-1 (Horowitz and Greenamyre, 2010; Vance et al., 2010). Familial PD accounts for less than 10% of all PD cases. The majority of PD cases are idiopathic (IPD) with links to susceptibility genes such as Tau, USP24, ELAVL4 and ApoE (Vance et al., 2010). Environmental factors for the disease include aging, male gender, pesticide and Mn exposure. Age is a strong risk factor in both monogenetic and sporadic PD. Males are approximately twice as likely to develop PD as females. This may be due to sex hormone effects and/or occupational exposure to toxicants. Several animal studies suggest that estrogen is neuroprotective in multiple models of PD. Specific gene-environment interactions have been discovered for PD. Single nucleotide polymorphisms (SNP) in the nitric oxide synthase genes in conjunction with pesticide exposure and smoking have been shown to increase risk of PD (Hancock et al., 2006; Hancock et al., 2008).

PD is an illustrative example of a disease that is largely determined by gene-environment interactions. Studies have shown that although there is a genetic component to PD, penetrance of the disease is variable and incomplete.

An example of this is the discordance rates between monozygotic twins. There is variability in disease presentation and age of disease onset (Wirdefeldt et al., 2011). Exposure to environmental toxicants can produce a form of parkinsonism that is indistinguishable from IPD. However, not all people exposed to these toxicants develop parkinsonian symptoms, thereby suggesting that there is a genetic susceptibility in a small number of people.

Possibility of gene-environment interactions in monogenetic disease

Although HD is a monogenetic autosomal dominant disease, the number of CAG repeats in the *HTT* gene only accounts for 60% of the variability in age of disease onset (Andrew et al., 1993; Brinkman et al., 1997; Duyao et al., 1995; Stine et al., 1993; Wexler et al., 2004b). Environmental exposure and/or other genetic factors account for the remaining variability in disease onset and therefore may accelerate or slow the age of disease onset and progression (Hannan, 2004; van Dellen et al., 2005; van Dellen and Hannan, 2004). Monozygotic twin studies have shown discordance in age of onset, symptom presentation and disease severity. Some authors ascribe the difference in disease to be environmental, while others ascribe it to epigenetic phenomenon (Anca et al., 2004; Friedman et al., 2005; Georgiou et al., 1999; Gomez-Esteban et al., 2007; Panas et al., 2008). Friedman et al (2005) was the only research team that identified potential environmental exposure that could result in differential disease phenotypes between monozygotic twins. The birth home of the twins was across the street from an industrial factory; the air was polluted

and there were numerous chemical spills throughout their childhood. After the factory closed, it was designated as a federal toxic site. The twin presenting with HD symptoms at the age of 65 had only recently stopped smoking within the previous year, while the unaffected twin stopped smoking at the age of 35. The unaffected twin also moved out of the birth home long before the affected twin, and therefore was not exposed to either cigarettes or industrial toxins as long as the affected twin. This is only one example where there is a probable link to environmental exposure playing a significant role in onset of HD. Further investigation of monozygotic twins and large epidemiological studies may shed further light on to how environmental exposure can modify the onset and progression of HD.

Evidence for gene-environment interactions in HD animal models

Animal models of HD also show gene-environment interactions in disease progression. Environmental enrichment (EE) involves placing novel items of various texture, shapes and sizes into cages with mice. EE has been shown to delay onset of motor symptoms in the R6/1 and R6/2 HD mouse models (Hockly et al., 2002; van Dellen et al., 2000). However, EE was not able to slow degeneration of striatal MSN (Spires et al., 2004). Dietary restriction through fasting was able to improve performance on the rotarod, increased brain derived nerve growth factor (BDNF) and increase life span in the HD N171-82Q mouse model (Duan et al., 2003). Another modification of the diet to include essential fatty acids reduced motor symptoms, but was not able to prevent a reduction in

striatal D1R and D2Rs in the R6/1 mouse model (Clifford et al., 2002). Supplementation of the YAC128 diet with the essential fatty acid ethyl-eicosapentaenoic acid (EPA) beginning at 7 months improved motor function, however there was no effect on progression of neurodegeneration (Van Raamsdonk et al., 2005a).

Interestingly, in human clinical trials, supplementation of the diet with EPA improved performance on the Unified Huntington's Disease Rating Scale (UHDRS) in two separate clinical trials (Clifford et al., 2002; Puri et al., 2005). A third trial failed to find an improvement in performance on the UHDRS, however there was no decline in performance observed suggesting that EPA was able to at least prevent a decline in performance (Vaddadi et al., 2002). The most recent clinical trial (TREND-HD) also failed to detect a difference between EPA and placebo in performance on the UHDRS (Investigators, 2008). These trials suggest that there is still much to be learned about HD and how environmental exposure may or may not have an effect on disease progression.

Gender as a factor in gene-environment interactions

Gender differences in the toxicokinetics of xenobiotics have been reported in the literature (Clewell et al., 2002; Fletcher et al., 1994; Nicolson et al., 2010). Multiple factors contribute to the gender differences; from differences in cytochrome P450 (CYP450) expression, transporter expression and influences of sex hormones on expression of these enzymes and transporters (Bonate, 1991;

Harris et al., 1995). Few studies have been conducted to examine the effect of gender on Mn exposure and HD.

Gender and metal toxicity

Studies conducted in the general population, unexposed to high levels of Mn, have shown conflicting results. Men have been shown to have lower ferritin levels, reduced Mn absorption from the gastrointestinal tract and slower Mn clearance than women (Finley et al., 1994). Some studies indicate that in a healthy unexposed population, serum Mn levels are higher in men than women (Davis and Greger, 1992; Greger et al., 1990). However, more recent reports indicate that there is no gender difference in baseline serum Mn levels (Diaz et al., 2001; Rukgauer et al., 1997). A recent study explored intellectual function of children living in a Mexican Mn mining district. Children exposed to Mn had 20x the amount of Mn in hair and blood than children unexposed to high Mn levels. Young girls exposed to Mn performed worse on the revised Wechsler Intelligence Scale for Children than Mn exposed boys (Riojas-Rodriguez et al., 2010). Although there were no gender differences in Mn levels of exposed children, this suggests that cognitive performance may be differentially affected in boys and girls. Gender differences in response to metal exposure are not unique to Mn. Human studies have found gender differences in accumulation, storage and sensitivity to metals including cadmium (Cd), lead (Pb), Mn, mercury (Hg) and nickel (Ni) (Akesson et al., 2002; Akesson et al., 2005; Bjorkman et al., 2000; Grandjean et al., 1998; Gulson et al., 1998; Jin et al., 2004; Kobayashi et al., 2006; Manton et al., 2003; McKeown-Eyssen et al., 1983; Meding et al., 2001;

Nielsen et al., 2002; Pounds et al., 1991; Uno et al., 2005; Vahter et al., 2007; Vahter et al., 2002). Animal studies also show gender differences in metal toxicokinetics and sensitivity. For example, male and female rats accumulated Mn differentially across body tissues following Mn exposure by inhalation; however, there was no difference in Mn accumulation in the striatum or other regions of the basal ganglia (Dorman et al., 2004). Gender differences in toxicokinetics following a single oral dose of the gasoline additive methylcyclopentadienyl manganese tricarbonyl (MMT) showed that female rats accumulated higher MMT levels than male rats due to slower clearance of MMT (Zheng et al., 2000). Erikson et al (2004a) exposed juvenile rats to airborne Mn for 13 weeks and found gender-specific changes in protein and mRNA expression of glutamine synthetase, metallothionein mRNA and glutathione levels in multiple regions of the brain. Gender differences in the toxicokinetics of Mn are present regardless of route of administration and Mn speciation. As with humans, rodents show gender differences upon exposure to other metals such as Pb and Hg (Fortoul et al., 2005; Magos et al., 1981; Sager et al., 1984).

Human studies have found gender differences in accumulation, storage and sensitivity to other metals including Cd, Pb, Hg and Ni (Vahter et al., 2007; Vahter et al., 2002). Cd accumulates in the renal cortex and exposure to low levels of Cd reduced the glomerular filtration rate in women (Akesson et al., 2005), however, men showed Cd-induced renal tubular effects at lower Cd levels than women (Jin et al., 2004; Kobayashi et al., 2006; Uno et al., 2005). Over 90% of Pb is stored in skeletal bone and release of Pb from bone parallels

increased bone turnover rates in women during pregnancy and lactation (Gulson et al., 1998; Manton et al., 2003; Pounds et al., 1991). A recent twin study in Sweden found that blood Pb levels have a larger genetic component in women than men (Bjorkman et al., 2000). Neurodevelopmental delays in children exposed to Hg prenatally are more prominent in boys than girls (Grandjean et al., 1998; McKeown-Eyssen et al., 1983). Females are more susceptible to topical Ni allergy, which may be related to an increase in exposure to Ni containing jewelry (Meding et al., 2001; Nielsen et al., 2002).

Animal studies also show gender differences in metal toxicokinetics and sensitivity. Female rats exposed to Pb by inhalation accumulated significantly higher levels of Pb than male rats. However, male rats lost more lung nonciliated bronchiolar cells and had a higher rate of necrosis (Fortoul et al., 2005). Female rats exposed to methylmercury (MeHg) by gastric gavage accumulate higher levels of the metal in the brain and have more damage to cerebellar granule layers than male rats (Magos et al., 1981). However, Sager et al. (1984) showed that male mice exposed to MeHg had fewer cells in the molecular and granule layers of the cerebellum than female mice. Male rats had a higher level of Mn in the blood, lung and olfactory bulb than female rats following Mn exposure by inhalation. Female rats had higher Mn levels in the cerebellum and liver, however there was no difference in Mn accumulation in the striatum or other regions of the basal ganglia (Dorman et al., 2004). Gender differences in toxicokinetics following a single oral dose of the gasoline additive MMT showed that female rats had a higher area under the curve (AUC), a longer half-life, a slower clearance

(CL) and elimination constant (kel). Overall, the female mice were exposed to more MMT than male mice and eliminated MMT from their system more slowly (Zheng et al., 2000). Erikson et al., (2004a) exposed juvenile rats to airborne manganese sulfate or manganese phosphate for 13 weeks and found gender-specific and Mn-species specific changes in protein and mRNA expression of glutamine synthatase, metallothionen mRNA and glutathione levels in multiple regions of the brain. This study suggests that gender-specific differences in sensitivity to Mn exposure may also depend on the species of Mn. A recent behavioral study suggests that male mice are more susceptible to Mn exposure than female mice and that the behavioral deficit may be related to reduced striatal DA following Mn exposure (Moreno et al., 2009; Simon et al., 1994). A similar behavioral deficit has been found in a PD mouse model (George et al., 2008).

Gender differences in Parkinson's disease

Gender differences in prevalence, age of onset and progression have been described for PD (Haaxma et al., 2007; Miller and Cronin-Golomb, 2010; Shulman, 2007). Females tend to have a later age of onset and less severe symptoms of PD. Gender studies in animal models of PD have also shown that estrogen plays a protective role in neuropathology and behavior. Survival of DA neurons following exposure to DA neurotoxicants, used in animal models of PD is sensitive to gender (Richardson et al., 2008; Tamas et al., 2005). A study examining gender effects of 6-hydroxydopamine (6-OHDA) lesions on behavior and neuropathology showed that male rats are more sensitive to this toxicant

than female rats. Male rats showed a greater loss of DA neurons in the SN and had greater deficits in locomotor activity than female rats (Tamas et al., 2005). This suggests that the nigrostriatal DA system is more sensitive to toxicants in male than female rodents.

Gender differences in Huntington's disease

Multiple animal models of HD have shown gender differences in neuropathology and motor phenotype. Transgenic HD rats carrying a truncated *HTT* fragment with 51 CAG repeats showed gender differences in striatal volume, D1 dopamine receptor density and 17-β-estradiol. Symptomatic male rats showed reductions in each of these measures at 14 months (Bode et al., 2008). Eight weeks of wheel running was shown to increase striatal levels of brain derived nerve growth factor (BDNF) in female, but not male, R6/1 mice (Zajac et al., 2010). Knock-in HD mice with 140 CAG repeats showed gender differences in behavior and striatal neurochemistry. Female knock-in mice showed habituation to the running wheel in the cage and spent more time running in the dark phase than male knock-in mice. Male knock-in mice showed a decrease in ascorbate release in the striatum that was no present in female knock-in mice (Dorner et al., 2007). Male N171-82Q HD mice showed a rotarod deficit that was not evident in female HD mice. BAG1 is a co-chaperone for HSP-70 which increases HSP-70 activity. Crossing the HD mice with a neuron specific BAG-1 overexpressing line reduced the motor phenotype and reduced synaptosomal *HTT* aggregates in male HD mice (Orr et al., 2008). A comprehensive examination of behavior phenotypes, including gender

differences, in numerous HD mouse models was reviewed by Menalled et al., (2009). These studies show that gender differences in HD animals can be detected in motor phenotype, neuropathology and neurochemistry. Furthermore, HD mice respond differently to therapeutic interventions based on gender (Dorner et al., 2007; Orr et al., 2008; Zajac et al., 2010).

Hypothesis and specific aims

Since the striatum is a common target for both HD pathology and Mn accumulation, this provides the opportunity to observe gene-environment (heretofore referred to as disease-toxicant) interactions. Data previously published by our research groups show that YAC128 mice accumulate less striatal Mn relative to wild-type (WT) mice (Williams et al., 2010a; Williams et al., 2010b). This phenomenon was restricted to the striatum because no significant differences in Mn levels between genotypes were observed in other brain regions. *In vitro* experiments by Williams et al. (2010b) and Kwakye et al. (2011), showed that a striatal cell line expressing mutant *HTT* ($STHdh^{Q111/Q111}$) accumulated less Mn and exhibited higher survival rates than striatal cells expressing WT *HTT* ($STHdh^{Q7/Q7}$). Based on these studies, we hypothesized that Mn exposure and mutant *HTT* would exhibit disease-toxicant interactions at the level of neuron morphology and neurochemistry in the striatum of YAC128 mice.

Specific Aims

This work aims to answer the following questions; (1) is there a disease-toxicant interaction between mutant *HTT* and Mn exposure in striatal neurochemistry and MSN morphology and (2) does gender play a role in the disease-toxicant interaction in MSN morphology?

Specific Aim 1

In this aim we determine if (1) Mn exposure, (2) mutant *HTT* expression and (3) the combination of Mn exposure and mutant *HTT* expression alters striatal neurochemistry and MSN morphology at two time points. In order to address the question if a disease-toxicant interaction between HD and Mn exposure alters striatal neurochemistry and MSN morphology, we exposed WT and YAC128 mice to vehicle (Veh) or Mn and examined striatal neurochemistry by HPLC and MSN morphology by Golgi staining.

Specific Aim 2

Based on the literature of gender differences in Mn exposure and HD animal models, we hypothesized that gender may be a factor in Mn and/or HD neuropathology. Therefore, we examined striatal MSN morphology and striatal Mn content 24 hours and 3 weeks following Mn exposure in mice of both genders and genotypes to determine (1) if gender has an effect on MSN morphology in the presence or absence of Mn exposure, (2) if gender is a factor in striatal Mn accumulation and (3) if gender differences in MSN morphology are present when Mn levels return to baseline.

CHAPTER II

MATERIALS AND METHODS

Chemical Reagents

Osmium tetroxide and glutaraldehyde were obtained from Electron Microscopy Sciences (Hatfield, PA), $MnCl_2$ from Alfa Aesar (Ward Hill, MA), paraformaldehyde from Fisher Scientific (Pittsburgh, PA), Phosphate Buffered Saline (PBS) from Mediatech Inc. (Manassas, VA), isoflurane from Phoenix Pharmaceutical Inc., (St. Joseph, MO) and all other chemicals were obtained from Sigma Chemical Company (St. Louis, MO).

Animal Housing and Mn Exposure

The FVB-Tg (YAC128)53Hay/J mouse line (YAC128) was purchased from JAX (#004938, Bar Harbor, ME) (Slow et al., 2003). All animal exposure protocols were approved by the Vanderbilt University Medical Center Institutional Animal Care and Use Committee (IACUC) and strictly adhered to in order to minimize the mice' pain. All treatment and procedures followed NIH laboratory animal care and use guidelines. Genotyping of the mice and confirmation of a static CAG-triplet repeat length in mutant animals was carried out by PCR according to a previously published protocol (#004938; from JAX) (Slow et al., 2003). Mice were distributed into exposure groups across multiple litters and the gender in each of the groups was balanced. The Mn exposure paradigm was

adapted from the previously published protocol (Dodd et al., 2005; Williams et al., 2010b) that resulted in a significant increase in striatal Mn levels without significant motor impairment on experimental day 7, 24 hours following the last Mn exposure. Twelve week old mice were subcutaneously (s.c.) injected at the hind leg with vehicle (water) or $MnCl_2$-$4H_2O$ (50 mg/kg) on experimental day 0, 3, and 6.

Quantification of Striatal Manganese Levels

Mice were decapitated on experimental day 7 (13 weeks, 7 mice per group) or 28 (16 weeks, 5 mice per group) and the striatum was rapidly dissected. The striatum was then placed in liquid nitrogen and stored at -80^{o}C. Samples were dried in glass vials on a heat block at 100^{o} C for 3 days underneath a beaker turned upside down and digested with 65-70% nitric acid for 3 hours at 90^{o} C. To each sample, 10 mL of 1 % nitric acid was added. Next, samples were filtered (Arcodisc, 0.45 μm HT Tuffryn membrane) and submitted for Inductively Coupled Plasma-Mass Spectrometry (ICP-MS) analysis. A Perkin-Elmer ELAN DRC II ICP-MS was calibrated and verified before reading the blank (1% nitric acid). 50 μL of In-115 at a concentration of 50 μg/L was added to each sample as an internal control. Analysis of each sample was read with the following settings: nebulizer flow 0.9-1 L/min, radio frequency power 1,250-1,300 W, plasma gas flow 15 L/min, lens voltage 6.5-7.5 V, auto lens on, 3 replicates per reading, 100 ms dwell time per atomic mass unit, 1000 ms integration time with peak hopping scan mode.

Golgi Silver Impregnation

Multiple Golgi staining methods have been used in the striatum, so we compared two methods to identify one that produced high quality staining of striatal MSNs. We first completed a pilot study comparing the FD Neurotechnologies Rapid GolgiStain Kit (Ellicott City, MD), published previously in our laboratory, with the single section rapid Golgi method that was optimized to stain MSNs (Garcia et al., 2010; Kusnoor et al., 2010). In our hands, the FD Neurotechnologies Rapid GolgiStain Kit did not fully impregnate a large number of neurons in the striatum. For example, there were numerous breaks in staining along the dendrite (Figure 23A, white arrow) or non-specific blebbing (Figure 23A, black arrow). In comparison to the FD Neurotechnologies Rapid GolgiStain Kit staining, the single section rapid Golgi method (Figure 23B) produced high quality staining without any breaks in staining or blebbing along the dendrites. For this reason, we chose to use the single section Golgi method for the full studies to analyze how the disease-toxicant interaction between mutant *HTT* and Mn modifies striatal MSN morphology.

On experimental day 7 (13 weeks) or day 28 (16 weeks) the mice were deeply anesthetized with isoflurane, and transcardially perfused with 15 mL 0.1M phosphate buffer (PB) followed by 40 ml of 2% paraformaldehyde and 2.5% glutaraldehyde in 0.1M PB. The brains were removed from the skulls and post-fixed for 3 hours at room temperature. Vibratome sections were cut in the coronal plane at 150 μm. The single-section Golgi silver impregnation method was

previously described (Garcia et al., 2010; Kusnoor et al., 2010). The sections were incubated in 1% osmium tetroxide for 20-40 minutes, transferred to 3.5% potassium dichromate and incubated overnight. The sections were then incubated in silver nitrate between two slides for 4-6 hours. Sections were washed in water, mounted on 0.5% gelatin coated slides, dehydrated and cleared and coverslipped. There were 4-5 mice per exposure group at 13 weeks and five mice in all groups at 16 weeks. The FD Neurotechnologies Rapid GolgiStain Kit (Ellicott City, MD) was used according to the manufacturer's instructions.

Neuron Reconstruction and Analysis

Golgi-impregnated striatal medium spiny neurons were reconstructed under 60x magnification using the NeuroLucida (MicroBrightfield, Inc., Williston, VT) system. One researcher, blinded to genotype and exposure conditions, selected, traced and analyzed the neurons. Four to six neurons were traced per animal and were selected for tracing based on the following strict criteria: location in the striatum (Bregma +0.14 mm to +0.86 mm), soma and dendrites must be fully impregnated without beading or breaks in staining along the dendrite, and must have at least 2 primary dendrites and reach the 3rd branch order. Neurons were analyzed using NeuroExplorer (MicroBrightfield, Inc., Williston, VT). Morphometric characteristics were either averaged over the entire neuron (total neuron measures) or analyzed as a function of distance from the soma. Dendritic length and spine number are summed over the entire dendritic tree to give total

dendritic length and total spine number, respectively. Total spine density is the number of spines per 10 μm. The point of each dendrite branching is termed a node. Therefore, the total number of nodes is the total number of branch points summed across the dendritic tree. The total number of ends refers to the number of dendrite endings. Concentric circles of 10 μm radiating outward from the center of the soma were used to analyze morphometric features as a function of distance from the soma. Branching complexity was measured by tallying the number of dendrites that cross each of the concentric circles (intersections). The space in between each of the concentric circles creates a shell in which morphologic features, such as dendrite length, spine number and spine density were measured. This information provides a more detailed view of neuron morphology (Sholl, 1953).

Amino Acid and Monoamine Neurochemistry Analysis

Mice were euthanized at week 13 or 16 by decapitation. The striatum was rapidly dissected, placed in liquid nitrogen and stored at -80^{o}C. Samples were submitted to the Center for Molecular Neuroscience/Kennedy Center Neurochemistry Core Lab at Vanderbilt University for measurement of amino acids (n=3-8 mice per group) and monoamine neurotransmitters (n = 4-6 mice per group) by HPLC.

Immunohistochemical Staining

On either day 7 or day 28 the animals were deeply anesthetized with isoflurane, and transcardially perfused with 0.1M PB followed by 4% paraformaldehyde in 0.1M PB. The brains were blocked and post-fixed overnight. The following day the brains were transferred into 30% sucrose for cryoprotection. Coronal sections (40 μm) were made using a cryostat to collect multiple sets of sections. Immunostaining was done according to previously published protocols (Bubser 2000, 1998? Deutch 1991 Cereb Ctx w/mods). Briefly, free-floating sections were washed in TBS, incubated in primary antibody overnight at room temperature, washed in TBS, incubated in a biotyinylated secondary antibody for 90 mins at room temperature, washed with TBS, and incubated in HRP-conjugated streptavidin for 1 hr at room temperature. Sections were washed in TBS and developed with (0.0005%) DAB in TBS plus (0.00009%) H_2O_2. The reaction was quenched by washing with TBS multiple times. Sections were mounted, cleared and coverslipped.

Antibodies

Sheep polyclonal tyrosine hydroxylase (TH, 1:3000 Millipore, Temecula CA, USA) was used to identify dopamine neurons in the substantia nigra. Mouse monoclonal glutamic acid decarboxylase 67 (GAD67, Millipore) was used to identify medium spiny neurons in the striatum. Biotinylated secondary antibodies (1:1600) and horseradish peroxidase (HRP) conjugated streptavidin (1:1000) were obtained from Jackson ImmunoResearch (Bar Harbor, MA, USA).

Statistical Models

Data were generated through various experimental methodologies and require different statistical models in order to meet critical assumptions required for each model. Grubb's outlier test was used prior to statistical analysis to find and eliminate outliers in data with the significance of alpha set to $p < 0.05$. Univariate, multivariate and repeated measures analysis of variance (ANOVA) followed by post-hoc analysis using Fisher's LSD multiple comparison test were performed using PASW Statistics 18 (SPSS, Inc, Chicago, IL). Striatal Mn levels, total neuron measures, striatal neurochemistry and immunohistochemistry were assessed by multivariate ANOVA with age, exposure, gender and genotype (when appropriate) as fixed factors. Age, exposure, gender and genotype (when appropriate) and radius were assigned as fixed factors in the analysis where neuron morphologic characteristics were measured as a function of distance from the soma. When ANOVA results were significant, *post-hoc* analysis of all pairwise combinations by Fisher's LSD was used to determine statistical differences between exposure groups.

CHAPTER III

MORPHOMETRIC ANALYSIS IN NEURODEGENERATIVE DISORDERS

Abstract

The study of dendritic length and spine density has become standard in the analysis of neuronal abnormalities, since a considerable number of neurological diseases have their foundation in alterations in these structures. One of the best ways to study possible alterations in neuronal morphometry is the use of Golgi impregnation. Introduced more than a century ago, it is still the standard and state-of-the-art technique for visualization of neuronal architecture. We successfully applied the Golgi method to mouse, rat, monkey, and human brain tissues for studying both the normal and abnormal morphology of neurons. We were able to discover subtle morphological alterations in neuronal dendrites and dendritic spines in different brain areas. Although Golgi preparations can be examined by electronic microscopy, we used light microscopy and reconstruction using Neurolucida software to quantitatively explore the relationship between total dendritic length and spine density in different types of neurons. This unit summarizes the methodology used to quantify neuronal abnormalities and discusses the utility of these techniques in different models of neurodegeneration.

Introduction

Basic protocol: Golgi-Cox Stain with Rapid GolgiStain™ kit

In our morphological studies and this unit we use the FD Rapid Golgi Staining Kit (FD Neurotechnologies, *http://fdneurotech.com/*), a commercial Golgi-Cox staining system that has been proven to produce good results in animal and post-mortem human brain tissues. This method results in an adequate number of well impregnated neurons with nicely visible spines. Tracing and quantitative neuronal morphology is performed with the use of the Neurolucida system (MBF Bioscience, *http://www.mbfbioscience.com/*). Neurolucida is an advanced scientific software for performing neuron tracing and morphometry, as well as brain and anatomical mapping. Neurolucida can be used with live images from color video cameras or with stored image sets from confocal microscopes, electron microscopes, and scanning tomographic sources. When used in connection with light microscopes, Neurolucida utilizes a computer-controlled motorized XYZ stage for integrated navigation through tissue sections. Once the tracing is complete, images can be transferred to NeuroExplorer, a three-dimensional visualization and morphometric analysis program designed for data analysis, permitting determination of total dendritic length and number of spines per neuron. A representative neuronal tracing from our previous study with monkey brain is presented in Figure 1.

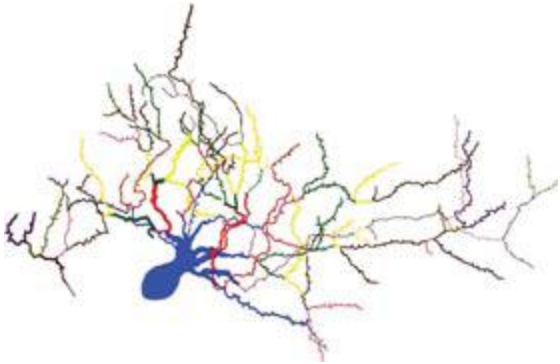

Figure 1. Golgi-impregnated Neurolucida-traced Purkinje cell from the monkey brain.

The following Basic Protocol is a description of the methodology for impregnation and staining of neuronal tissue; the Anticipated Results section in the Commentary describes concrete examples of quantitative characterization of neuronal morphology in studies conducted by our laboratories. For our staining, we use the FD NeuroTechnologies Rapid Golgi Staining kit (FD kit); it is based on the Golgi-Cox method of Ramon-Moliner (1970) and Glaser and Van der Loos (1981). It has been used in multiple animal species, as well as human post-mortem tissue, to assess neuronal morphometry in a variety of brain regions. The kit is simple and easy to use with few technical requirements. *NOTE:* All protocols involving living animals must first be reviewed and approved by an Institutional Animal Care and Use Committee (IACUC) and must conform to governmental regulations regarding the care and use of laboratory animals.

Materials

- Experimental animal, e.g., mouse, rat, monkey
- FD Rapid Golgi Stain Kit (FD NeuroTechnologies, cat. no. PK-401)
- 50%, 70%, 95%, and 100% ethanol
- Xylenes
- Paraffin
- 1% (w/v) bovine serum albumin (Sigma A3912) in PBS
- Tissue-Tek O.C.T. Compound (Sakura Finetek, cat. no. 4583)
- 0.1% cresyl violet
- Histo-Clear (National Diagnostics; optional)

- Cytoseal XYL mounting solution (Thermo Fisher Scientific)
- Dissecting equipment
- Razor blade (e.g., surgical carbon steel #12, single edge, VWR 55411-055)
- 15-ml conical plastic tubes
- Histology cassettes
- Automated histology processor, e.g., Thermo Scientific Shandon Excelsior
- Embedding molds
- Automated rotary microtome (Leica RM 2235) or manual rotary microtome (Leica
- RM 2125)
- Superfrost Plus microscope slide (25 × 75 × 1–mm; e.g., VWR, cat. no. 48311-703)
- Histology oven
- Cryostat and chuck
- Gelatin-coated microscope slides (see recipe)
- Slide box
- Plastic staining dishes and rack (e.g., Sakura Finetek 4451)
- Coverslips (24 × 50–mm, no. 1 1⁄2; e.g., VWR, cat. no. 48393-241))
- Light microscope, e.g., Olympus BX62 with motorized stage
- Neurolucida and NeuroExplorer software (MBF Bioscience, *http://www.mbfbioscience.com*)

- Additional reagents and equipment for anesthesia (Donovan and Brown, 1998) and euthanasia (Donovan and Brown, 2006) of animals

NOTE: Keep containers closed tightly at all times. Protect tissues from light during and after exposure to Solutions A and B. Perform all procedures at room temperature, unless specified.

Tissue preparation

1. Clean and rinse all containers with distilled water.
    a. *Plastic containers are preferred, but glass containers are acceptable. Do not use metal implements when Solutions A and B from the FD Kit are present.*
2. At least 48 hr prior to experiment, prepare impregnation solution by combining equal volumes of Solutions A and B from the FD Rapid Golgi stain kit, gently mix (do not stir), and leave in the dark. Transfer 5- to 10-ml aliquots into 15-ml tubes. Prepare at least 5 ml of impregnation solution per cm3 of tissue.
    a. CAUTION*: Solutions A and B contain mercuric chloride, potassium dichromate, and potassium chromate, and are toxic to the skin and potentially fatal if swallowed.*
3. Deeply anesthetize experimental animals (Donovan and Brown, 1998) prior to sacrifice (Donvan and Brown, 2006).
4. Remove the brain from the skull quickly, but avoid damage to the brain.

5. Dissect the brain using a surgical razor blade.
    a. *The dissection procedure should depend on the specific brain regions of interest. Avoid processing tissue pieces with volume >1 cm3, which may result in incomplete tissue impregnation.*
6. Briefly rinse tissue with double distilled or Milli-Q water to remove blood from the surface.

Silver Impregnation

7. Place tissue into 15-ml conical tubes containing 10 ml of the impregnation solution (see step 2; use ≥5 ml solution/cm3 of tissue) for 2 weeks at room temperature in the dark.
    a. *Only use the top part of the impregnation solution and avoid the precipitate.*
8. Replace the impregnation solution with fresh impregnation solution on the next day.
    a. CAUTION*: Dispose of the impregnation solution in accordance with your institution's hazardous waste regulations.*
9. Transfer the tissue into Solution C from the kit (in a 15-ml tube) and store in the dark at 4◦C for 5 to 7 days.
10. Replace Solution C on the next day.
11. After 1 week processing in Solution C in the dark at 4◦C, transfer the tissue into a new 20-ml scintillation vial and fill with water. Wash the tissue under running water overnight at room temperature.

12. Place the very well rinsed tissue in a histology cassette, immerse cassette in 70% ethanol, and process in an automated histology processor as described in the following steps.
    a. *All submitted tissue should be placed in cassettes and properly labeled with a unique identification number.*

Tissue processing in automated tissue processor

After fixation (3 weeks: 2 weeks with Solutions A and B and 1 week with Solution C; steps 7 to 11) and preparatory procedures, the tissue is ready to go through the process of dehydration, clearing, infiltration, and embedding. Tissue processing and embedding in wax provide a support matrix for the tissue. Tissue must be completely fixed before processing. Processors have many containers of reagents into which the samples are transferred sequentially (using a carousel) and are pumped in or out.

13. Immerse tissues in increasing concentrations of ethanol to remove water from the tissue (once in 70% ethanol, three times in 95% ethanol, three times in 100% ethanol, each time for 1 hr). Following dehydration, clear samples in xylene (twice, each time for 1 hr) and infiltratewith paraffin, three times, each time for 1 hr using the automated processor.
    a. *Poor dehydration results in poor processing. Too much time in alcohol can cause artifacts such as vacuolization and shrinkage. Incubation in clearing agents for too long can harden tissue and*

make sectioning difficult. Tissue processing schedules for automated processors are devised according to brain size.

14. Using embedding molds, immerse samples in melted paraffin wax, which when solidified provides a support matrix.

Paraffin block sectioning

15. Section paraffin blocks at 50 to 80 µm on a rotary microtome.
16. Float sections in purified water at 10◦C below the melting point of the wax used, then pick them up on BSA-coated charged (Superfrost Plus) slides.
    a. *Slides are coated by immersing in 1% BSA in PBS for ≥30 min, then rinsing with water.*
    b. *Two sections may be placed on each slide.*
17. Drain slides upright and dry at 37◦C for a minimum of 20 min.
18. Leave sections in histology oven at 60◦C for at least 1 hr (preferably overnight) to improve adhesion.

Cryostat sectioning

Following processing with Solution C and washing (step 11), processed tissue can be frozen and sectioned with a cryostat (although the authors usually use paraffin-embedded tissue since paraffin sections are more stable):

a. Rapidly freeze tissue block by gently wrapping it in aluminum foil and placing in the cryostat chamber for at least 10 min.

b. Apply O.C.T. tissue-embedding compound on the chuck and allow it to solidify. Set the cryostat thickness to ~100 μm and cut through the embedding compound until a flat surface large enough to accommodate the tissue is obtained.
c. Orient the tissue so that the side of least importance is facing the chuck. Place a small amount of O.C.T. tissue-embedding compound on the side of the tissue that is least important and rapidly freeze tissue on the flat surface of the chuck. Place a small amount of tissue-embedding compound around the edge of the tissue to secure it to the chuck. Allow tissue embedding compound to solidify for ~5 min.
d. Cut 50- to 150-μm thick sections quickly on a cryostat at −22°C. Set the chamber temperature to 1°C colder than the specimen head temperature. Set the cryostat temperature the evening before use to allow sufficient time for the chamber to reach the desired temperature.
e. Fill the dropper from the FD Golgi Stain kit with Solution C and place a drop of Solution C at each position on the gelatin-coated microscope slide where each section will be placed. Make sure that the sections are not placed too close to the edge of the slide. This will cause bubbles to form in the mounting medium and render the slides unusable.

f. Transfer each section onto a drop of Solution C using the glass specimen retriever from the kit to mount on gelatin-coated microscope slides.
g. Absorb excess solution using a strip of filter paper or Kimwipe. Absorb excess solution so that sections do not fall off of the slides.
h. Dry sections flat at room temperature overnight in the dark without the use of a heating source or fan.
i. Dried sections should be processed as soon as possible, but they may be stored for up to 1 week in a slide box at room temperature. Proceed to step 20.

Deparaffinization and staining procedure

19. Deparaffinize sections by incubating for 5 min successively in three changes of xylene in Sakura Finetek staining dishes.
20. Hydrate sections by immersing successively twice, each time for 5 min, in 100%, 95%, 70% and 50% ethanol in Sakura Finetek staining dishes.
21. Rinse in distilled water.
22. Rinse sections in double distilled or Milli-Q water twice for 2 min each.
23. Place sections in a mixture consisting of 1 part Solution D, 1 part Solution E (both from the FD Rapid Golgi Stain kit), and 2 parts double-distilled or Milli-Q water, for 10 min in a Sakura Finetek staining dish.
    a. Solution D 10 ml
    b. Solution E 10 ml

c. Water 20 ml.

i. *Prepare working solution just before use. It may be used for up to 200 sections (e.g., mouse brain) per 100 ml, depending on the size of sections. Cover the bottle and staining jar containing the working solution to prevent vaporization of the reagent.*

24. Rinse sections in double distilled or Milli-Q water twice, each time for 4 min.

    a. *The distilled water should be renewed frequently.*

25. Stain sections by immersing in 0.1% cresyl violet for 10 min. Quickly rinse in distilled water.

    a. *Although the FD Rapid Golgi Staining Kit fully impregnates and stains neurons, cresyl violet counterstaining provides better visualization of brain and results in images especially desirable for publication purposes. Staining in warmed cresyl violet solution (preheated in a 37^{o} to 50^{o}C oven) can improve penetration and enhance staining.*

<u>Tissue dehydration and coverslipping</u>

26. Dehydrate sections by immersing successively twice, each time for 5 min in 95% ethanol.
27. Continue tissue dehydration by immersing successively in two changes of 100% ethanol, each time for 5 min.

28. Clear by immersing slides in xylenes or Histo-Clear two times, each time for 5 min.
29. Take one slide out of the staining rack at a time and drain off excess solution on a paper towel.
30. Add a sufficient amount of Cytoseal to cover the slide (or area with sections) and carefully place coverslip on slide. Place more Cytoseal around the edge of the coverslip to ensure that a complete seal is made. Make sure no air bubbles form between the coverslip and slide.
    a. *Cover either the area with the sections or the entire slide with mounting medium. Two drops of Cytoseal solution are sufficient to mount the coverslips.*
31. Dry the slides at room temperature for 24 to 48 hr, or until completely dry.
    a. *Slides should be protected from light.*
    b. *Stained slides are now ready to be microscopically evaluated using a light microscope (Olympus BX62) and Neurolucida software.*

<u>Alternative protocol: Single section rapid Golgi stain</u>

The rapid Golgi method has been cited in the literature as staining in a finer more detailed manner than the Golgi-Cox method than the kit is derived from (Rosoklija et al., 2003). This protocol is based on the Gabbott and Somogyi single section rapid Golgi method (Gabbott and Somogyi, 1984). While this method is more labor intensive, one clear advantage of this protocol is that the turnaround time is much shorter than the kit method. Complete neuron

impregnation from this method is superior is some brain regions, but poor or nonexistent in others.

Additional Materials

- Heparin sodium (Sigma H9399)
- 0.1 M Sodium Phosphate Buffer (pH 7.3)
- 2% (w/v) Paraformaldehyde + 2.5% (v/v) glutaraldehyde (Electron Microscopy Sciences 16210) in 0.1 M sodium phosphate buffer (pH 7.3-7.4)
    - Heat 100 ml of water 55°C. Add 4.0 g paraformaldehyde and stir to dissolve. Cool solution to room temperature and pass through a whatman filter #1. Add 20 ml 25% glutaraldehyde, 20 ml water and 50 ml 0.1 M sodium phosphate buffer. Make solution fresh before use or store at 4^{o}C overnight following filtration of 4% paraformaldehyde. Solutions can be stored for up to one week at 4^{o}C, but it is best to use the solution as fresh as possible.
- Whatman filter paper, grade 1
- Funnel
- Peristaltic pump
- Vibratome
- Feather blades (Ted Pella 121-9)
- 1% (v/v) aqueous osmium tetroxide (Electron Microscopy Sciences 19190)
- Paint brush

- 12 well plates (BD Biosciences 351143)
- 3.5% (w/v) Potassium dichromate (Sigma P5271)
- 1% (w/v) Silver nitrate (Sigma S6506)
- Lab tape
- 0.5% gelatin coated slides
    - Heat 100 mL water to 55^{o}C and add 0.5 g porcine gelatin type A and stir until completely dissolved. Dip slides 3 times into gelatin and dry in a 95^{o}C oven for at least 15 minutes or until dry. Store slides in slide box or slide rack at room temperature indefinitely.

Day 1

Tissue preparation

1. After opening the chest cavity for perfusion, inject 300 µl of 5.9% heparin sodium in 0.9% saline into the heart of the mouse.
2. Flush with 0.1 M sodium phosphate buffer.
3. Perfuse with about 40 ml of 2% (w/v) paraformaldehyde plus 2.5% (v/v) glutaraldehyde.
4. Place the brain into a brain block and use razor blades to block the region of interest.
5. Post-fix the brain at room temperature in the fixative solution for 3 hours.
6. Cut 150 µm sections on the vibratome using a high amplitude and low advance speed to minimize tissue damage.
7. Collect sections in 0.1 M sodium phosphate buffer.

Tissue processing

8. Make a fresh 1% (v/v) osmium tetroxide solution in double distilled or Mili-Q water. Put 1 ml of solution in each well of the 12-well plate. Using a paint brush, place 1-2 sections per well and incubate for 20-40 minutes or until sections are stiff and dark.
9. Make fresh 3.5% (w/v) potassium dichromate solution in double distilled or Milli-Q water. Put 1 ml of solution in each well of a fresh 12-well plate. Transfer sections into potassium dichromate with paintbrush and incubate overnight, about 17 hours, in the dark.

Day 2

Tissue processing continued

10. Make a fresh solution of 1% (w/v) silver nitrate in double distilled or Milli-Q water and filter with Whatman chromatography paper. Fill a glass jar and plastic incubation chambers about 1/3 full with filtered silver nitrate.
11. Use a paintbrush to transfer one section to a microscope slide. Orient the microscope slide such that the long edge is vertical and place the section near the bottom of the slide also oriented vertically. *Ensure that the region of interest is directly exposed to the sliver nitrate solution by cutting off excess brain tissue that may block impregnation.*
12. Place another microscope slide on top to make a sandwich and tape the top of the slides together. Carefully dip the sandwich into the glass jar of silver

nitrate and make sure there are no bubbles under the section. Place the sandwich in a staining container with silver nitrate in it and store in the dark at room temperature. Repeat this with all of the remaining sections.

Developing the silver stain

13. Check the neuron impregnation with a light microscope after 2 hours and every 30 minutes following. Once the neurons are fully impregnated, dendrites and spines fully impregnated, begin disassembling the sandwiches.
14. Wash each section quickly in double distilled or Milli-Q water 2-3 times and mount onto gelatin coated slides. Absorb excess water with a kimwipe and begin incubation in ethanol (EtOH) solutions.
15. Incubate slides in 50%, 70%, 90% x 3, 100% x 3 EtOH and Histoclear x 3 for 3 minutes each. Place DPX on slide and coverslip as directed above.

Neuron reconstruction

Select neurons for reconstruction.

It is important to be careful about which neurons are chosen to be traced for morphometric measurements. Knowledge of typical neuron morphology in the brain region of interest is crucial to making accurate measurements of the correct neuronal subtype. Roitman et al. (2002) describes criteria that neurons are required to meet in order to be considered for morphometric analysis. Selection criteria may include complete filling of the cell body, no beading or breaks in staining along the dendritic branches, limited crossing of dendrites from other

neurons, a minimum number of dendritic branches originating from the soma, and a minimum number of subsequent branch points.

Trace neurons meeting selection criteria

Full reconstruction of the individual neurons is time consuming, but provides the most information about the neurons. Information includes parameters such as soma size, total dendritic length, total spine number, total dendritic spine density, spine density as a function of distance from the soma, and spine density as a function of branch order. If prior knowledge exists about damage to specific regions of the neuron in a particular disease state or toxicant exposure, then full reconstructions may not be necessary and neuronal tracings may be restricted to the affected areas. This should only be done in circumstances where there are ample and consistent data available to support the use of partial reconstructions.

Statistical Analysis

Collect data from at least five neurons in a number of sections from at least four animals. The ultimate animal and neuron number should be determined by the use of power calculations. Perform statistics as in standard experimental situations. In the case of two experimental groups, a Student t-test should be utilized, and if there are more than two experimental groups, ANOVA should be used in combination with appropriate post-hoc tests. See Chapter II for specific discussion.

Commentary

Golgi background information

In spite of being developed more than 130 years ago by Camillo Golgi (Golgi, 1873), the impregnation method that bears his name continues to be used as the standard for visualization of dendrites and dendritic spines. Successful impregnation of brain tissue with this method allows qualitative and quantitative characterization of neuronal morphology. The method's uniqueness lies in the fact that only a small fraction (fewer than 5%) of the neuronal elements are stained (Spacek, 1989). Groups of nerve cells are stained randomly, and many times selected parts appear completely stained while neighboring areas are devoid of staining. Absence of background staining allows visualization of neuronal structures and makes it possible to follow dendritic trees even in thick sections. However, since the cell bodies, as well as the processes, are filled with silver precipitate, cytoplasmic details cannot be examined.

One of the fine structures that were first revealed by the Golgi method, and which caught the eye of Santiago Ramón y Cajal, were the dendritic spines. They were first described as small thorns that projected from the dendrites of cerebellar Purkinje cells (Ramon y Cajal, 1888). Although originally thought to be an artifact, dendritic spines are today known to represent centers of information processing that are able to control their own protein synthesis and degradation (Halpain et al., 2005; Melendez-Ferro et al., 2009). As principal sites of synaptic

input, spines play a key role in connectivity throughout the brain. Dendritic spine distribution and structure is altered in response to subtle variations in their extracellular milieu due to a number of different factors, including synaptic activity, drugs, toxic exposure, and disease (Fiala et al., 2002). In addition to spine pathology, alterations in the total dendritic length, dendritic branching, and soma size have been observed in a number of neurodevelopmental, neurodegenerative, and psychiatric disorders, such as Fragile X mental retardation, Down's syndrome, Alzheimer's disease, Parkinson's disease, Huntington's disease, and schizophrenia (Blanpied and Ehlers, 2004; Fiala et al., 2002; Garey et al., 1998; Glantz and Lewis, 2000; Irwin et al., 2000; Kaufmann and Moser, 2000; Knobloch and Mansuy, 2008; Stephens et al., 2005; Zaja-Milatovic et al., 2005). These structural neuronal changes are usually found to correlate with the disease symptoms. Exercise, stress, and hormonal alterations have also been shown to cause alterations in neuron morphology (Alfarez et al., 2009; Chen et al., 2009; Eadie et al., 2005; Fuchs et al., 2006; Leggio et al., 2005; Shansky et al., 2009; Stranahan et al., 2007). Therefore, the optimal visualization of neuronal architecture allowed by the Golgi method is of primary importance for studies of altered neuronal activity and associated morphology in different models of brain disorders.

Currently, there are many variations of the original Golgi method (Millhouse, 1981); most rely on a two-step procedure to impregnate and label cell profiles in the central nervous system (CNS) (Angulo et al., 1994). In the first step, tissue specimens are exposed to a chromating solution containing

potassium chromate and/or potassium dichromate. In the second step, the tissue is exposed to a silver nitrate solution, which results in the formation of silver chromate crystals (Gabbott and Somogyi, 1984; Izzo et al., 1987; Jones, 1988; Spacek, 1992). Other procedures eliminate the silver nitrate step, and instead add mercuric chloride directly to the chromating solution; the tissue is then exposed to ammonia to darken the resulting mercury-based precipitate (e.g., Golgi-Cox). There are three major variants of the Golgi method, each exhibiting its advantages and disadvantages, depending upon the condition of the tissue and the particular needs of the study. The Rapid Golgi method utilizes osmium, which can increase the number of cells stained, stabilize the membranes of cells allowing complete impregnation (Spacek, 1992), and promote the rate of crystal formation (Millhouse, 1981). This method works well with fresh tissue (Marin-Padilla, 1995), or tissue that has been fixed in formalin for a very short period of time, from a few hours to a few days. The Golgi-Cox method utilizes a mixture of potassium dichromate and mercuric chloride and has been shown to be highly successful in rats (Gibb and Kolb, 1998; Glaser and Van der Loos, 1981). The Golgi–Cox method has been reported to be the optimal method for ensuring the staining of entire dendritic trees of cortical neurons, but not for impregnation of dendritic spines (Buell, 1982; Ramón-Moliner, 1970), or for studying subcortical structures (Riley, 1979). It reportedly gives reliable, progressive, controlled impregnation of neuronal processes, and stains dendrites very darkly (Buell, 1982). However, this method produces a much lighter background than the rapid Golgi technique and is successful in young brains, as well as heavily myelinated

adult brain tissue (Millhouse, 1981). The Golgi–Kopsch method uses formaldehyde and glutaraldehyde as replacement for osmium tetroxide (Colonnier, 1964; Kopsch, 1896). This method is successfully used in numerous studies for tissues that were fixed in formalin for many years (D'Amelio, 1983), as well as for tissues from perfused animals, immediately taken after brain perfusion and extraction (Angulo et al., 1996; Riley, 1979).

Expected results

The protocol in this unit describes the utility of the FD Rapid Golgi Stain Kit for the study of neuronal morphometry in animal and human brain tissue. Our studies show that this impregnation technique is suitable for the analysis of parameters of neuronal morphology, such as dendritic length and spine density, both in fresh brain and archived brains fixed in formalin up to several years. We have used the Neurolucida system with NeuroExplorer quantitative analysis, exploring alterations in neuronal morphology in several models of neurodegeneration including innate immunity activation (Milatovic et al., 2003; Milatovic et al., 2004), excitotoxicity generated by kainic acid (KA) (Zaja-Milatovic et al., 2008), and neurotoxicities associated with Mn exposure (Milatovic et al., 2009) and anticholinesterase agents (Gupta et al., 2007; Milatovic et al., 2009).

In the mouse model of activated innate immunity, we have evaluated the integrity of pyramidal neurons from the CA1 hippocampal area. As detailed in the previous section, we have used Golgi-impregnated (FD Rapid Golgi Stain Kit) 50-μm thick hippocampal sections from paraffin-embedded blocks. For glial innate

immune response we have used a single intracerebroventricular (ICV) injection of lipopolysaccharide (LPS, 5 µg/5 µl), a major component of Gram-negative bacterial cell walls. Data from this study revealed that, coinciding with the peak in oxidative damage to cerebral neuronal membranes at 24 hr post LPS injection, a significant reduction in the spine density and dendritic length of pyramidal neurons occurred in the CA1 sector of hippocampus. Since LPS itself has no direct toxic effect on neurons, LPS-activated glial innate immune response leads to indirect neuronal oxidative damage and synaptodendritic degeneration exclusively through a CD14-dependent mechanism (Milatovic et al., 2004; Montine et al., 2002). Representative Golgi-impregnated Neurolucida-traced pyramidal neurons from theCA1 hippocampal area of control animals and LPS-treated animals are presented in Figure 2. Interestingly, both the dendritic-spine density and dendritic length returned to near basal levels by 72 hr post ICV LPS injection, again coinciding with resolution of oxidative damage in neurons (Milatovic et al., 2004; Montine et al., 2002).

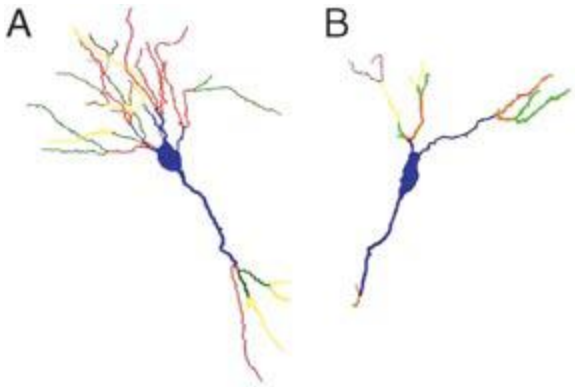

Figure 2. Neurolucida tracings of representative Golgi-impregnated dorsal hippocampal CA1 neurons.

A. Dorsal hippocampal CA1 neuron from control mice. **B.** Mice subjected to intracerebroventricular injection of LPS induced degeneration of the hippocampal dendritic system and decrease in total length of dendrite and spine density of hippocampal pyramidal neurons. Colors indicate the degree of dendritic branching (blue = 1◦; red = 2◦; green = 3◦; yellow = 4◦; brown = 5◦).

Dendrites have also been quantified according to the centrifugal method of Sholl (Sholl, 1953), where spine density and length of dendrites arising from the soma are determined in the first- (50 μm), second- (50 to 100 μm), and third-order segments (100 μm to 150 μm) from the center of the soma. Results of this study demonstrated that LPS exposure caused a significant decrease in total dendrite length in the proximal (0 to 50 μm) and intermediate (51 to 100 μm) Sholl compartments of CA1 pyramidal neurons (Figure 3A). Results also revealed that LPS exposure induced a significant decrease in spine density (number of spines per 100 μm dendrites) in all three (proximal, intermediate, and distal) Sholl compartments of CA1 pyramidal neurons (Figure 3B).

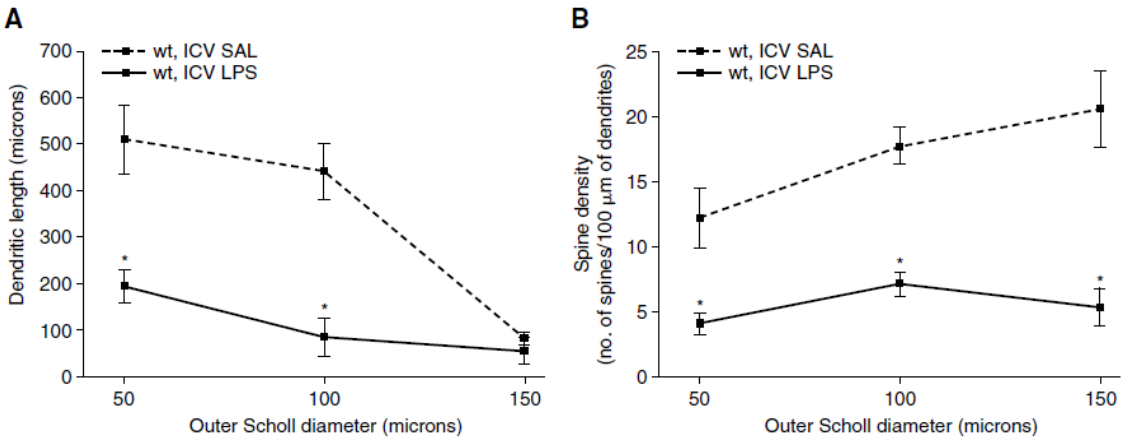

Figure 3. Dendritic length and spine density in each Sholl compartment of pyramidal neurons from CA1 hippocampal area of mice following ICV injections of LPS.

Brains from rats exposed to LPS were collected 24 hr post injection ($n \geq 4$). **A)** Dendritic length in 50 and 100 micron compartments was significantly reduced upon exposure to LPS. **B)** Spine density was reduced in all compartments following exposure to LPS. Asterisk (*) indicates that one-way ANOVA had $p < 0.001$ with Bonferroni's multiple comparison tests showing significant difference for Sholl compartment ($p < 0.05$) from control (SAL) versus LPS treatment.

The integrity of hippocampal dendritic system was also evaluated in the model of anticholinesterase neurotoxicity. We have used diisopropylphosphorofluoridate (DFP) as a model compound for organophosphorus (OP) insecticides or nerve agents, and investigated if oxidative/nitrosative damage induced by anticholinesterase exposure is accompanied by dendritic damage in the CA1 sector of hippocampal neurons. Rats treated acutely with DFP (1.25 mg/kg, s.c.) developed onset of toxicity, including seizures and fasciculations, within 60 min. At this time point, DFP caused significant increases in biomarkers of cerebral oxidative damage. Furthermore, quantitative neuronal analysis of pyramidal neurons with no breaks in staining along the dendrites from the CA1 area revealed significant reductions in dendritic lengths and spine density (Zaja-Milatovic et al., 2009). Representative images of Golgi-impregnated hippocampal sections with their traced pyramidal neurons from control and DFP-exposed animal are presented in Figure 4. Additional morphometric analysis with the Sholl method of concentric circles confirmed early neuronal damage and showed that anticholinesterase induced brain hyperactivity targeted the dendritic system with profound dendrite regression of hippocampal neurons (Zaja-Milatovic et al., 2009).

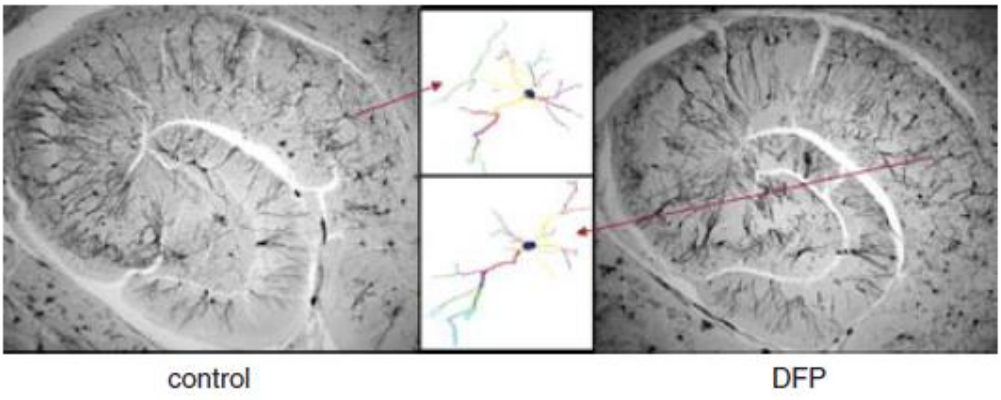

Figure 4. Photomicrographs of rat hippocampi (2.5×) with pyramidal neurons (10×) from CA1 hippocampal area of rat brains.

Hippocampal pyramidal neurons were examined 1 hr after saline (control) and diisopropylphosphorofluoridate (DFP; 1.25 mg/kg, s.c) injections. Treatment with DFP induced degeneration of the hippocampal dendritic system and decrease in total length of dendrite and spine density of hippocampal pyramidal neurons. Tracing and counting were done using a Neurolucida system at 100× under oil immersion. Colors indicate the degree of dendritic branching (yellow = 1◦; red = 2◦; purple = 3◦; green = 4◦; turquoise = 5◦; gray = 6◦).

Manganism (Mn poisoning) is associated with alterations in integrity of the dopaminergic innervation of striatal neurons. The MSNs are the target of the dopaminergic innervation of the striatum, comprising more than 90% of striatal neurons (Deutch et al., 2007). MSNs have radially projecting dendrites that are densely studded with spines, synapsing with dopamine and glutamate axons and providing the site of integration of several key inputs and outputs of the striatum (Day et al., 2006). Consequently, alterations in dendritic length and dendritic spine number may destabilize the structural basis of synaptic communication, and thus compromise MSN function. Therefore, we investigated if dendritic degeneration of MSNs was present in the striatum of mice exposed to a single injection or multiple injections of $MnCl_2$. Representative images of Golgi-impregnated (FDRapid GolgiStain Kit) striatal section with the traced MSN from control animal are presented in Figure 5. NeuroExplorer-assisted neuronal morphometry revealed progressive spine degeneration (total number of spines per neuron) of MSNs in mice with increase in time and dose of $MnCl_2$ exposure. Consistent with these effects, Mn also induced dose- and time-dependent progressive dendritic damage (total dendritic length per neuron) of MSNs (Milatovic et al., 2009).

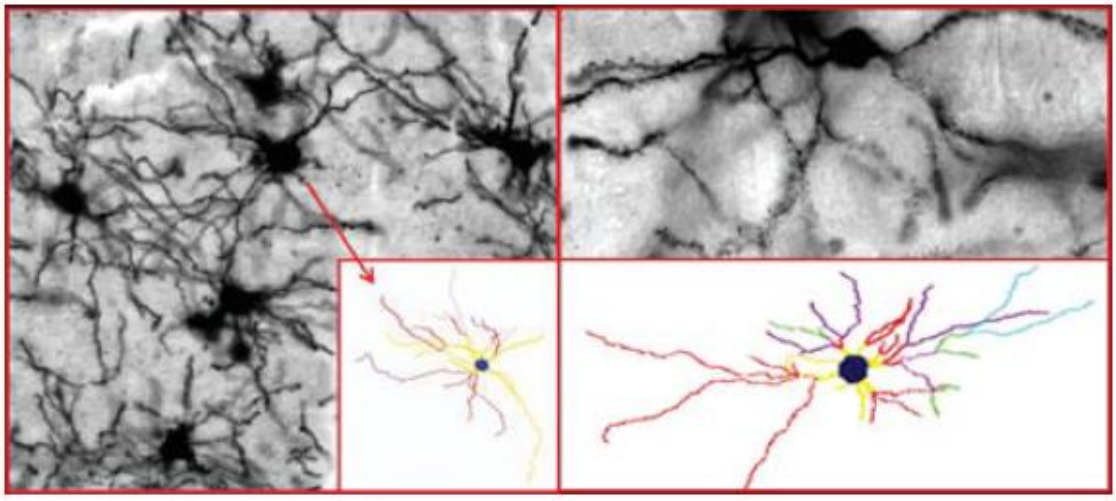

Figure 5. Photomicrographs of mouse striatal sections with representative tracings of medium spiny neurons (MSN) from mice treated with saline.

Tracing and counting were done using a Neurolucida system at 60× or 100× under oil immersion. Colors indicate the degree of dendritic branching (yellow = 1◦; red = 2◦; purple = 3◦; green = 4◦; turquoise = 5◦).

In these animal models of neuroinflammation, seizures, and metal neurotoxicity, we have performed Golgi impregnation (FD Rapid Golgi Stain Kit) of fresh brain tissue (immediately after the extraction). However, we have used the same impregnation procedure for human brain that has been fixed in formalin for several years, and investigated if dendritic degeneration in neostriatal MSN is associated with Parkinson's disease (PD). We have used brains from patients diagnosed with PD and controls matched for age and for time in formalin, obtained via autopsies at the University of Washington performed between 1987 and 2003. The time in fixative for PD cases averaged 9.7 years (median, 12.5 years) and for controls averaged 9.6 years (median, 12.0 years). Portions of fixed putamen (~0.3 cm3) were taken from three consecutive tissue slabs: immediately caudal to the anterior commissure (precommissural), at the anterior commissure, and immediately rostral to the anterior commissure (postcommissure). Tissue was sectioned by Vibratome in the coronal plane at 80 µm and Golgi impregnation and morphometric analysis performed by an observer blinded to diagnosis. Results from that study showed that spine density in all three regions in controls remained essentially constant across regions of putamen, but progressively decreased across precommissural to postcommissural regions in patients with PD. Morphometric values from three different regions of putamen from patients with PD or controls are presented in Figure 6. Importantly, morphometric analysis of MSNs from these Golgi impregnated formalin-fixed brains showed no correlation of time in fixative with

dendritic length or spine density in all three regions in control or patients with PD (Zaja-Milatovic et al., 2005).

The Neurolucida system and morphometric analysis has also been used in our in vitro experimental models. Confocal immunofluorescent images of neurons previously probed with neuronal markers (MAP2, drebrin, or spinophilin) were traced with the Neurolucida system, and dendritic length or spine density per neuron or the segment evaluated by NeuroExplorer in control and amyloid beta (Aβ)–exposed primary neuronal cultures. Representative confocal images, neuronal tracings, and morphometric evaluation (dendritic length) of the neurons are presented in Figure 7.

Additionally, we have employed the Rapid Golgi method and evaluated impregnation and visualization of dendrites and dendritic spines from fresh mouse brain tissue. Our preliminary results showed successful impregnation of brain tissue with this method, allowing quantitative characterization of neuronal morphology. A Rapid Golgi–impregnated dendritic segment from a mouse MSN is presented in Figure 8.

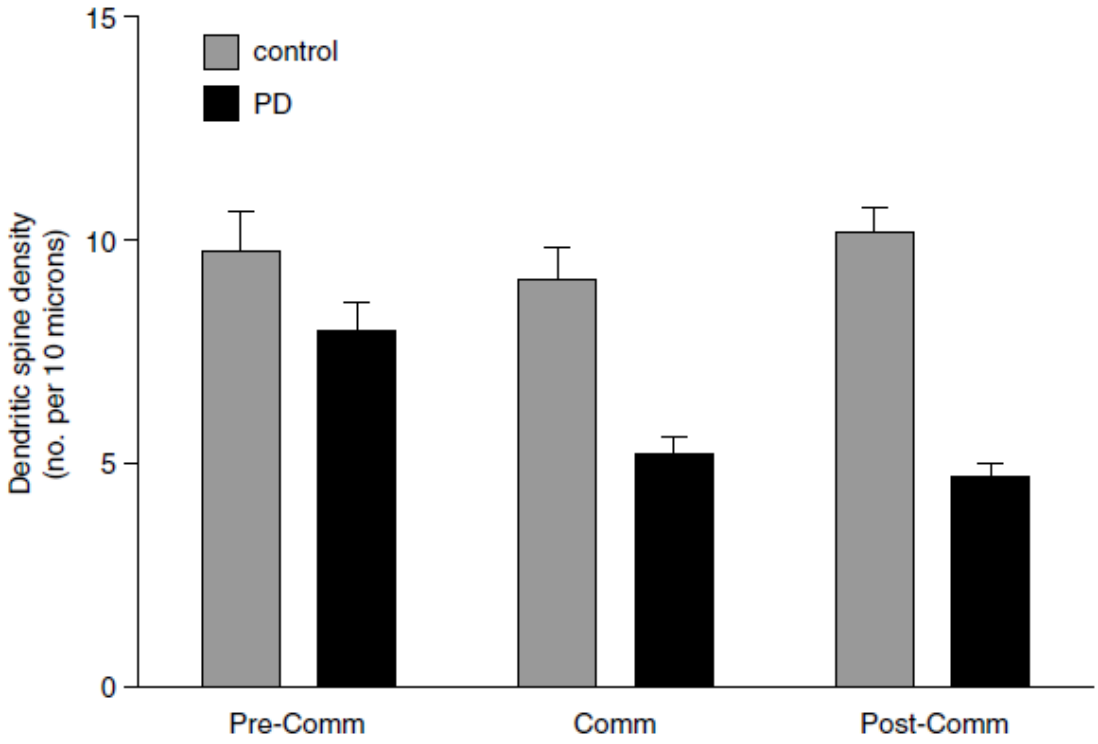

Figure 6. Morphometric values (spine density) from three different regions of putamen from patients with PD or controls.

6 to 8 neurons were evaluated in each section and the average value obtained for each region in each individual. These individual averages were then combined to yield a grand average (± SEM) for each region in PD patients (black) and controls (gray). Two-way ANOVA for spine density (F42, 2, 1) had $p < 0.001$ for control versus PD, $p < 0.01$ for region, and $p < 0.05$ for interaction between these two terms. Bonferroni-corrected post-tests showed that spine density was significantly less in PD patients than controls for commissural and post-commissural regions ($p < 0.001$) but not pre-commissural region ($p > 0.05$). Adapted from Zaja-Milatovic et al. (2005) with kind permission from Walter Kluwer Health.

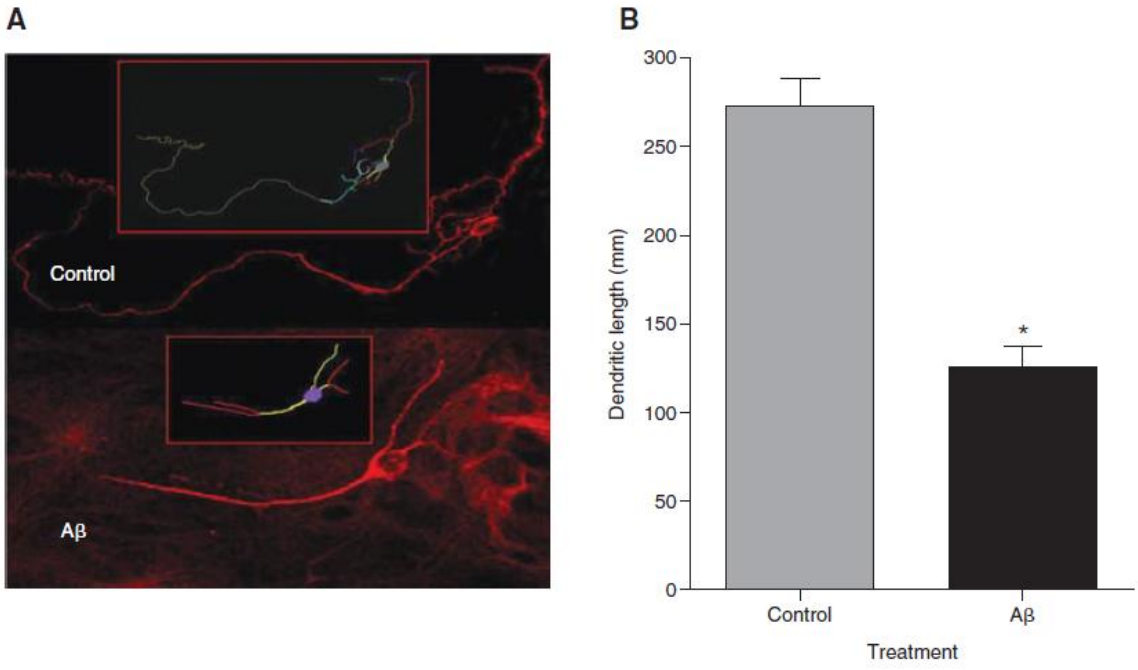

Figure 7. Representative confocal immunofluorescent images, Neurolucida tracings, and NeuroExplorer-assisted morphometric evaluation of neurons from control and Aβ-exposed mixed cerebral and hippocampal neuronal culture.

A) The neurons were probed for MAP2 with mouse anti MAP-2 monoclonal antibody (5 µg/ml). MAP2 was visualized withCy3-donkey anti-mouse secondary antibody (1:100). **B)** Control and Aβ-exposed neurons were traced out in the Neurolucida program followed by quantitation of the dendritic length in NeuroExplorer. Aβ-treated values were significantly different from control ($p < 0.01$).

Figure 8. Mouse MSN dendritic segment impregnated by the rapid Golgi method.

This image shows a striatal MSN impregnated by the rapid single-section Golgi method. Dendritic branching is clearly visualized as well as dendritic spines.

Altogether, we have showed the validity of the use of Golgi impregnation technique (FD Rapid Golgi Stain Kit) for the study of human and animal brain tissue, as well as for studies on neuronal cultures in vitro. In addition to minimal background precipitation, this technique produced good clarity of dendrites and dendritic spines in different brain areas. Our preliminary findings with the Rapid Golgi technique also showed good neuronal impregnation and sharpness of dendritic spines. Moreover, we have shown that the Neurolucida system is effective in evaluating neuronal morphometry both in vivo and in vitro.

Critical parameters and troubleshooting

Tissue sectioning on the cryostat and vibratome are critical parameters in the success of either protocol. Trials should be conducted in order to determine the optimal temperature for sectioning on the cryostat and optimal blade advance and amplitude speeds are critical for sectioning tissue on the vibratome. Optimal section thickness should also be determined in a trial experiment to make sure that there are routinely enough neurons with complete dendritic arbors visible. The developing stage in the FD Neurotechnologies kit is another critical step, if the sections are left in the developing solution (Solutions D and E) for too long, the tissue will be over stained. This also holds true for the silver nitrate incubation in the rapid Golgi protocol, which is why it is important to check the sections periodically to ensure they are not being over stained.

Time considerations

Using the FD kit, it takes about 3 weeks to complete processing of the tissue. The process of sectioning and staining is less time consuming, and it takes 1 to 2 days to section, dry, and stain already processed sections. Alternatively, the single section rapid Golgi method only takes 2 days to completely process the tissue. It is easier to do a larger number of animals at one time using the FD kit because the rate limiting step is sectioning tissue on the cryostat. In contrast, the limit for the single section rapid Golgi method is 6-8 animals per day. The rate limiting factor for this method is how quickly the sandwiches can be made, taken apart and slides coverslipped without the sections being over stained or dried out. Trials should be performed for each protocol prior to conducting a full experiment to reduce unnecessary animal usage and to optimize staining for the brain region of interest. The time investment required to reconstruct the Golgi stained neurons should also be considered because it is a laborious and time intensive commitment to trace the Golgi stained neurons. It takes ~2 hr to reconstruct a well preserved pyramidal neuron. It can take even longer to reconstruct a well preserved Purkinje cell.

CHAPTER IV

CONFOUNDING FACTORS IN MORPHOMETRY

Introduction

Neuron morphometry gives keen insight into the health and function of the neuron being studied. Dendritic spines are rapidly changing key players in neuron function since they are the primary structure receiving excitatory inputs from other neurons. Examination of neuron morphology can reveal whether a neuron is healthy or if it is degenerating in a disease state. Although neuron morphometry can give insight into health of the neuron, there are caveats that one must be aware of prior to initiation of these studies. Like many experiments, Golgi impregnation and study of neuron morphology requires controls and proper experiment design in order to obtain useful information. This chapter will discuss confounding factors that need to be taken into consideration when designing neuron morphology experiments.

Results

Method of Golgi impregnation

There are many methods of Golgi impregnation that have been developed since Camillo Golgi first described silver impregnation of neurons in 1807 (Golgi, 1873). The two methods of silver impregnation that were described in Chapter III

were compared prior to initiation of experiments described in Chaper V and Chapter VI to determine which method yielded optimal impregnation for analysis.

FD Neurotechnologies Rapid GolgiStain Kit

While the single-section rapid Golgi method was being optimized, a small group of animals was used to test the FD NeuroTechnologies Rapid GolgiStain™ kit (henceforth referred to as the FD kit method). Wild-type vehicle (WT-Veh) (n = 2) and Mn exposed (WT-Mn) (n = 3) mice were used in this trial. There was no difference in soma size or total spine number (Figure 9A and Figure 9B). Total spine density (Figure 9C) on MSNs was significantly decreased in WT-Mn mice ($p < 0.05$). There was only a trend towards an increase in total dendritic length (Figure 9D) of WT-Mn MSNs ($p = 0.08$), which was driving the difference in total spine density. Examination of neuron morphology as a function of distance from the soma failed to find a significant difference in dendritic branching (Figure 10A) or dendrite length (Figure 10B) as a function of distance from the soma between Veh and Mn exposed mice. Spine number (Figure 10C) and spine density (Figure 10D) as a function of distance from the soma were significantly reduced in Mn exposed mice ($p < 0.05$). Spine density as a function of branch order (Figure 11) was reduced in Mn exposed mice across all branches. Spine density was only significantly reduced along the 3rd branch order ($p< 0.05$), however there was a strong trend towards a significant reduction along the 2nd branch order ($p = 0.051$). Overall, the FD kit method of Golgi staining found a significant difference in neuron morphology between WT-Veh and WT-Mn exposed mice.

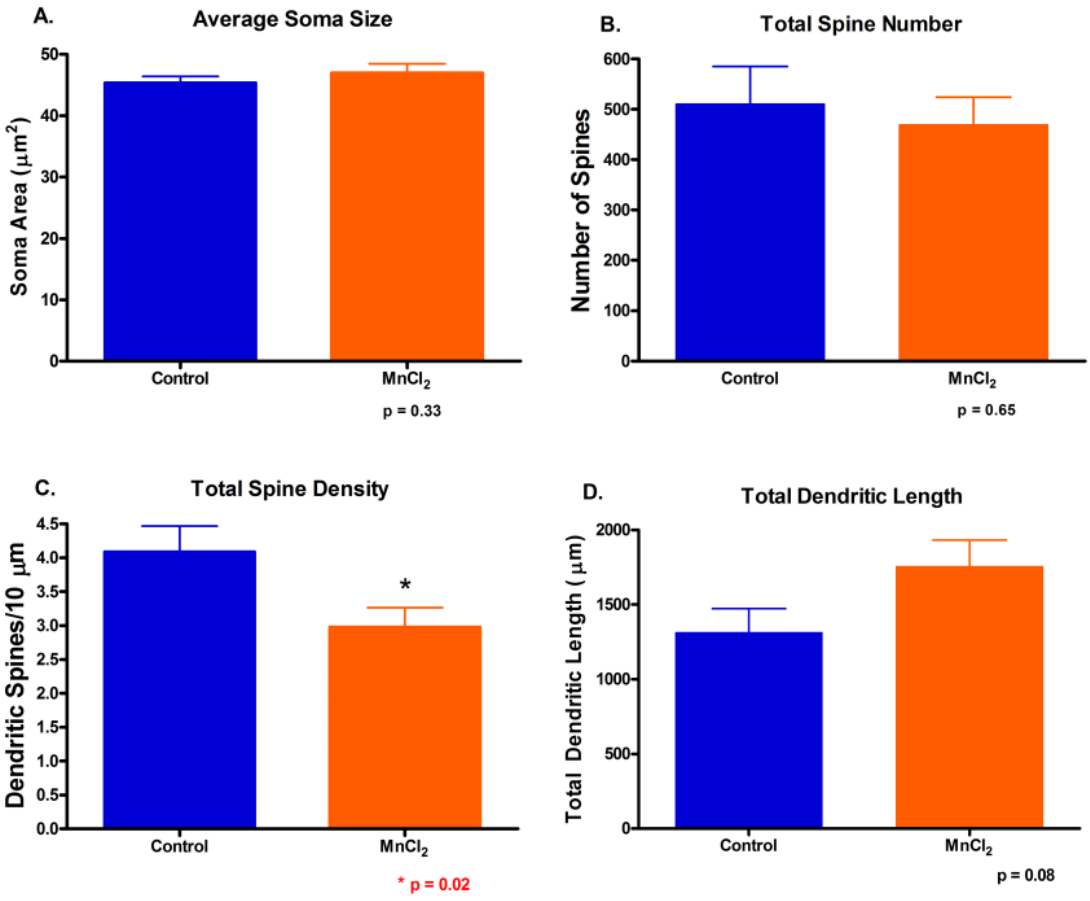

Figure 9. FD Kit Golgi neuron morphology in WT mice.

A) Soma size is unchanged following Mn exposure in WT mice. **B)** Mn exposure does not significantly affect total spine number. **C)** Mn exposure significantly decreases total spine density ($p < 0.05$). **D)** There is a trend toward an increase in total dendritic length in Mn exposed WT mice ($p = 0.08$).

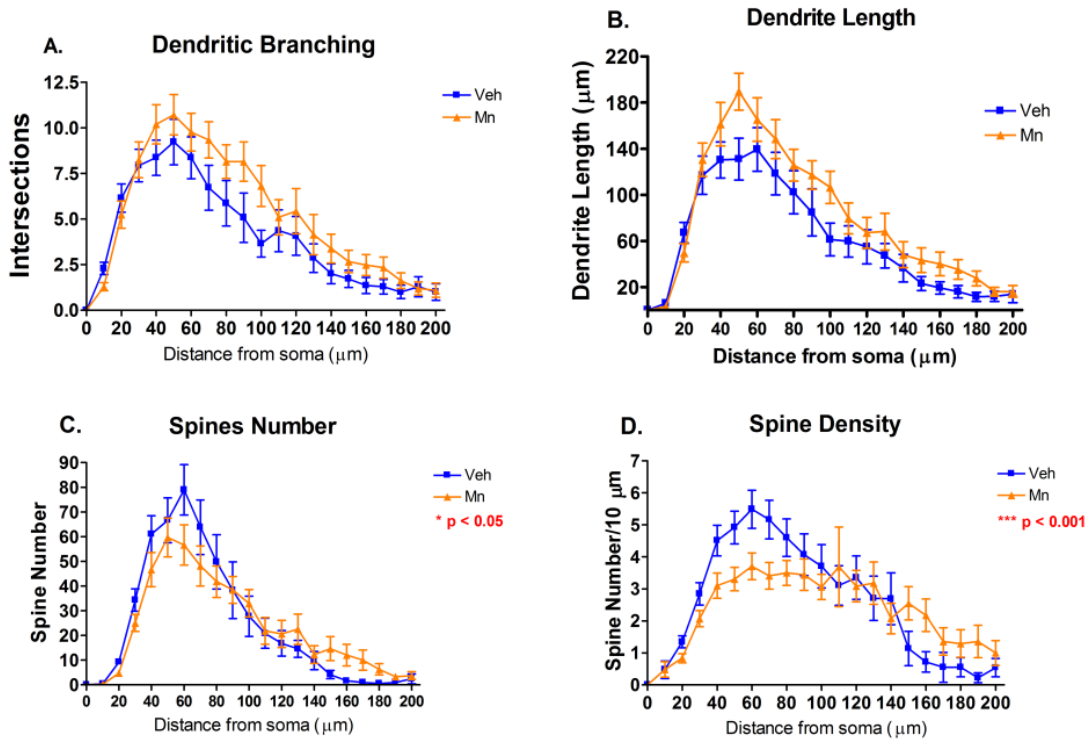

Figure 10. FD Kit Golgi morphometric measures as a function of distance from the soma.

A) Dendritic branching as a function of distance from the soma is unchanged following Mn exposure in WT mice. **B)** Mn exposure does not significantly affect dendrite length as a function of distance from the soma. **C)** Mn exposure significantly decreases spine number as a function of distance from the soma ($p < 0.05$). **D)** Mn exposure significantly decreases spine density as a function of distance from the soma ($p < 0.001$).

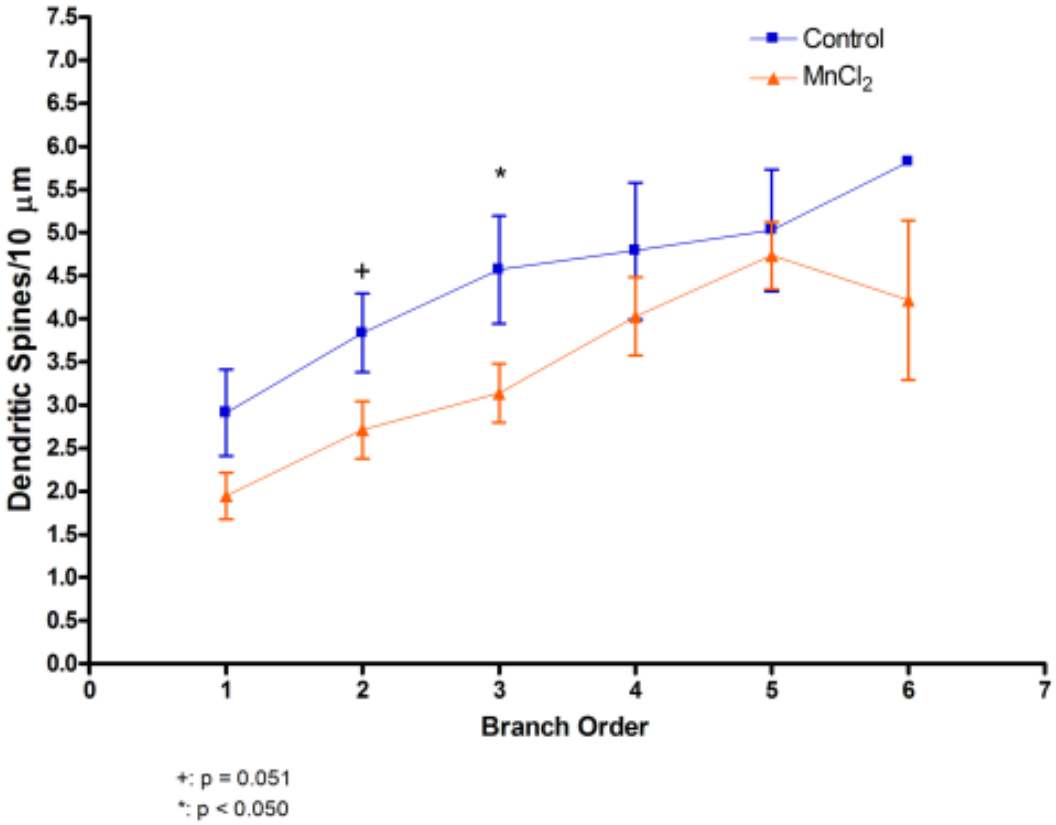

Figure 11. Spine density as a function of branch order is reduced in WT-Mn MSN.

Spine density as a function of distance from the soma is decreased on branch order 3 ($p < 0.05$), however there is a strong trend toward a significant decrease in spine density on branch order 2 ($p = 0.051$).

Comparison of Golgi methods

We compared the results of the FD kit method to the single-section rapid Golgi method. The first thing that was noticed was the difference in staining pattern and quality between the methods (Figure 12). The impregnation of MSNs with the FD kit method was inconsistent and not of high quality. There were frequent breaks in staining along the dendrite, which renders that neuron unusable for inclusion in the experiment. Also common were blebs, or large blobs, of precipitate along the dendrite. These neurons are also unable to be included in the experiment. The single-section rapid Golgi method produced clear staining of neurons without breaks or extraneous staining of the neurons.

We compared total spine density of WT-Veh animals from each staining method with values reported in the literature to ensure that our staining was comparable to published data (Figure 13). A literature search of Golgi staining in the striatum was conducted and the average total spine density from fully reconstructed neurons was determined (Day et al., 2006; Klapstein et al., 2001; Lee et al., 2006; Spires et al., 2004). We found that the average total spine density of MSNs in the literature was between 6-9 spines/10 μm. The average total spine density of WT-Veh MSNs from the FD kit method was 4.1 spines/10 μm. MSNs from WT-Veh mice using the single-section rapid Golgi method had an average total spine density of 5.8 spines/10 μm, which was only slightly below the average published density. Based on the fact that the silver impregnation was more consistent and total spine density was closer to the average in the

literature, we chose to complete our investigation with the single-section Golgi method.

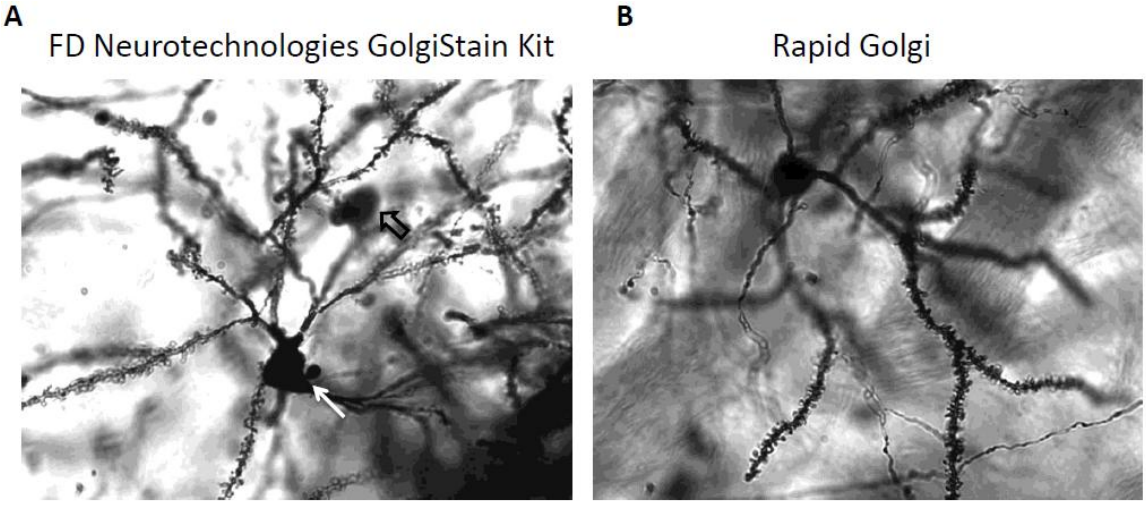

Figure 12. Comparison of Golgi staining efficacy between FD kit and single-section Rapid Golgi.

A) Example of a striatal MSN stained using the FD Neurotechnologies Kit. The white arrow indicates breaks in dendrite filling which renders that neuron unusable for tracing studies. The black arrow indicates nonspecific filling or blebbing along the dendrite. **B)** Typical striatal MSN staining using the Rapid Golgi method. No breaks in dendrite filling or blebs along the dendrite were found in any neurons with the Rapid Golgi method.

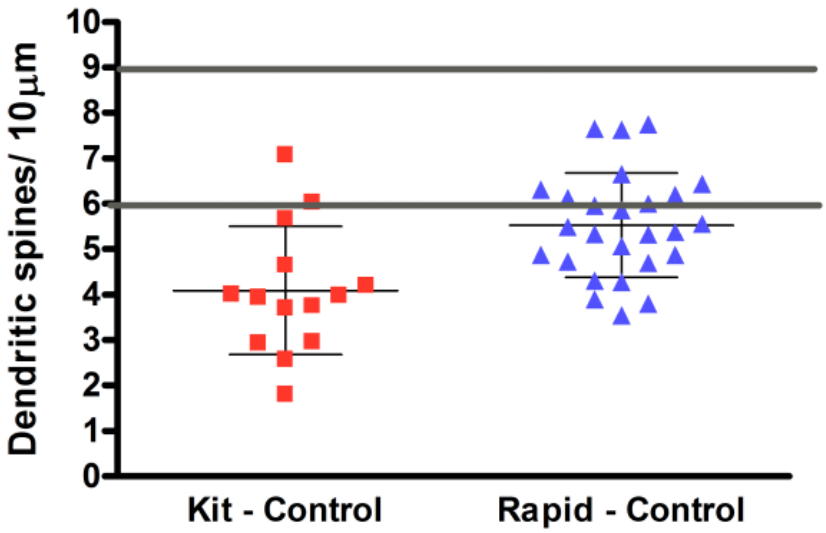

Figure 13. Comparison of Total Spine Density from FD Kit and single-section Rapid Golgi.
WT-Veh exposed mice were used to compare Golgi impregnation methods. Total spine density was assessed from FD Kit and single-section rapid Golgi impregnated neurons. The gray lines represent the range of total spine density reported in the literature for MSNs. Total spine density in MSNs impregnated using the FD Kit method fell below the total spine density reported in the literature. The mean total spine density in single section rapid Golgi impregnated MSNs was much closer to the range reported in the literature.

Golgi processing strategy

The time it takes to complete Golgi staining varies greatly between Golgi impregnation methods. The kit method takes weeks to complete the staining process, while the single-section Golgi method takes only two days. However, many more animal tissues can be processed at one time using the kit method. The single-section Golgi staining procedure has time critical steps that are the rate limiting factor in how many animals can be processed at one time. The limit on the number of animals that can be processed at once requires an experiment with a large number of subjects to be conducted over a prolonged period of time. This in and of itself can result in problems with staining because of the capricious nature of Golgi staining.

Our experiment was conducted using the single-section Golgi method over a period of 8 weeks. Animals from all treatment groups were processed during each Golgi experiment to minimize staining bias during each processing event (Figure 14). In order to ensure that a systematic error in processing did not occur, we analyzed total dendritic length across processing events (Figure 15). There was no increase or decrease in dendritic length across processing events for all exposure groups. However there was an increase in total dendritic length for WT-Veh and WT-Mn groups, but no change in total dendritic length across processing events for YAC128-Veh or YAC128-Mn exposure groups. This indicates that the changes in dendritic length were due to alterations in neuron morphology, not due to a Golgi staining error.

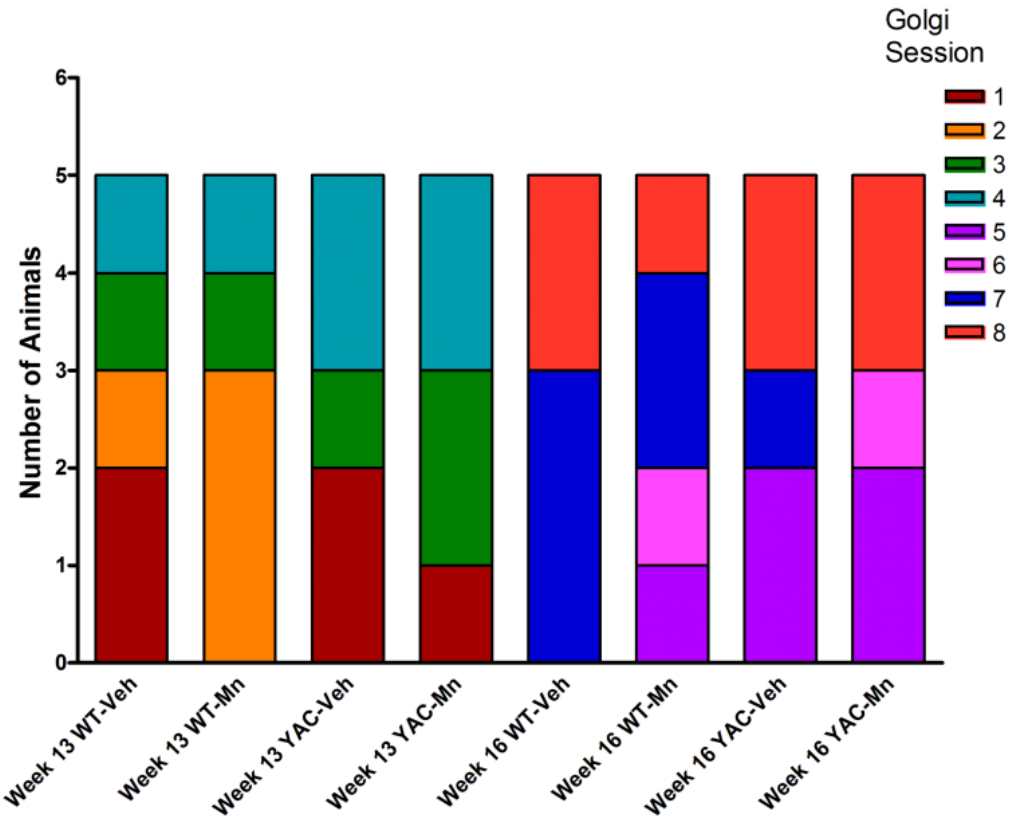

Figure 14. Distribution of animals in each exposure group across Golgi processing sessions.

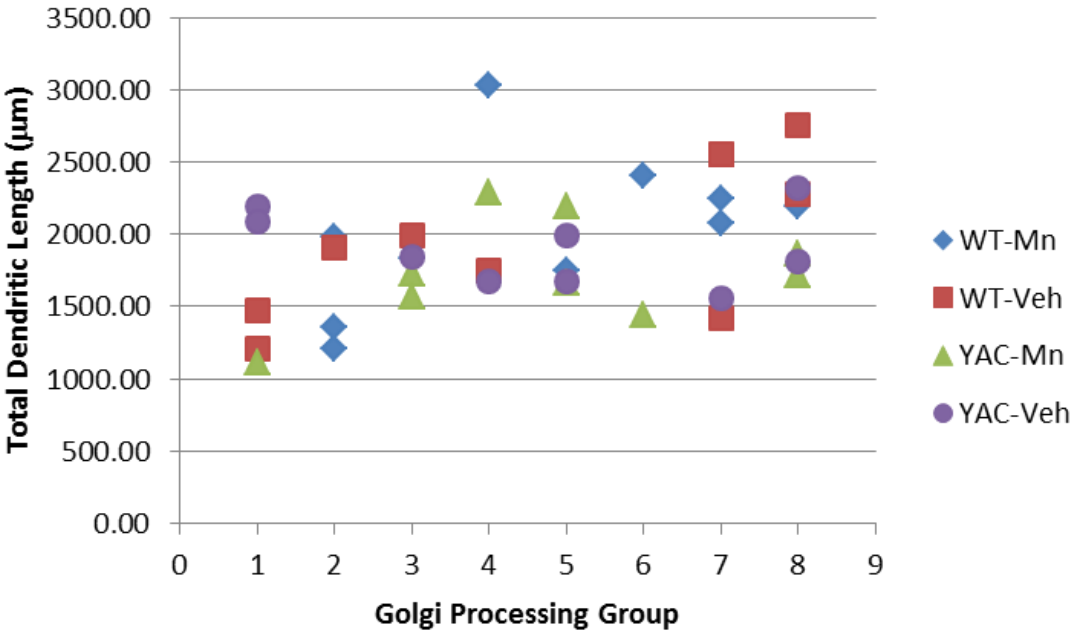

Figure 15. Total dendritic length across Golgi processing group.

Golgi processing date did not have an effect on total dendritic length. Animals from each exposure group were processed across multiple days and total dendritic length did not change due to a systematic error caused by processing tissue across multiple sessions.

Litter

Litter is an important factor to consider when distributing animals across exposure groups. The litter-of-origin had a significant effect on rotarod performance for the R6/2 HD mouse model, but not on WT littermates (Hockly et al., 2003). In this case the R6/2 mice performed more similar to their littermates than to other R6/2 mice of the same generation. The ideal distribution of animals among exposure groups is to use only one animal per litter. However, this is usually not feasible with in-house breeding because of the large number of litters that would be required to produce the number of animals needed at the same time. For our experiments, we distributed WT and YAC128 mice from each litter across exposure groups as evenly as possible (Figure 16). All exposure groups contained animals from at least two litters and most litters had animals in more than one exposure group. Examining dendrite length across litters (Figure 17), there is no significant effect of litter at the early ($F_{(4,89)}$=1.592, p = 0.138) or late ($F_{(4,105)}$=0.962, p = 0.432) time point. In this case, litter is not a significant factor in neuron morphology.

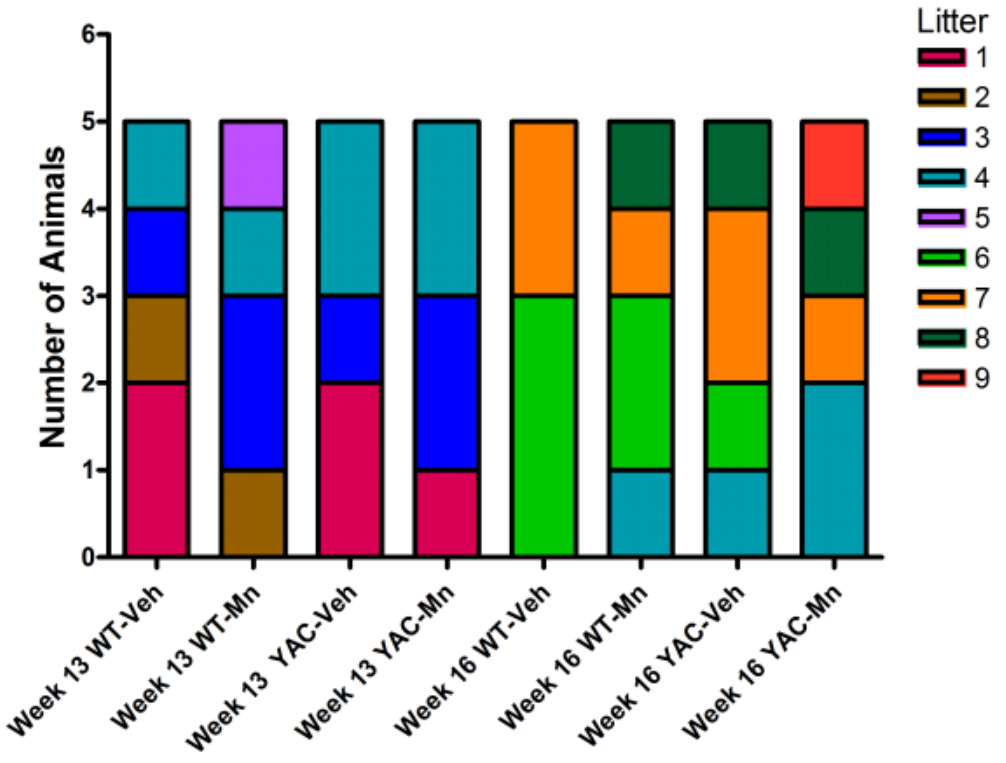

Figure 16. Distribution of litters across expsoure groups.

Mice from each litter were distributed across multiple exposure groups. Each exposure group, in turn, was composed on animals from at least two litters.

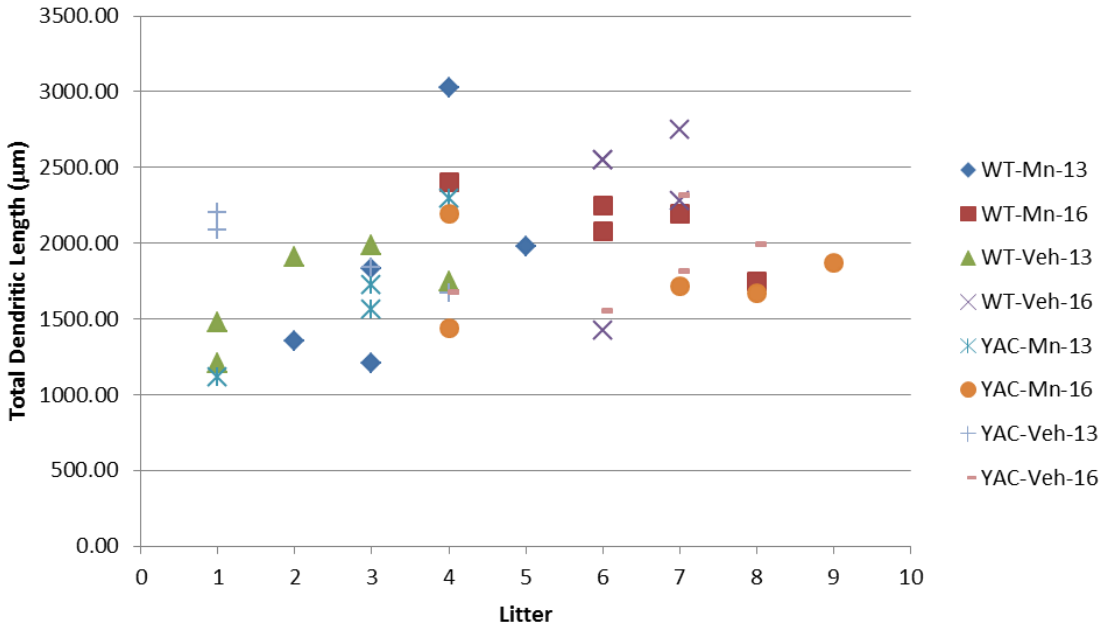

Figure 17. Total dendritic length is not affected by litter.
Total dendritic length was compared across litter. Litter was not shown to have an effect on total dendritic length.

Gender

Another important factor in experimental design is gender (Figure 19). This factor is often overlooked in multiple ways. First, the vast majority (40-60%) of *in vivo* neuroscience or pharmacology experiments uses only male animals (Wald, 2010). Only 10-20% of neuroscience or pharmacology experiments use both genders. Approximately 5-20% use animals of unspecified gender and a very small percentage, less than 20%, use female animals only (Figure 20). Secondly, even when both genders are included in experiments, only two-thirds of those manuscripts included gender as a factor in data analysis (Wald and Wu, 2010). An argument for including both genders in early *in vivo* experiments is to determine if a gender difference is present at early stages of research before such it is translated into human treatment. This may improve medical treatments for women, who do not necessarily respond to drugs in the same manner as men. Analysis of our neuron morphology data showed a strong influence of gender. These data will be discussed further in Chapter VI.

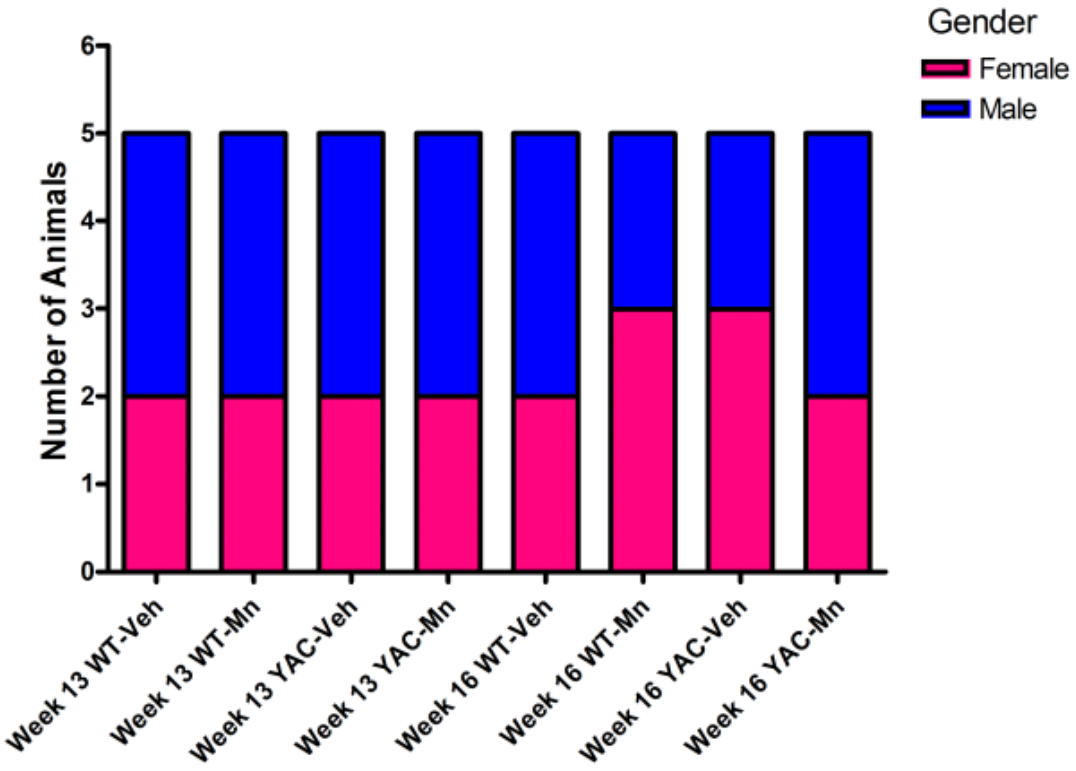

Figure 18. Distribution of mice of each gender across exposure groups.

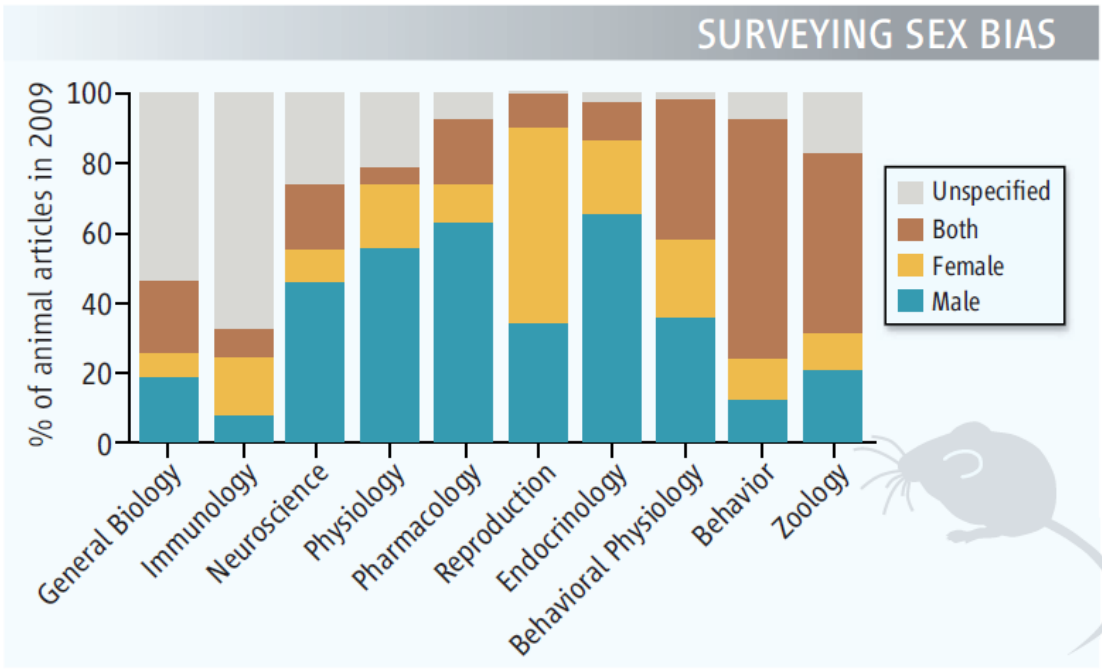

Figure 19. Surveying sex bias.
A survey of journal article from 2009 found the strongest bias toward male animals in fields most likely to translate to humans.

Discussion

This chapter focused on factors that are important to take into consideration prior to initiating experiments designed for analysis of neuron morphology, but the general ideas are applicable to other *in vivo* experimentation. As discussed in here and Chapter III, the method of Golgi impregnation is crucial to obtaining optimal neuron staining. One needs to first consider which method produces better impregnation of the brain region of interest. The second consideration is the number of animals required to complete the study and in what timeframe Golgi impregnation experiments will take place. The kit method can easily accommodate a large number of animals to be stained simultaneously, but the single-section Golgi method can only accommodate a limited number of animals per day. If the latter method is chosen, safe guards must be put in place to ensure that animals from each experimental group are evenly distributed across Golgi impregnation events. One should also consider performing analysis of the neuron morphology data to confirm that processing the tissue over multiple independent events did not cause a change in impregnation.

Distribution of animals into experimental groups is a key factor. Animals from multiple litters should be used in each experimental group. Similarly, animals from a single litter should be distributed across experimental groups to ensure that a single litter does not solely affect one experimental group. The contribution of litter to differences in neuron morphology should be statistically analyzed to rule out a litter effect. In the same way, male and female animals should be equally represented in each experimental group. This ensures that if a

gender effect is present, it is detectible. Inclusion of both genders in disease-toxicant experiments such as ours, increase knowledge about this specific interaction, it allows us to tease out potential disease interventions that may be more beneficial to one gender over another.

In summary, important factors such as how many independent experimental sessions will be required to complete the study, litter and gender should be well thought out and planned prior to embarking on an experimental plan. Each of these factors introduces a bias into interpreting the experimental results. However, with careful planning and post-experimental statistical analysis these factors can be eliminated as potential confounding factors in data analysis. In fact, including animals from both genders can result in novel and interesting results if it does influence the experimental results.

CHAPTER V

EARLY CHANGES IN STRIATAL NEUROCHEMISTRY AND MEDIUM SPINY NEURON MORPHOLOGY IN HUNTINGTON'S DISEASE MOUSE MODEL ARE MODIFIED BY MANGANESE EXPOSURE

Abstract

YAC128 Huntington's disease (HD) transgenic mice accumulate less manganese (Mn) in the striatum relative to wild-type (WT) littermates. We hypothesized that Mn and mutant *Huntingtin* (*HTT*) would exhibit gene-environment interactions at the level of neurochemistry and neuronal morphology. Twelve-week-old WT and YAC128 mice were exposed to $MnCl_2$-$4H_2O$ (50 mg/kg) on days 0, 3 and 6. Striatal medium spiny neuron (MSN) morphology as well as neurotransmitter and amino acid content were analyzed at 13 weeks (7 days from initial exposure) and 16 weeks (28 days from initial exposure). No genotype-dependent differences in MSN morphology were apparent at 13 weeks, but an age-dependent genotype-specific increase in dendrite length and branching complexity in WT mice that was absent in YAC128 mice was identified. Mn exposure and genotype exhibited both positive and negative interactions and single-factor effects on a subset of striatal amino acids. Striatal monoamine levels were unaltered at 13 weeks; however at 16 weeks, (a) Mn exposure reduced dopamine (DA) and metabolites in WT mice, (b) YAC128 mice had reduced DA and metabolites similar to Mn exposed WT mice, and (c) YAC128 mice were protected from further decreases

in DA following Mn exposure. YAC128 mice exhibited elevated amino acids at 16 weeks, and this difference versus WT was fully reversed by exposure to Mn. Taken together, these results demonstrate Mn-HD disease-toxicant interactions at the onset of striatal dendritic neuropathology in YAC128 mice. Furthermore, Mn-exposure of the HD mice ameliorates some mutant *HTT*-dependent changes in striatal neurochemistry while exacerbating phenotypes, including dendritic pathology.

Introduction

Huntington's disease (HD) is an autosomal dominant inherited disease caused by expansion of a CAG triplet-repeat within the first exon of the *Huntingtin (HTT)* gene (Huntington's Disease Collaborative Research, 1993). The primary neuropathology in HD is loss of striatal, followed by cortical neurons (de la Monte et al., 1988). HD causes proliferative and/or degenerative changes in striatal MSNs (MSNs) as evidenced by post-mortem studies (Ferrante et al., 1991; Graveland et al., 1985a; Vonsattel et al., 1985). Changes in MSN morphology precede gross striatal neuron loss (Ferrante *et al*. 1991). Analysis of MSN morphology can identify early neuropathology prior to death of MSNs and further loss of striatal neurons.

Mn is an essential trace metal that is critical for many physiological processes including reproduction, formation of connective tissue and bone and normal brain function including neurotransmitter synthesis and metabolism (Aschner et al., 2005; Erikson et al., 2005; Golub et al., 2005; Roth and Garrick,

2003). Exposure to high Mn levels causes neurotoxicity, especially in brain regions where Mn preferentially accumulates including the globus pallidus, striatum, substantia nigra and the subthalamic nucleus (Olanow, 2004; Pal et al., 1999). Rodent studies examining MSN morphology following Mn exposure found a decrease in total dendritic length and spine number (Milatovic et al., 2009). Various striatal amino acid and monoamine neurotransmitter levels are also affected by Mn overexposure, however these studies have predominantly focused on just a single amino acid, broad-based assessment of multiple amino acids in the same samples have not been reported (Autissier et al., 1982; Burton et al., 2009; Gianutsos and Murray, 1982; Gwiazda et al., 2002; Kontur and Fechter, 1988; Lipe et al., 1999; Olanow et al., 1996; Reaney et al., 2006; Struve et al., 2007; Takeda et al., 2002; Takeda et al., 2003; Vidal et al., 2005). An increase in brain Mn levels is also known to cause motor dysfunction in humans (Aschner, 2000; Calne et al., 1994; Olanow, 2004; Pal et al., 1999) and mice (Guilarte et al., 2006; Vezer et al., 2005). Since the striatum is a common target for both HD and Mn accumulation, this provides the opportunity to observe a disease-toxicant interaction.

Data previously published by our group shows that following Mn exposure YAC128 mice exhibit decreased striatal accumulation of Mn relative to wild-type (WT) mice (Williams et al., 2010a; Williams et al., 2010b). This phenomenon was restricted to the striatum as no significant differences in Mn levels between genotypes were observed in other brain regions. *In vitro* work by Williams et al. (2010b) and Kwakye et al. (2011), showed that a striatal cell line expressing

mutant *HTT* (STHdh$^{Q111/Q111}$) accumulated less Mn upon exposure, exhibit a basal Mn deficiency under normal culture conditions and were resistant to Mn cytotoxicity relative to wild-type striatal cells (STHdh$^{Q7/Q7}$). Based on these studies, we hypothesized that YAC128 mice would exhibit altered responses to Mn exposure *in vivo* at the level of striatal MSN morphology and striatal neurochemistry. We reasoned that a variety of gene-environment interactions could be observed given the impaired striatal Mn accumulation we have previously reported (Williams et al., 2010a; Williams et al., 2010b). First, decreased Mn accumulation in mutant animals could diminish Mn-dependent toxic effects. Second, Mn exposure could suppress striatal phenotypes in the YAC128 mice that are caused by a Mn handling deficit in these animals. Lastly, expression of the toxic mutant HTT protein in YAC128 animals could interact with striatal Mn neurotoxicity to elicit or enhance changes in dendritic morphology or neurochemistry. Thus, a series of studies were carried out to investigate these possibilities by examining MSN architecture and striatal neurotransmitter and amino acid content following Mn exposure in WT and YAC128 mice.

Although CAG repeat length is inversely related to the age of disease onset in humans, it only accounts for 60% of the variability in disease onset (Andrew et al., 1993; Brinkman et al., 1997; Duyao et al., 1995; Stine et al., 1993; Wexler et al., 2004a). Environmental and/or other genetic factors account for the remaining variability in disease onset and therefore may accelerate or slow the age of disease onset and progression (Anca et al., 2004; Georgiou et al., 1999; Hannan, 2004; van Dellen and Hannan, 2004). Disruption in metal homeostasis

has been associated with many neurodegenerative diseases including Parkinson's disease, Huntington's disease and Alzheimer's disease (Yokel, 2006). Here we explore the possibility that exposure to manganese (Mn) may modulate HD pathophysiology.

There are many mouse models of HD that express either fragments or the full-length mutant *HTT* gene. We use the full-length YAC128 model because the onset of motor symptoms and neuropathology recapitulate many aspects of the human disease (Carroll et al., 2011; Slow et al., 2003). Changes in YAC128 striatal volume are not observed until 9 months of age despite a procedural learning deficit at 2 months and motor phenotype onset at 3 months (Menalled et al., 2009; Slow et al., 2003; Van Raamsdonk et al., 2005b). At 12 months, cortical volume, neuron area and striatal neuron numbers are reduced in YAC128 mice (Slow et al., 2003). Degenerative changes in MSN morphology have been found in multiple HD models (Guidetti et al., 2001; Klapstein et al., 2001; Nithianantharajah et al., 2009; Spires et al., 2004), however, striatal MSN morphology has been examined in YAC128 mice only at one month of age with no alterations identified (Milnerwood et al., 2010; Slow et al., 2003). Therefore, we focused our studies on mice at the age of motor dysfunction onset in an attempt to characterize the earliest changes in MSN morphology and also to match the age at which we found a defect in striatal Mn accumulation in our previous study (Williams et al., 2010a; Williams et al., 2010b).

Results

YAC128 mice accumulate less Mn in the striatum immediately following exposure

The striatum represents a target region for Mn neurotoxicity and also degeneration in HD (de la Monte et al., 1988; Ferrante et al., 1991; Graveland et al., 1985a; Olanow, 2004; Pal et al., 1999). Accordingly, studies were carried out to address the effect of mutant *HTT* and Mn toxicity on striatal MSN morphology and striatal neurotransmitter content in 13 and 16 week old YAC128 and WT mice. Twelve-week old mice were exposed to vehicle (Veh, s.c.) or Mn (50 mg/kg $MnCl_2$-$4H_2O$, s.c.) on experimental day 0, 3 and 6. Mice were sacrificed on experimental day 7 (13 weeks postnatal) or day 28 (16 weeks postnatal) (Figure 20A). Mice were subsequently used for either measurement of striatal metals by ICP-MS, Golgi impregnation for analysis of striatal MSN morphometry or striatal neurochemistry analysis.

Our first objective was to measure striatal Mn concentrations by ICP-MS 24 hours (experimental day 7, 13 weeks old) and 3 weeks (experimental day 28, 16 weeks old) following the last Mn injection. At 13 weeks, levels of striatal Mn (Figure 20B) were significantly increased in both Mn exposed WT and YAC128 mice ($F_{(1,23)}$=783.43, $p < 0.0001$). There was a significant genotype x exposure interaction with YAC128 mice accumulating significantly lower levels of striatal Mn compared to WT ($F_{(1,23)}$=5.33, $p < 0.05$), corroborating graphite furnace atomic absorbance spectroscopy (GFAAS) results in an independent study

(Williams et al., 2010b). At 16 weeks, (Figure 20C) this exposure effect persisted ($F_{(1,16)}$=9.19, $p < 0.01$) and Mn levels in the striatum of WT mice were dramatically reduced, but remained significantly elevated compared to vehicle injected mice ($p < 0.01$), but there was no difference in striatal Mn levels between WT-Vehicle (WT-Veh), YAC128-Veh and YAC128-Mn groups at 16 weeks. In addition to Mn, other metals were simultaneously analyzed by ICP-MS in the striatum of these mice. Striatal levels of copper (Cu) and zinc (Zn) and other metals showed no significant differences across the exposure groups at either time point (data not shown). These results demonstrate that the sub-acute Mn exposure paradigm can significantly and specifically elevate striatal Mn levels immediately following exposure. Excess Mn was completely eliminated from YAC128 striatum by 3 weeks post exposure, however WT mice still had slightly elevated levels of striatal Mn.

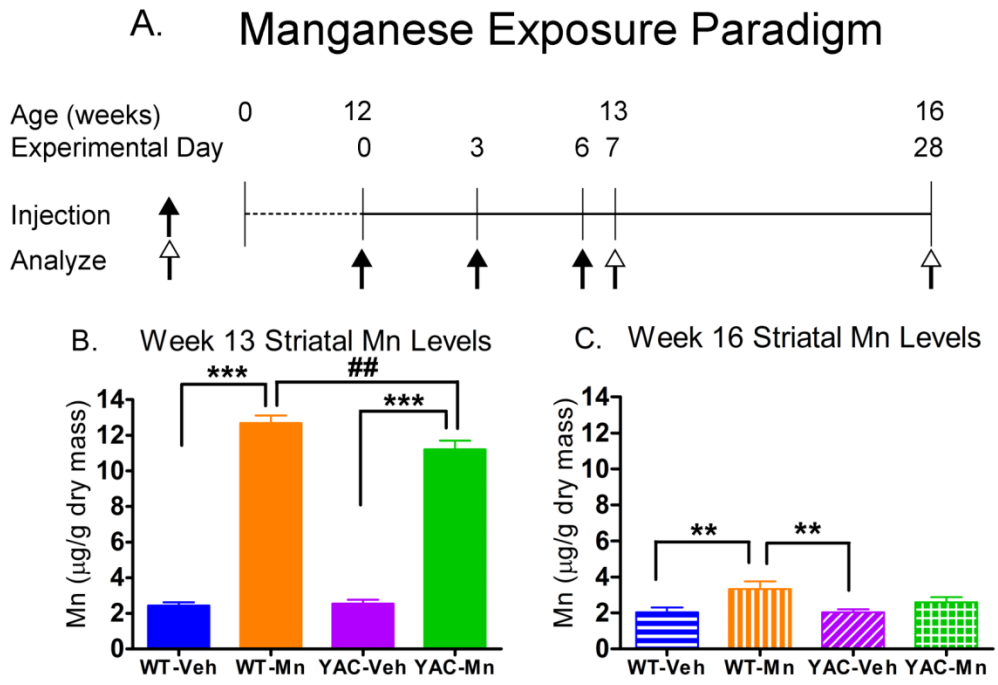

Figure 20. Striatal Mn levels are significantly elevated in WT-Mn over YAC128-Mn mice at week 13 but are elevated only above vehicle exposed mice at week 16.

A) Mn exposure paradigm. 12 week-old WT and YAC128 mice were exposed to $MnCl_2$-$4H_2O$ (50 mg/kg s.c.) or vehicle (filled arrow) on days 0, 3, 6, and were sacrificed (open arrow) on experimental day 7 (13 weeks) or day 28 (16 weeks) for striatal Golgi impregnation or neurochemistry analysis. **B)** Striatal Mn levels, measured by ICP-MS, at week 13 (n = 7) are significantly higher in Mn exposed mice compared to their vehicle controls at week 13 ($F_{(1,23)}$=783.43, $p < 0.0001$). There is a genotype x exposure interaction whereby significantly less Mn accumulated in the YAC128-Mn exposed group compared to WT-Mn exposed mice ($F_{(1,23)}$=5.33, $p < 0.05$). **C)** At week 16 (n = 5), Mn levels dropped, but a exposure effect still remains ($F_{(1,16)}$=9.19, $p < 0.001$) with Mn levels significantly higher in WT mice. Average striatal Mn concentrations +/- SEM. Significant results of *post-hoc* t-tests: **p < 0.01, $^{\#\#}$p < 0.005 and ***p < 0.001.

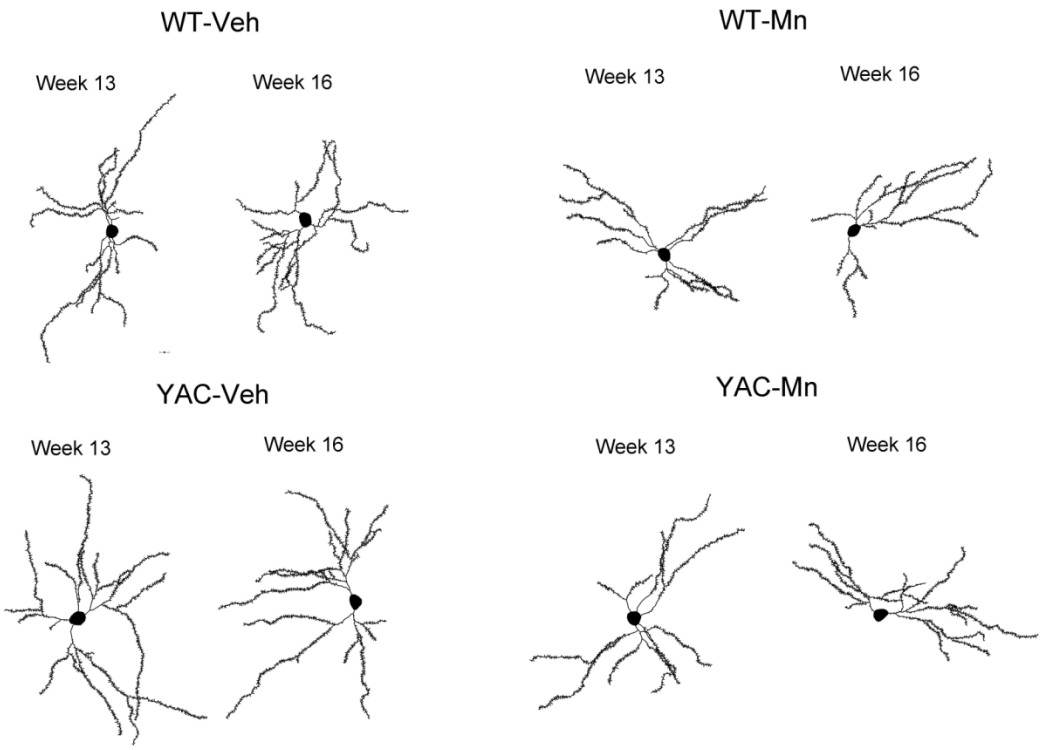

Figure 21. Representative reconstructions of striatal MSN in week 13 and 16 mice.

Mice were exposed on day 0, 3, 6 with vehicle or $MnCl_2$-$4H_2O$ (50 mg/kg s.c.), sacrificed on experimental day 7 (week 13, n = 4-5) or 28 (week 16, n = 5) and the striatum was processed for Golgi impregnation. Neurons were traced and analyzed using Neurolucida and Neuroexplorer, respectively (NeuroBrightField, Inc). Representative neurons were within 5% of the mean total dendritic length for each exposure group

Genotype influences neuron morphology at 16 weeks

Figure 21 depicts representative reconstructions of neurons in each exposure group at 13 weeks (experimental day 7) and 16 weeks (experimental day 28). We failed to observe any overt differences in neuron morphology based on visual inspection of neuronal traces for each group (Figure 21). MSN morphology was unaffected by genotype or Mn exposure at week 13 (Figure 22, Table 1), however changes in neuron morphology were observed at week 16. There was a significant main effect of genotype ($F_{(1,109)} = 7.503$, $p < 0.01$) at 16 weeks on total dendritic length (Figure 22B, Table 2). YAC128 mice in both the Veh and Mn exposure groups exhibited shorter total dendritic lengths compared to WT-Veh MSNs. *Post-hoc* tests revealed that total dendritic length of YAC128-Mn MSNs were significantly shorter than WT-Veh ($p = 0.014$). There were trends towards statistical significance in the differences between WT-Veh and YAC128-Veh MSNs ($p = 0.06$) as well as WT-Mn and YAC128-Mn ($p = 0.051$) MSNs, which also contributed to the overall significant main effect of genotype. At 16 weeks there was a main effect of genotype ($F_{(1,109)}= 7.99$ $p < 0.01$) on total spine density (Figure 22D, Table 2). YAC128 mice as a group had higher total spine densities than WT mice. *Post-hoc* analysis showed that YAC128-Mn MSNs had a significantly higher spine density than WT-Veh and WT-Mn ($p < 0.05$). The higher dendritic spine density in YAC128 mice was strongly driven by the reduction in total dendritic length, as we failed to observe a significant difference in total spine number or total ends at 13 or 16 weeks (Figure 22 E and Figure 22F, Table 1 and Table 2). There was a significant main effect of genotype ($F_{(1,109)}= 4.06$ $p <$

0.05) on the number of dendrite endings at week 16 (Figure 22H). *Post-hoc* analysis revealed a significant reduction in the number of dendrite endings in YAC128-Veh compared to WT-Veh mice ($p < 0.05$). These data consistently show that genotype plays a significant role in morphological differences observed in MSNs at 16 weeks.

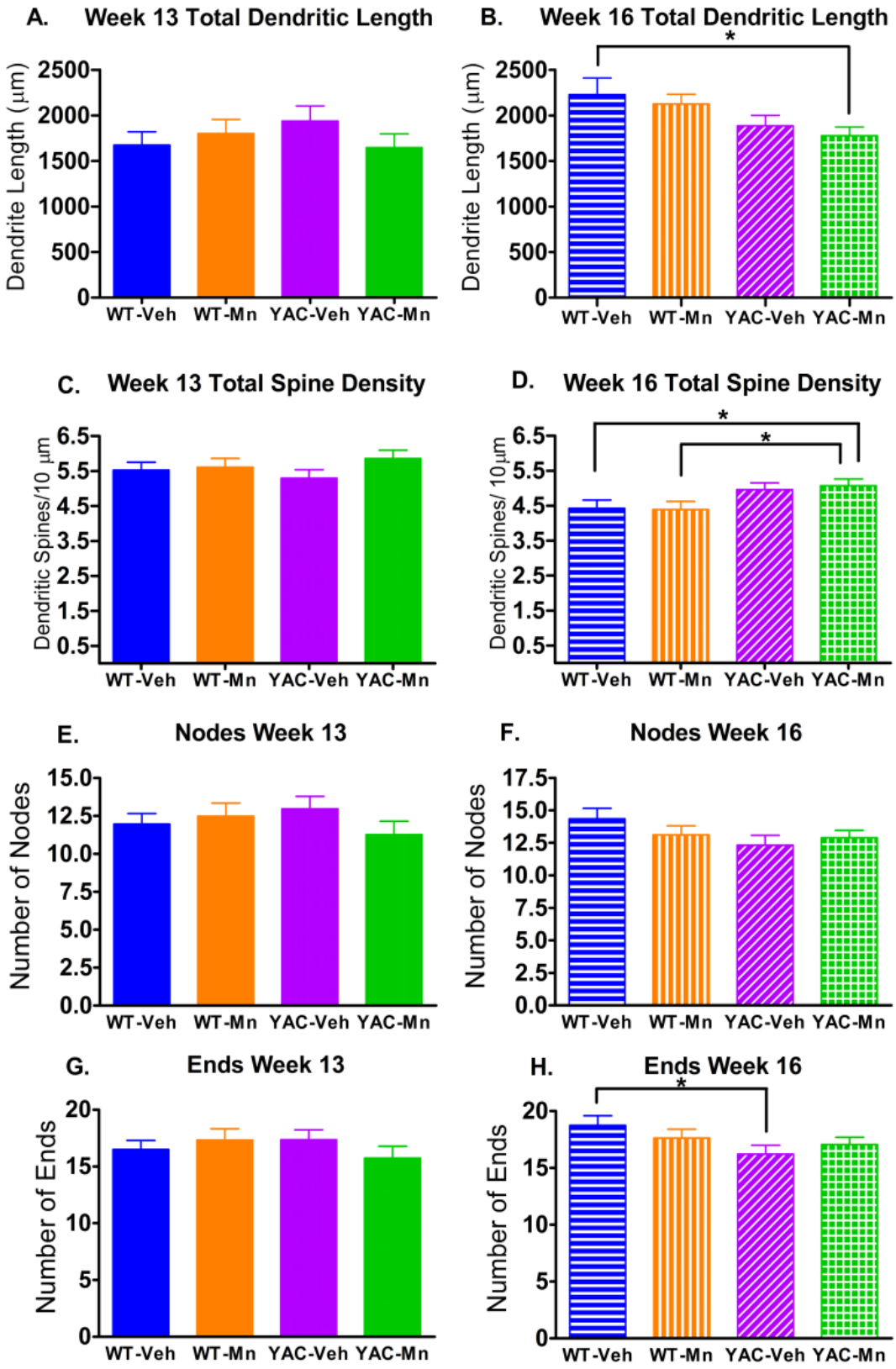
A. Week 13 Total Dendritic Length
Dendrite Length (µm)
2500
2000
1500
1000
500
0
WT-Veh
WT-Mn
YAC-Veh
YAC-Mn
B. Week 16 Total Dendritic Length
*
Dendrite Length (µm)
2500
2000
1500
1000
500
0
WT-Veh
WT-Mn
YAC-Veh
YAC-Mn
C. Week 13 Total Spine Density
Dendritic Spines/10 µm
6.5
5.5
4.5
3.5
2.5
1.5
0.5
WT-Veh
WT-Mn
YAC-Veh
YAC-Mn
D. Week 16 Total Spine Density
*
*
Dendritic Spines/ 10µm
6.5
5.5
4.5
3.5
2.5
1.5
0.5
WT-Veh
WT-Mn
YAC-Veh
YAC-Mn
E. Nodes Week 13
Number of Nodes
15.0
12.5
10.0
7.5
5.0
2.5
0.0
WT-Veh
WT-Mn
YAC-Veh
YAC-Mn
F. Nodes Week 16
Number of Nodes
17.5
15.0
12.5
10.0
7.5
5.0
2.5
0.0
WT-Veh
WT-Mn
YAC-Veh
YAC-Mn
G. Ends Week 13
Number of Ends
20
15
10
5
0
WT-Veh
WT-Mn
YAC-Veh
YAC-Mn
H. Ends Week 16
*
Number of Ends
20
15
10
5
0
WT-Veh
WT-Mn
YAC-Veh
YAC-Mn

Figure 22. Total dendritic length and total number of endings are reduced while total spine density is increased in YAC compared to WT mice at 16 weeks.

A) Total dendritic length is unchanged in WT and YAC mice at week 13. **B)** Total dendritic length is reduced in YAC vs WT mice revealing a significant main genotype effect at 16 weeks ($F_{(1,109)} = 7.50$, $p < 0.01$). **C)** Total spine density is unchanged across exposure groups at week 13. **D)** The increased total spine density in YAC vs WT mice reveals a significant main effect of genotype at week 16 ($F_{(1,109)} = 7.99$, $p < 0.01$). **E)** There is no difference in total number of nodes at 13 weeks. **F)** At 16 weeks there is no difference in total number of nodes between groups. **G)** No significant difference in total number of endings was observed at 13 weeks. **H)** Total number of endings were reduced in YAC128-Veh vs WT-Veh mice revealing a significant genotype effect ($F_{(1,109)}= 4.06$ $p < 0.05$). Week 13: n = 4-5 mice per group, 4-6 neurons/animal. Week 16: n = 5 mice/group, 4-6 neurons/animal. Error bars indicate SEM. Significant differences by *post-hoc* t-test indicated by *p < 0.05.

Table 1. Two-way ANOVA statistics for total dendritic measures at 13 weeks.

	Genotype	Exposure	Genotype x Exposure
Total Dendritic Length	F(1,93) = 0.125 p = 0.724	F(1,93) = 0.287 p = 0.593	F(1,93) = 1.855 p = 0.176
Total Spine Density	F(1,93) = 0.001 p = 0.978	F(1,93) = 1.831 p = 0.179	F(1,93) = 1.00 p = 0.320
Total Spine Number	F(1,93) = 0.143 p = 0.707	F(1,93) = 0.002 p = 0.966	F(1,93) = 0.902 p = 0.345
Soma Area	F(1,93) = 0.602 p = 0.440	F(1,93) = 0.308 p = 0.581	F(1,93) = 0.126 p - 0.724
Total Nodes	F(1,93) = 0.019 p = 0.892	F(1,93) = 0.514 p = 0.475	F(1,93) = 1.817 p = 0.181
Total Ends	F(1,93) = 0.154 p = 0.696	F(1,93) = 0.178 p = 0.674	F(1,93) = 1.687 p = 0.197

Table 2. Two-way ANOVA statistics for total dendritic measures at 16 weeks.

	Genotype	Exposure	Genotype x Exposure
Total Dendritic Length	F(1,109) = 7.503 **p = 0.007**	F(1,109) = 0.669 p = 0.405	F(1,109) = 0.000 p = 0.986
Total Spine Density	F(1,109) = 7.993 **p = 0.006**	F(1,109) = 0.033 p = 0.857	F(1,109) = 0.113 p = 0.737
Total Spine Number	F(1,109) = 0.155 p = 0.649	F(1,109) = 0.136 p = 0.713	F(1,109) = 0.027 p = 0.869
Soma Area	F(1,109) = 3.228 p = 0.075	F(1,109) = 0.324 p = 0.570	F(1,109) = 0.000 p = 0.998
Total Nodes	F(1,109) = 2.549 p = 0.113	F(1,109) = 0.218 p = 0.641	F(1,109) = 1.695 p = 0.196
Total Ends	F(1,109) = 4.058 **p = 0.046**	F(1,109) = 0.026 p = 0.871	F(1,109) = 1.668 p = 0.199

Morphometric measures as a function of distance from the soma are altered by genotype and Mn exposure

Several measures of neuron morphology as a function of distance from the soma were examined in order to gain a detailed understanding of the MSN morphology in these mice. Dendritic arborization is an important morphological characteristic that determines how the neuron integrates synaptic inputs. Sholl analysis measures branching complexity of the neuron by tallying the number of dendrites that intersect a series of evenly spaced concentric circles centered at the soma (Sholl, 1953). At 13 weeks, there was a significant effect of distance on dendritic branching (as expected for Sholl analysis), but no significant interactions between distance x genotype, distance x exposure, or three-way interaction effects (Figure 23A and Table 3). At 16 weeks (Figure 23B and Table 4) there was a significant effect of distance x genotype ($F_{(30,3270)}$=1.71, p = 0.01) and as well as a further effect of Mn exposure (distance x genotype x exposure interaction effect ($F_{(30,3270)}$=1.71, p < 0.01)). *Post-hoc* analysis revealed that the basis of the disease-toxicant interaction effect is a significant difference in branching complexity between WT-Veh and YAC-Mn mice at 16 weeks (p < 0.05). There was also a trend towards reduced branching complexity in YAC128-Mn compared to WT-Mn mice (p = 0.06). These data demonstrate that the combined effect of Mn-exposure and the HD mutant genotype caused a decrease in dendritic branching complexity greater than either factor alone.

We examined dendrite length, spine number and spine density as a function of distance from the soma as further measures of dendritic arborization

and synaptic integration. These morphological characteristics of dendrites were measured in each shell made by the concentric circles used for Sholl analysis (Figure 23). None of these measures showed significant differences at 13 weeks (Table 3). Dendrite length as a function of distance from the soma closely resembled the results from Sholl analysis at 16 weeks (Figure 23D, Table 4). There was a main effect of distance x genotype ($F_{(30,3270)}$ =2.26, $p < 0.0001$) and a distance x genotype x exposure interaction ($F_{(30,3270)}$ =1.61, $p < 0.019$). Spine number as a function of distance from the soma (Figure 23F) also showed distance x genotype ($F_{(30,3270)}$=1.72, $p < 0.01$) and distance x genotype x exposure ($F_{(30,3270)}$=3.01, $p < 0.0001$) effects at 16 weeks (Table 4). There were significant distance x genotype ($F_{(17,1853)}$=1.73, $p = 0.032$) and distance x exposure interactions ($F_{(17,1853)}$=1.89, $p = 0.015$) at 16 weeks for spine density as a function of distance from the soma (Figure 23H, Table 4). These data corroborate the findings by Sholl analysis, and further demonstrate complex disease-toxicant interaction effects between HD and Mn exposure that become apparent 3 weeks post-exposure.

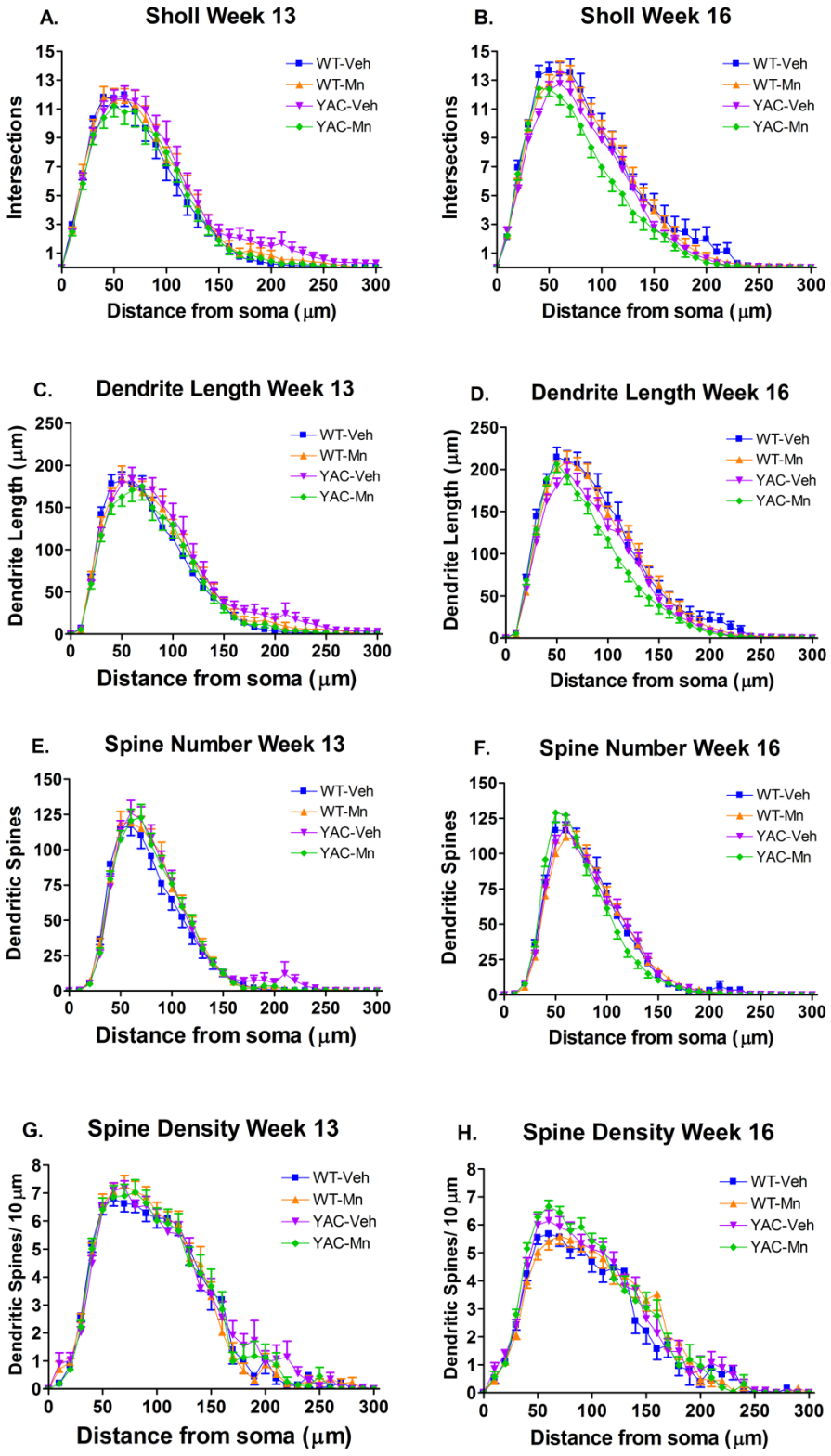
A.
Sholl Week 13
Intersections
Distance from soma (μm)
WT-Veh
WT-Mn
YAC-Veh
YAC-Mn
B.
Sholl Week 16
Intersections
Distance from soma (μm)
C.
Dendrite Length Week 13
Dendrite Length (μm)
Distance from soma (μm)
D.
Dendrite Length Week 16
Dendrite Length (μm)
Distance from soma (μm)
E.
Spine Number Week 13
Dendritic Spines
Distance from soma (μm)
F.
Spine Number Week 16
Dendritic Spines
Distance from soma (μm)
G.
Spine Density Week 13
Dendritic Spines/ 10 μm
Distance from soma (μm)
H.
Spine Density Week 16
Dendritic Spines/ 10 μm
Distance from soma (μm)

Figure 23. YAC128-Mn exposed mice have decreased branching complexity at 16 weeks.
Morphological characteristics of MSNs were assessed using the Sholl method. Concentric rings at 10 μm intervals were centered at the soma and intersections of dendrites at each radius were counted to determine branching complexity. **A)** Dendritic branching complexity is not significantly different between groups at 13 weeks. **B)** Main effects of distance x genotype and distance x genotype x exposure for dendritic branching complexity were observed only at 16 weeks. **C)** Dendrite length as a function of distance from the soma is unaltered at 13 weeks. **D)** At 16 weeks, dendrite length as a function of distance from the soma is subject to distance x genotype and distance x genotype x exposure effects. **E)** Spine number as a function of distance from the soma is unchanged at 13 weeks. **F)** A distance x genotype and distance x genotype x exposure effect were observed at 16 weeks for spine number as a function of distance from the soma. **G)** At 13 weeks spine density as a function of distance from the soma was unaffected. **H)** Spine density as a function of distance from the soma was subject to effects of distance x genotype and distance x exposure.

Table 3. Repeated measures two-way ANOVA statistics for dendritic measures as a function of distance from the soma at 13 weeks.

	Distance x Genotype	Distance x Exposure	Distance x Genotype x Exposure
Sholl	F(39, 3627) = 0.877 p = 0.687	F(39, 3627) = 0.177 p = 1.000	F(39, 3627) = 0.510 p = 0.995
Dendritic Length	F(39, 3627) = 1.013 p = 0.448	F(39, 3627) = 0.211 p = 1.000	F(39, 3627) = 0.772 p = 0.845
Spine Number	F(39, 3627) = 0.933 p = 0.589	F(39, 3627) = 0.470 p = 0.998	F(39, 3627) = 0.741 p = 0.881
Spine Density	F(17, 1581) = 0.299 p = 0.997	F(17, 1581) = 0.632 p = 0.869	F(17, 1581) = 0.825 p = 0.665

Table 4. Repeated measures two-way ANOVA statistics for dendritic measures as a function of distance from the soma at 16 weeks.

	Distance x Genotype	Distance x Exposure	Distance x Genotype x Exposure
Sholl	F(30,2370) = 1.709 **p = 0.0095**	F(30,2370) = 0.558 p = 0.975	F(30,2370) = 1.713 **p = 0.0093**
Dendritic Length	F(30,2370) = 2.264 **p = 0.0001**	F(30,2370) = 0.730 p = 0.8571	F(30,2370) = 1.613 **p = 0.0187**
Spine Number	F(30,2370) = 1.717 **p = 0.0090**	F(30,2370) = 0.649 p = 0.9287	F(30,2370) = 3.001 **p < 0.0001**
Spine Density	F(17,1853) = 1.733 **p = 0.0315**	F(17,1853) = 1.890 **p = 0.0151**	F(17,1853) = 1.513 p = 0.0812

Onset of striatal neuropathology occurs by 16 weeks in YAC128 mice

Comparing total dendritic length and total spine density across age revealed that there was a significant effect of age for both neuron measures and an age x genotype interaction for total dendritic length (Table 5). While there was a significant increase in total dendritic length in WT (Veh + Mn) MSNs from 13 to 16 weeks ($p = 0.002$), there was no significant difference in YAC128 (Veh + Mn) MSNs at these time points (Figure 24A). *Post-hoc* t-tests revealed a significant difference in total dendritic length between WT and YAC128 groups at week 16 ($p = 0.007$). Based on this novel result, we decided to directly compare WT-Veh and YAC128-Veh mice (Figure 24B). There was a significant age x genotype interaction for total dendritic length between WT-Veh and YAC128-Veh ($F_{(1,100)}=4.01$, $p < 0.05$). Total dendritic length increased in WT-Veh mice from 13 to 16 weeks ($p = 0.011$), while YAC128-Veh mice showed no significant difference in total dendritic length across age. Similarly, total spine density (Figure 24C) decreased from week 13 to 16 in both genotypes ($p < 0.05$). However, at 16 weeks total spine density was higher in YAC128 MSNs compared to WT MSNs ($p = 0.005$). Next, we directly compared total spine density in WT-Veh and YAC128-Veh mice. Total spine density decreased from 13 to 16 weeks in WT-Veh MSNs ($p = 0.001$), but there was not a significant decrease in total spine density in YAC128-Veh MSNs across age (Figure 24D). The absence of an age-dependent increase in total dendritic length and decrease in total spine density of MSNs in YAC128 mice is the earliest sign of neuropathology identified to date in this model of HD.

Analyses of neuron morphology measures as a function of distance from the soma across age revealed significant effects of distance x age for dendritic branching, dendrite length and spine density (Figure 24 and Table 6). Additionally, distance x age x genotype interactions were detected for dendritic branching, dendrite length and spine number (Figure 24 and Table 6). *Post-hoc* analysis confirmed that the genotype effect was driven by a significant increase in branching complexity between 13 and 16 weeks in WT mice (Figure 24E) ($p < 0.05$). Importantly, there was no significant difference between 13 and 16 week branching complexity in YAC128-Veh MSNs (Figure 24I). Therefore, changes in dendritic branching that normally occurred in WT-Veh mice *did not* occur in YAC128-Veh mice, indicating an onset of neuropathological changes between 13 and 16 weeks of age. Similar results were found for dendrite length as a function of distance from the soma (Figure 24). WT mice had longer dendrite lengths per shell at 16 weeks compared to 13 weeks ($p < 0.05$), but there was no difference in dendrite length per shell between the time points in YAC128-Veh mice (Figure 24F and Figure 24J). Spine number as a function of distance from the soma was not changed between 13 and 16 weeks in either genotype (Figure 24G and 24H). Sixteen-week old WT-Veh mice had significantly decreased spine density per shell (Figure 24H) compared to 13 week WT-Veh mice ($p < 0.05$), but there was no difference between spine densities in YAC128 mice from week 13 to 16 (Figure 24L). This parallels the changes observed in total spine density across age groups. Together these data corroborate that subtle neuropathological changes in MSN morphology commence as early as 16 weeks of age and that

the disease-toxicant interaction between Mn and mutant *HTT* has a subtle effect on dendrite length in YAC128 mice.

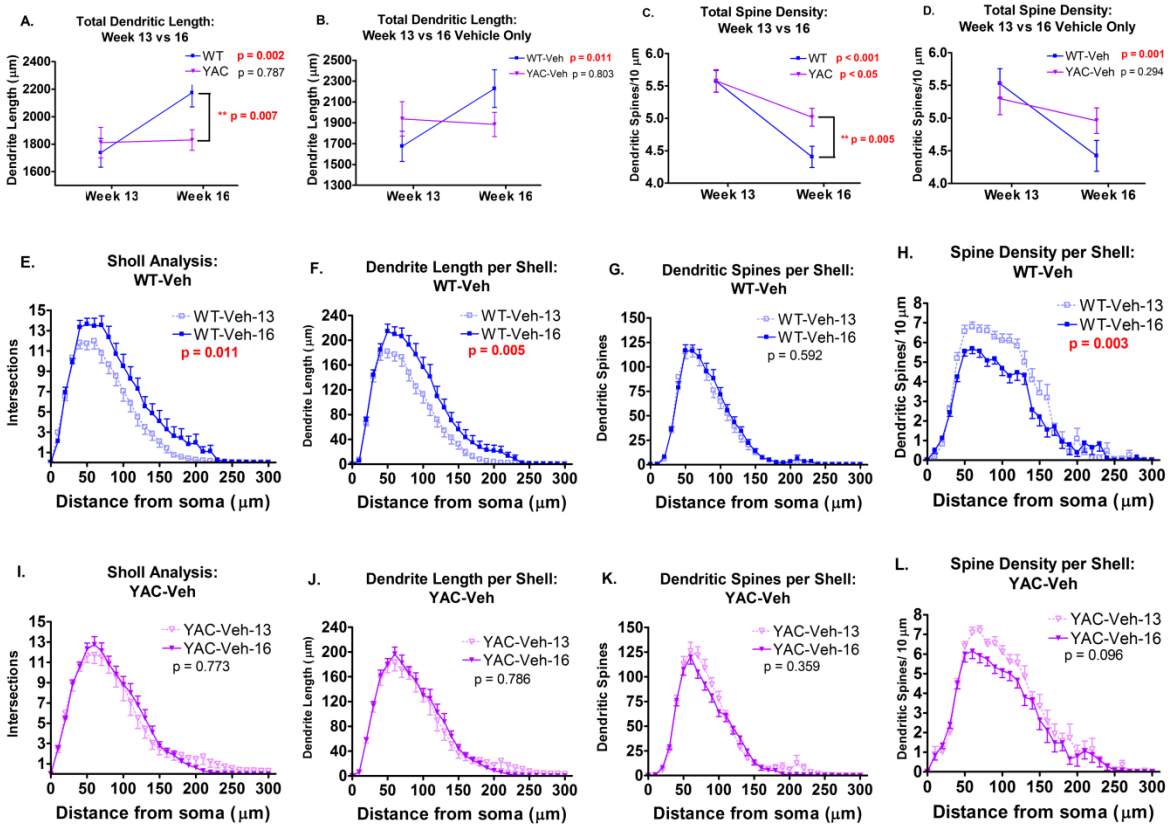

Figure 24. Onset of striatal neuropathology in YAC128 mice.
A) Total dendritic length of WT mice increased from week 13 to week 16, but was unchanged in YAC128 mice. **B)** Total dendritic length increased in WT-Veh mice from week 13 to week 16, but was unchanged in YAC128-Veh mice. **C)** Dendritic branching, measured by Sholl analysis, increased from week 13 to week 16 in WT-Veh mice. **D)** Dendrite length as a function of distance from the soma also increased from week 13 to week 16 in WT-Veh mice. **E)** Spine number as a function of distance from the soma was unchanged from week 13 to week 16 in WT-Veh mice, recapitulating the similarity between total spine number at 13 and 16 weeks. **F)** Spine density as a function of distance from the soma was decreased from week 13 to week 16 in WT-Veh mice. **G)** There was no change in dendrite branching in YAC128-Veh mice from week 13 to 16. **H)** There was no change in dendrite length as a function of distance from the soma from week 13 to 16 in YAC128-Veh mice. **I)** There was no change in spine number as function of distance from the soma in YAC128-Veh mice. **J)** There was only a slight decrease in spine density as a function of distance from the soma, which is reflected in total spine density across age. Week 13: n = 4-5 mice per group, 4-6 neurons/animal. Week 16: n = 5 mice/group, 4-6 neurons/animal. Average values +/- SEM; p-values from *post-hoc* t-tests are on each graph, significant values indicated in bold. ** $p < 0.01$.

Table 5. Multivariate ANOVA statistics for total dendritic measures across age.

	Genotype	Exposure	Age	Genotype x Expsoure	Age x Genotype	Age x Exposure	Age x Genotype x Exposure
Total Dendritic Length	F(1,202) = 2.194	F(1,202) = 0.909	F(1,202) = 5.843	F(1,202) = 1.149	F(1,202) = 4.131	F(1,202) = 0.014	F(1,202) = 1.103
	p = 0.140	p = 0.342	**p = 0.017**	p = 0.285	**p = 0.043**	p = 0.906	p = 0.295
Total Spine Density	F(1,202) = 3.677	F(1,202) = 1.272	F(1,202) = 28.812	F(1,202) = 0.941	F(1,202) = 3.522	F(1,202) = 0.785	F(1,202) = 0.269
	p = 0.057	p = 0.261	**p < 0.0001**	p = 0.333	p = 0.062	p = 0.377	p = 0.604
Total Spine Number	F(1,202) = 0.002	F(1,202) = 0.041	F(1,202) = 0.528	F(1,202) = 0.406	F(1,202) = 0.299	F(1,202) = 0.072	F(1,202) = 0.719
	p = 0.965	p = 0.840	p = 0.468	p = 0.525	p = 0.585	p = 0.788	p = 0.397
Soma Area	F(1,202) = 0.414	F(1,202) = 0.001	F(1,202) = 0.104	F(1,202) = 0.067	F(1,202) = 3.197	F(1,202) = 0.630	F(1,202) = 0.069
	p = 0.521	p = 0.981	p = 0.748	p = 0.795	p = 0.075	p = 0.428	p = 0.793
Total Nodes	F(1,202) = 0.005	F(1,202) = 1.040	F(1,202) = 0.001	F(1,202) = 2.51	F(1,202) = 3.197	F(1,202) = 0.002	F(1,202) = 0.181
	p = 0.944	p = 0.309	p = 0.974	p = 0.115	p = 0.075	p = 0.961	p = 0.671
Total Ends	F(1,202) = 0.016	F(1,202) = 0.649	F(1,202) = 0.021	F(1,202) = 1.757	F(1,202) = 0.075	F(1,202) = 0.032	F(1,202) = 0.369
	p = 0.901	p = 0.421	p = 0.886	p = 0.186	p = 0.784	p = 0.859	p = 0.544

Table 6. Repeated measures multivariate ANOVA statistics for dendritic measures as a function of distance from the soma across age.

	Distance x Genotype	Distance x Exposure	Distance x Age	Distance x Genotype x Exposure	Distance x Age x Genotype	Distance x Age x Exposure	Distance x Age x Genotype x Expsoure
Sholl	F(39,7878) = 1.196	F(39,7878) = 0.329	F(39,7878) = 3.831	F(39,7878) = 1.257	F(39,7878) = 1.714	F(39,7878) = 0.415	F(39,7878) = 0.773
	p = 0.188	p = 1.000	**p <0.0001**	p = 0.132	**p = 0.004**	p = 1.000	p = 0.843
Dendritic Length	F(39,7878) = 1.222	F(39,7878) = 0.268	F(39,7878) = 3.932	F(39,7878) = 1.542	F(39,7878) = 2.355	F(39,7878) = 0.642	F(39,7878) = 0.679
	p = 0.162	p = 1.000	**p <0.0001**	**p = 0.017**	**p <0.0001**	p = 0.959	p = 0.937
Spine Number	F(39,7878) = 0.568	F(39,7878) = 0.248	F(39,7878) = 1.010	F(39,7878) = 1.917	F(39,7878) = 1.922	F(39,7878) = 0.836	F(39,7878) = 1.374
	p = 0.986	p = 1.000	p = 0.309	**p = 0.0005**	**p <0.0005**	p = 0.755	p = 0.061
Spine Density	F(17,3434) = 0.748	F(17,3434) = 1.104	F(17,3434) = 6.458	F(17,3434) = 0.783	F(17,3434) = 1.041	F(17,3434) = 1.219	F(17,3434) = 1.464
	p = 0.755	p = 0.343	**p <0.0001**	p = 0.715	p = 0.409	p = 0.240	p = 0.098

YAC128 mice were more sensitive to Mn-dependent changes in striatal amino acids

In addition to striatal neuron morphology, we examined total levels of striatal amino acids and monoamine neurotransmitters to identify neurochemical changes that may underlie the alterations in MSN dendritic morphology. Many of these amino acids act both as neurotransmitters and in metabolic pathways. Striatal amino acids levels have not been previously reported in YAC128 mice or following Mn exposure, except as noted in the introduction. Mutant *HTT* and Mn exposure had varied effects on striatal amino acids, though most were unchanged by either genotype or exposure. Amino acids that were affected by mutant *HTT* and/or Mn exposure included γ-amino butyric acid (GABA, Figure 25A and 25E), citrulline (Cit, Figure 25B and 25F), glycine (Gly, Figure 25C and 25G), serine (Ser, Figure 25D and 25H) histidine and alanine (data not shown). Mutant *HTT* and Mn-effects were specific, with striatal levels of aspartate, glutamate, leucine, lysine, methionine, ornithine, phenylalanine, proline, taurine and tyrosine remaining unchanged relative to their respective controls at both time points (Figure 26).

Striatal GABA levels at 13 weeks (Figure 25A) were significantly elevated by Mn exposure ($F_{(1,16)}$=9.53, $p < 0.01$). WT- and YAC128-Veh exposed animals had nearly identical levels of striatal GABA, but Mn exposure resulted in significantly higher GABA levels in both genotypes compared to their respective Veh exposed counterparts ($p < 0.05$). YAC128-Mn striatal GABA levels were also elevated over WT-Veh ($p < 0.05$). Striatal GABA levels at 16 weeks (Figure 25E)

were significantly affected by a genotype x exposure interaction ($F_{(1,14)}$=5.14, p < 0.05). YAC128-Mn animals had significantly lower levels of striatal GABA compared to WT-Mn (p = 0.019). Cit levels in the striatum were significantly elevated by Mn exposure ($F_{(1,16)}$=14.87, p < 0.001) at 13 weeks (Figure 25B). Mn exposure resulted in an increase in striatal Cit levels for both genotypes ($F_{(1,14)}$=5.14, p < 0.05) above Veh exposed mice of both genotypes (p < 0.05). However, by 16 weeks when Mn was no longer elevated, striatal Cit in Mn exposed mice (Figure 25F) was equivalent to WT-Veh.

Gly levels in the striatum at 13 weeks (Figure 25C) were affected by genotype ($F_{(1,16)}$=4.64, p < 0.05). *Post-hoc* tests revealed that YAC128-Mn mice had significantly higher levels of striatal Gly compared to WT-Veh and WT-Mn mice (p < 0.05). At 16 weeks there was a significant main effect of genotype ($F_{(1,14)}$=7.43, p = 0.016) and a genotype x exposure interaction ($F_{(1,14)}$=11.43, p < 0.005) on striatal Gly levels (Figure 5G). YAC128-Veh mice had an increase in striatal Gly levels over WT-Veh (p = 0.002) mice at 16 weeks. Gly levels were only transiently elevated in Mn exposed mice at 13 weeks because at 16 weeks Gly levels were at the same level as WT-Veh when Mn levels returned to normal. Elevated Gly levels in the YAC128-Veh mice were returned to WT-Veh levels in Mn exposed YAC128 mice (YAC128-Mn vs YAC128-Veh p = 0.006). At 13 weeks striatal Ser levels (Figure 25D) were affected by genotype ($F_{(1,16)}$=4.66, p < 0.05) and exposure ($F_{(1,16)}$=12.38, p < 0.005). *Post-hoc* tests revealed that levels of Ser in YAC128-Mn mice were significantly elevated above WT-Veh (p < 0.001), WT-Mn (p < 0.05), and YAC128-Veh (p < 0.005). At 16 weeks striatal Ser

levels (Figure 25H) were subject to significant main effects of genotype ($F_{(1,14)}$=9.12, $p < 0.01$) and exposure ($F_{(1,14)}$=5.75, $p < 0.05$). Striatal Ser levels were normalized to WT-Veh levels in Mn exposed mice following clearance of Mn from the striatum. YAC128-Veh mice had an increase in striatal Ser compared to WT-Veh that was normalized to WT-Veh levels in Mn exposed YAC128 mice ($p < 0.05$).

In analyzing striatal amino acids across age groups it is possible to gain insight into the effects of Mn on the levels of amino acids over time. There was a significant age x exposure interaction for striatal Ser ($F_{(1,36)}$=12.20, $p < 0.001$), Gly ($F_{(1,36)}$=4.72, $p < 0.05$), Cit ($F_{(1,36)}$=19.95, $p < 0.001$) and GABA ($F_{(1,36)}$=9.70, $p < 0.005$). The age x exposure interaction is illustrated by the changing effect of Mn over time. Immediately after Mn exposure at 13 weeks, striatal Mn levels were significantly elevated and at the same time striatal Ser, Gly, Cit and GABA levels were elevated in Mn exposed animals. This may be due to an acute response to elevated Mn present in the striatum. Mn was almost completely eliminated from the striatum 3 weeks following the end of Mn exposure. At this time point, the amino acids that were elevated immediately after Mn exposure normalized compared to WT-Veh.

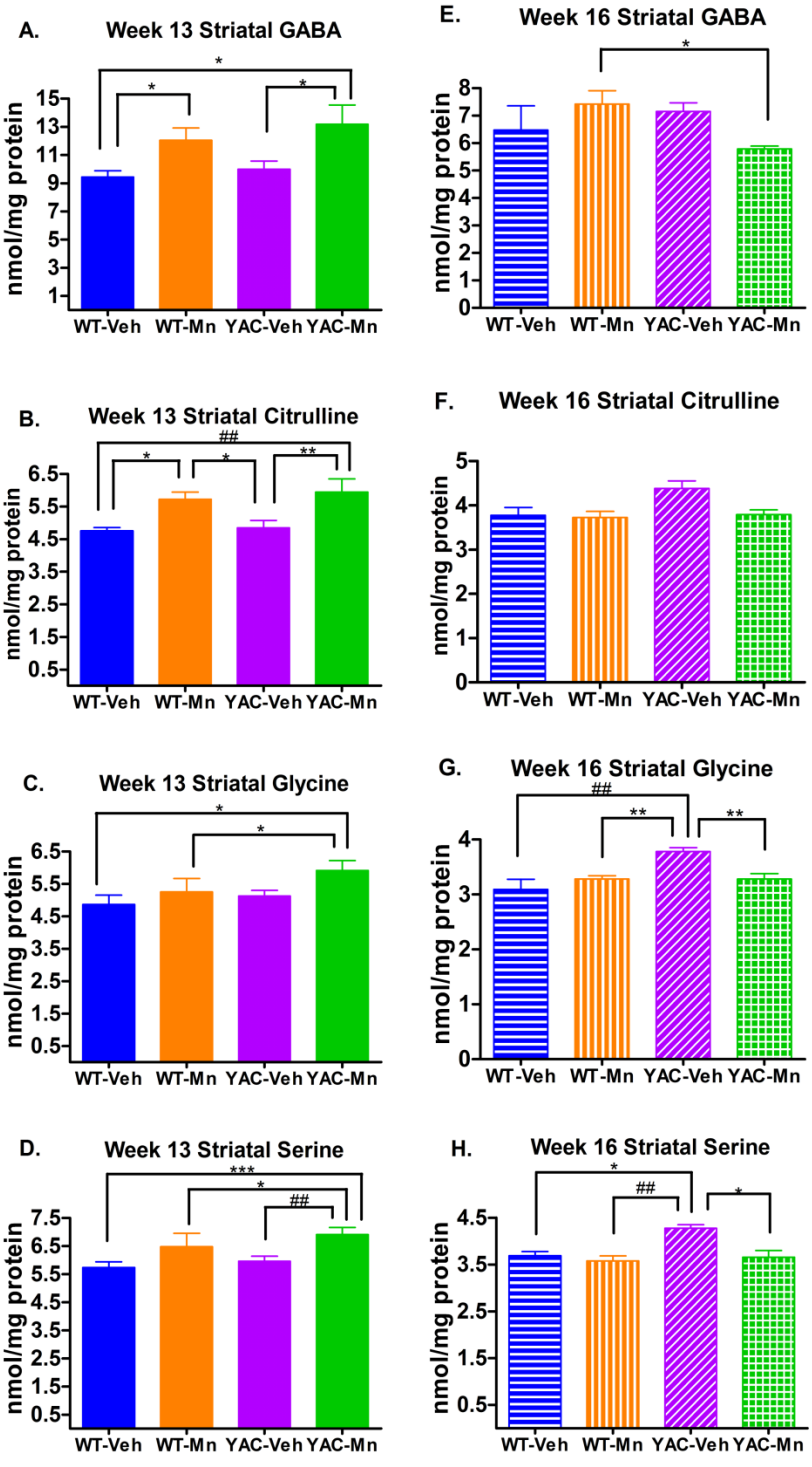
A.
Week 13 Striatal GABA
nmol/mg protein
WT-Veh
WT-Mn
YAC-Veh
YAC-Mn
B.
Week 13 Striatal Citrulline
C.
Week 13 Striatal Glycine
D.
Week 13 Striatal Serine
E.
Week 16 Striatal GABA
F.
Week 16 Striatal Citrulline
G.
Week 16 Striatal Glycine
H.
Week 16 Striatal Serine

Figure 25. Striatal amino acids are altered by Mn exposure and genotype at 13 and 16 weeks.

A) There is a main effect of treatment on GABA at week 13 ($F_{(1,16)}$=9.53, $p < 0.01$) WT-Mn and YAC-Mn are significantly elevated above WT-Veh ($p < 0.05$) YAC-Mn is also elevated above YAC-Veh ($p < 0.05$). **B)** Mn treatment ($F_{(1,16)}$=14.87, $p < 0.001$) caused an increase in striatal citrulline (Cit) levels. Mn treated animals of both genotypes are elevated above both vehicle treated groups. **C)** There is a main effect of genotype on Gly concentration in the striatum ($F_{(1,16)}$=4.64, $p < 0.05$) at week 13. Levels of Gly in YAC128-Mn are significantly higher than WT-Veh and WT-Mn, but do not reach significance compared to YAC128-Veh ($p = 0.052$). **D)** There are significant main effects of genotype ($F_{(1,16)}$=4.66, $p < 0.05$) and exposure ($F_{(1,16)}$=12.38, $p < 0.005$) on striatal Ser levels at 13 weeks. **E)** There is a significant genotype x treatment interaction for striatal GABA levels ($F_{(1,14)}$=5.14, $p = 0.04$). Striatal GABA is much lower in YAC-Mn compared to WT-Mn animals ($p < 0.02$). **F)** There is no significant difference in Cit levels at week 16. **G)** At week 16 there is a main effect of genotype ($F_{(1,14)}$=7.43, $p < 0.02$) and a genotype x exposure interaction ($F_{(1,14)}$=11.43, $p = 0.04$) on striatal Gly levels. YAC128-Veh Gly levels are elevated over WT-Veh, WT-Mn and YAC128-Veh ($p = 0.002$, $p = 0.009$, $p = 0.006$, respectively). **H)** There are significant main effects of genotype ($F_{(1,14)}$=9.12, $p < 0.001$) and exposure ($F_{(1,14)}$=5.75, $p < 0.05$) on striatal Ser at 16 weeks. Amino acid neurotransmitter means (week 13 n = 5-6 and week 16 n = 4-8) are plotted +/-SEM. Significant differences established by *pos-hoc* t-tests *$p < 0.05$, **$p < 0.01$, ##$p < 0.005$, and ***$p < 0.001$.

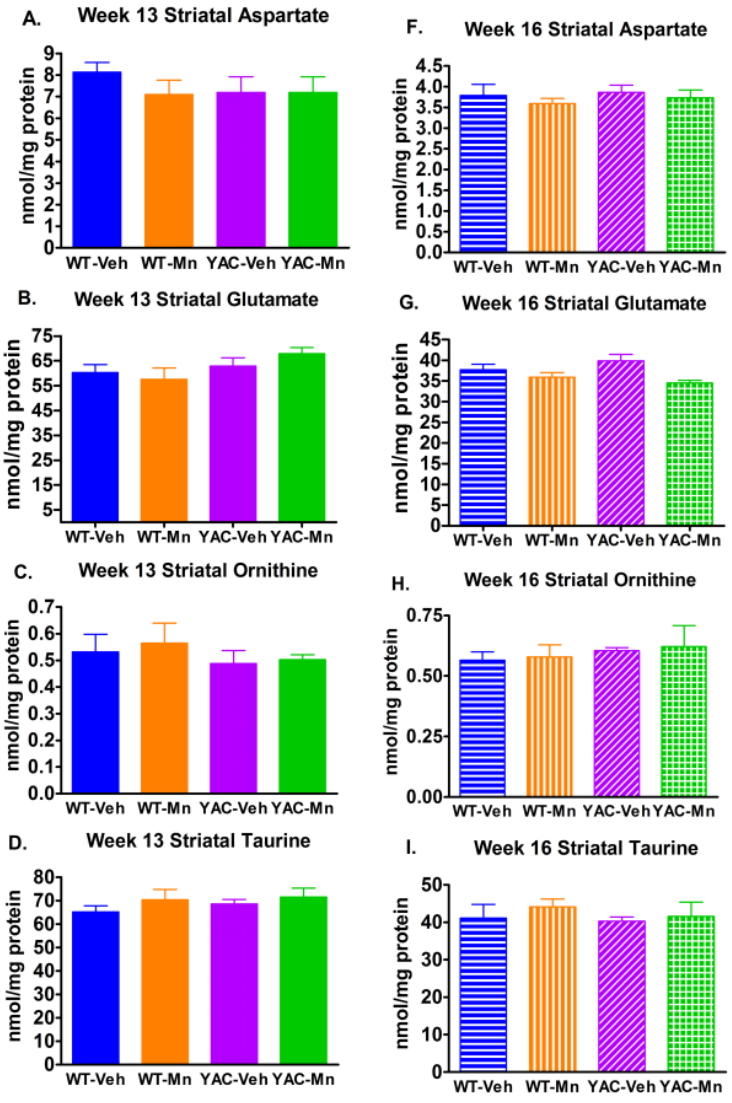

Figure 26. Striatal amino acids unaffected by Mn and genotype. Striatal amino acids including aspartate (**A, F**), glutamate (**B,G**), ornithine (**C, H**), taurine **(D,I)** and tyrosine (**E, J**) are unaffected by Mn and mutant *HTT* at 13 and 16 weeks. Additionally, isoleucine, leucine, valine, methionine, and phenylalanine were unaltered by Mn or mutant *HTT* (data not shown).

Striatal monoamine neurotransmitters were altered by Mn exposure and mutant *HTT* expression at 16 weeks

Monoamine neurotransmitters and metabolites, which have not been previously reported in the YAC128 mice, were also measured in the striatum at 13 and 16 weeks by HPLC. At 13 weeks, serotonin (5-HT) and the metabolite 5-hydroxyindoleacetic acid (5-HIAA, data not shown), dopamine (DA, Figure 27A) and its metabolites (Figure 27B), 3,4-dihydroxyphenylacetic acid (DOPAC), homovanillic acid (HVA) and, 3-methoxytyramine (3-MT), were not significantly different between genotype and exposure groups although the DA turnover rate, measured by the DOPAC/DA ratio (Figure 27B), was significantly affected by genotype ($F_{(1,18)}$=6.67, $p < 0.05$). DA turnover was reduced in YAC128-Mn compared to WT-Mn mice ($p < 0.05$). Overall, at 13 weeks there were no changes in striatal monoamine neurotransmitter levels, but the DA turnover rate was significantly affected by genotype.

By 16 weeks there were significant exposure and genotype effects on monoamine neurotransmitter levels in the striatum. Significant main effects of exposure occur for 5-HIAA ($F_{(1,17)}$=6.53, $p < 0.05$, data not shown), DA (Figure 27C, $F_{(1,17)}$=6.11, $p < 0.05$), DOPAC (Figure 27D, $F_{(1,17)}$=7.65, $p < 0.05$), and HVA (Figure 27D, $F_{(1,17)}$=12.91, $p < 0.005$) levels in the striatum. There were also significant main effects of genotype on DA ($F_{(1,17)}$=6.32, $p < 0.03$) and its metabolites DOPAC ($F_{(1,17)}$=6.77, $p < 0.02$) and HVA ($F_{(1,17)}$=7.22, $p < 0.02$). Serotonin levels were unaffected by Mn exposure or mutant *HTT*, but the 5-HT metabolite 5-HIAA was significantly reduced by Mn exposure (data not shown).

In Mn-exposed WT mice there was a non-significant reduction in 5-HIAA (p = 0.087) compared to vehicle, while YAC128 mice had a significant reduction in 5-HIAA levels in the striatum following Mn exposure (p = 0.016).

Striatal DA and its metabolites exhibited genotype and exposure effects at 16 weeks. DA levels (Figure 27C) were reduced by Mn exposure in WT mice ($p < 0.05$). YAC128-Veh mice had decreased striatal DA levels ($p < 0.05$) that were indistinguishable from WT-Mn levels. Unlike in WT mice, Mn exposure failed to decrease DA levels in YAC128 mice. Striatal DA levels in YAC128-Mn mice were similar to YAC128-Veh and WT-Mn levels. DA metabolites DOPAC and HVA (Figure 27D) were similarly affected by genotype and Mn exposure. Mn exposure reduced DOPAC and HVA levels in WT mice ($p < 0.01$). Similarly, YAC128-Veh mice had DOPAC and HVA levels reduced by approximately the same degree as WT-Mn versus WT-Veh ($p < 0.05$). DA metabolites in YAC128 mice were not further affected by Mn exposure with DOPAC and HVA levels were similar between YAC128-Mn, YAC128-Veh and WT-Mn mice. The DOPAC and HVA metabolite, 3-MT, was not significantly different in any group at 16 weeks (Figure 27D). The DOPAC/DA ratio was also unaltered at 16 weeks (Figure 27D). Analysis of striatal neurochemistry across time points revealed an age x exposure interaction for DOPAC ($F_{(1,37)}=4.28$, $p < 0.05$) and HVA ($F_{(1,37)}=5.12$, $p < 0.05$). These data revealed an effect of Mn exposure and genotype on the nigrostriatal dopaminergic system that only occurred at the later time point. Overall, at 16 weeks, Mn exposure reduced striatal DA and metabolites specifically only in WT animals. Mutant *HTT* reduced striatal DA and metabolites

as well, relative to WT-Veh. However, Mn exposure failed to show an effect on striatal DA and its metabolites in YAC128 mice.

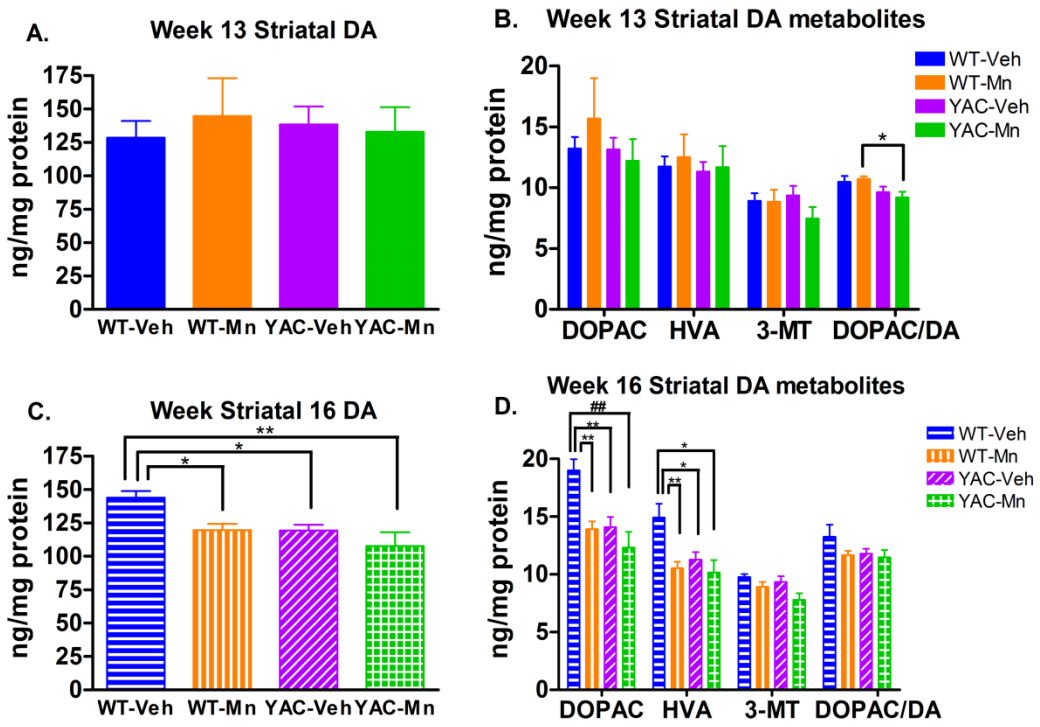

Figure 27. Striatal monoamine neurotransmitters and metabolites are more strongly affected at week 16 by Mn exposure and genotype.

A) There are no significant differences in striatal DA levels at week 13. **B)** There is no difference between striatal levels of DOPAC or HVA at week 13, however there is a significant main effect of genotype on ratio DOPAC/DA ($F_{(1,18)}$=6.67, $p < 0.02$). The turnover rate of DA is significantly lower in YAC128-Mn than WT-Mn ($p < 0.04$), and although lower it does not reach statistical significance compared to WT-Veh mice ($p = 0.053$). **D)** At week 16 there is a significant effect of genotype ($F_{(1,17)}$=6.32, $p = 0.022$ and treatment ($F_{(1,17)}$=6.11, $p = 0.024$) on striatal DA levels. WT-Mn, YAC128-Veh and YAC128-Mn have lower levels of striatal DA than WT-Veh mice ($p = 0.028$, $p = 0.033$ and $p =0.007$ respectively). **E)** There are also significant genotype and treatment effects on DA metabolites DOPAC (genotype: $F_{(1,17)}$=6.77, $p = 0.019$; treatment: $F_{(1,17)}$=7.66, $p = 0.013$) and HVA (genotype: $F_{(1,17)}$=7.22, $p = 0.016$; treatment: $F_{(1,17)}$=12.91, $p = 0.002$) at week 16. Levels of striatal DOPAC and HVA in WT-Mn, YAC128-Veh and YAC128-Mn are significantly lower than in WT-Veh mice ($p < 0.01$ and $p < 0.015$ respectively). Monoamine neurotransmitter and metabolite averages (week 13 n = 4-6 and week 16 n = 3-8) are graphed +/- SEM. Significance by *post-hoc* t-test *$p < 0.05$, **$p < 0.01$ and $^{\#\#}p < 0.005$.

Discussion

This study identifies novel *in vivo* correlates of a recently discovered gene-environment interaction between the disease-causing allele of *HTT* and Mn exposure revealed by analysis of striatal neurochemistry and MSN dendritic architecture. Additionally, we identified the age of onset for striatal dendritic neuropathology and neurochemical phenotypes in the YAC128 HD mouse model to be between 13 and 16 weeks of postnatal life, approximately corresponding to the age of onset for motor phenotypes (Menalled et al., 2009; Slow et al., 2003; Van Raamsdonk et al., 2005b).

Onset of YAC128 striatal neuropathology

Neuron morphology studies of striatal MSNs in R6/1(Spires et al., 2004), R6/2 (Klapstein et al., 2001), HD48 and HD89 (Guidetti et al., 2001) mice showed a decrease in spine density across branch order that was only evident in symptomatic mice (Klapstein et al., 2001). In the YAC128 mice, hyperkinetic activity is present at the initiation of Mn exposure at 12 weeks and motor impairment was just beginning at 16 weeks when we observed morphological changes in MSNs (Van Raamsdonk et al., 2005b). Milnerwood et al. (2010) found no morphological differences in striatal MSNs in YAC128 mice at 4 weeks of age. We detected no morphological or neurochemical associated abnormalities in YAC128-Veh mice at 13 weeks (Figure 22, Figure 23, Figure 25 and Figure 27). Our measurements on total dendritic length and total spine density for the 13 week WT-Veh and YAC128-Veh groups are nearly identical to

values reported by Milnerwood et al. (2010) (Figure 22). Morphological and neurochemical changes in the striatum of the YAC128 mice were observed at 16 weeks. YAC128 mice failed to show an increase in total dendritic length and dendritic branching that was apparent in WT mice from 13 to 16 weeks (Figure 24) indicating the onset of MSN neuropathology in YAC128 mice. YAC128 mice also failed to show a significant decrease in total spine density at 16 weeks (Figure 24). These subtle changes in neuron morphology may have large effects on synaptic input integration and transmission.

The morphological changes that we observed in YAC128-Veh mice at 16 weeks (Figures 22 thru 24) may be related to alterations in striatal neurotransmitter content. At 16 weeks YAC128-Veh mice had significantly lower levels of DA and its metabolites, DOPAC and HVA, (Figure 27) compared to WT-Veh mice. Reduced striatal DA levels and disturbances in dopaminergic signaling have also been observed in the R6/1 (Ortiz et al., 2011) and R6/2 mouse models of HD (Bibb et al., 2000; Cha et al., 1998; Johnson et al., 2006; Ortiz et al., 2010); however striatal DA levels were only altered in L-DOPA treated YAC128 mice (Tang et al., 2007). Not only was the nigrostriatal DA system altered in 16-week old YAC128-Veh mice, but the amino acids Gly and Ser were also elevated in the striatum (Figure 25). Elevated levels of Gly have also been detected in HD patient platelets (Reilmann et al., 1997) and CSF (Nicoli et al., 1993). Not only do YAC128 animals have an increase in NMDAR co-agonsists Ser and Gly, they also have an increase in NR2B expressing extrasynaptic NMDA receptors (Milnerwood *et al.* 2010). YAC128 animals are known to be sensitive to NMDAR

excitotoxicity and signaling through extrasynaptic NMDARs that have been shown to contribute to apoptosis of MSNs in these animals (Fernandes et al., 2007; Graham et al., 2009; Graham et al., 2006; Tang et al., 2005; Zeron et al., 2004; Zeron et al., 2002). Collectively, our data are consistent with N-methyl-D-aspartate receptor (NMDAR) dependent excitotoxicity in YAC128 mice at the 16-week time point. First, we found a reduction in striatal DA (Figure 27) that may result in less modulation of glutamatergic signaling at dendritic spines (Bamford et al., 2004). Secondly, an increase in striatal levels of NMDAR co-agonists Ser and Gly (Figure 25), which includes the metabolic pool of amino acids, may facilitate signaling through the NMDAR (Johnson and Ascher, 1987; Kartvelishvily et al., 2006). The facilitation of NMDAR signaling and dysregulation of glutamate release likely contributes to an excitotoxic environment (Milnerwood et al., 2010; Okamoto et al., 2009).

Mn exposure caused acute and chronic changes in striatal neurochemistry of WT mice

Mn exposure in WT mice influenced striatal neurochemistry at both 13 and 16 weeks (Figure 25 and Figure 27). Acute effects of Mn exposure included an increase in GABA and Cit (Figure 25) in WT mice at 13 weeks. These effects are likely a temporary response to Mn levels, as by 16 weeks these neurotransmitters levels returned to baseline levels. Mn exposure has been shown to increase expression of the enzyme nitric oxide synthase (NOS) that converts arginine into Cit and nitric oxide (NO) (Moreno et al., 2008). Cit levels

were elevated in the striatum only while Mn levels were elevated, suggesting that the effect of Mn on NOS expression is readily reversible. There was a significant decrease in striatal DA, HVA and DOPAC (Figure 27) at week 16 in WT-Mn mice, which was not present at 13 weeks. Previous studies using different Mn exposure paradigms have found similar alterations in striatal GABA and DA levels (Autissier et al., 1982; Gianutsos and Murray, 1982; Gwiazda et al., 2002; Lipe et al., 1999; Reaney et al., 2006; Struve et al., 2007; Vidal et al., 2005), although conflicting studies found that Mn exposure did not influence striatal Gly or DA levels (Burton et al., 2009; Kontur and Fechter, 1988; Olanow et al., 1996; Takeda et al., 2002; Takeda et al., 2003). The alterations in striatal neurotransmitter levels at 16 weeks have the potential to cause morphologic changes in MSNs. However, we failed to observe any significant effect of Mn exposure on MSN morphology at either age in WT mice (Figures 22 thru 24). This contrasts with our own previously published data suggesting that sub-acute Mn exposure results in morphological changes to striatal MSNs (Milatovic et al., 2009). One possible explanation for this discrepancy may be that the animals in the previous study were younger (6 to 8 weeks vs. 13 to 16 weeks postnatal herein) and a different inbred strain (C57Bl/6 vs. FVB). Nevertheless, data reported herein are consistent with other reports in the literature of Mn neurotoxicity causing damage to the nigrostriatal DA system (Guilarte et al., 2008; Guilarte et al., 2006; Stanwood et al., 2009).

Disease-toxicant interaction caused alteration in striatal neurochemistry

YAC128 mice showed less striatal Mn accumulation one day after final Mn exposure at 13 weeks compared to WT littermates (Figure 21). These data replicate findings from a previous study that utilized GFAAS to measure striatal Mn levels in similarly exposed YAC128 mice (Williams et al., 2010b). There are several potential mechanisms that may influence the differential Mn accumulation between genotypes; mutant *HTT* may interfere with import of Mn into the striatum or increase efflux of Mn from the striatum. Additional research is needed to determine the exact mechanism for differential striatal Mn accumulation between YAC128 and WT mice.

Mn exposure had significant effects on striatal neurochemistry in YAC128 mice. Changes in neurochemistry between 13 and 16 weeks in Mn exposed YAC128 and WT mice were complex. At 13 weeks, there were no significant morphological differences among the exposure groups (Figure 22 and Figure 23), but there were neurochemical changes in the striatum of YAC128-Mn mice. Mn exposure elevated striatal GABA and Cit in both genotypes, but Gly and Ser were only elevated in YAC128 mice (Figure 25). Proteomic analysis in the striatum of YAC128 mice exposed to Mn using the same exposure paradigm revealed an increase in D-3 phosphoglycerate dehydrogenase (PHGDH) levels at 13 weeks (unpublished data). The reaction catalyzed by PHGDH is the first and rate-limiting step in the synthesis of Ser and its activity regulates synthesis of D-Ser (Pizer, 1964; Yang et al., 2010). A direct correlation between levels of Gly

and Ser has been demonstrated in PHGDH deficiency (Klomp et al., 2000). Elevation of these amino acids at 13 weeks may represent an acute compensatory response to Mn exposure because the levels of these amino acids were normalized at 16 weeks (Figure 25) once Mn is cleared from the striatum. Interestingly, at 16 weeks the increased levels of Gly and Ser seen in YAC128-Veh mice compared to WT-Veh, were normalized by Mn exposure (Figure 25). D-Ser and Gly are co-agonists at the NMDAR and the increased levels of these amino acids in the striatum at 13 weeks may facilitate signaling through the NMDAR (Johnson and Ascher, 1987; Kartvelishvily et al., 2006). Additionally, Cit and therefore NO levels were elevated at 13 weeks in Mn exposed mice of both genotypes (Figure 25). NO has been shown to amplify Glu signaling, block Glu transporters and increase Glu release, thereby increasing the possibility of NMDAR excitotoxicity (Garthwaite, 2008; Guevara-Guzman et al., 1994; Lonart and Johnson, 1994; Pogun et al., 1994; Taskiran et al., 2003; West and Galloway, 1997). YAC128 mice express high levels of extrasynaptic NMDARs which may sensitize them to NMDAR excitotoxicity (Fernandes et al., 2007; Graham et al., 2009; Milnerwood et al., 2010; Shehadeh et al., 2006; Zeron et al., 2004; Zeron et al., 2002). The changes in striatal neurochemistry following Mn exposure did not affect every neurotransmitter; for example, 5-HT was unaffected by Mn at both 13 and 16 weeks (data not shown) and exposure to Mn did not reduce striatal DA levels in YAC128-Mn mice below YAC128-Veh or WT-Mn levels at 16 weeks (Figure 27).

The gene-environment interaction between mutant *HTT* and Mn is complex. For some phenotypes Mn exposure may suppress pathological changes occurring within the striatum of YAC128 HD mice. For example by restoring striatal Ser and Gly back to wild-type levels (Figure 25G and 25H). Such effects may be due to an amelioration of phenotypes caused by alterations in cellular Mn handling. For other phenotypes, YAC128 animals may suppress Mn-dependent phenotypes. For example, Mn exposure of YAC128 mice failed to lower striatal DA and metabolite levels further than YAC128-Veh mice (Figure 27C and 27D). Finally, for other phenotypes YAC128 animals may show increased sensitivity to Mn exposure. For example, acute elevations in striatal amino acids Gly and Ser at week 13 and morphological changes in striatal MSN at 16 weeks were all more severe in the YAC128 animals. Further studies need to be carried out to better understand this recently discovered disease-toxicant interaction. Nonetheless, our data strongly suggest that Mn exposure has the potential to influence HD onset or progression.

Conclusions

We set out to determine if Mn, mutant *HTT* or the combination of the two would alter striatal neurochemistry or MSN morphology. Overall, the answer is yes – but the direction and degree of the effects and interactions were varied and depended upon the specific phenotype being examined. We found that Mn exposure acutely alters striatal amino acid levels, but these acutely influenced amino acids return to baseline when Mn is eliminated from the striatum. Mn

exposure also has chronic effects on neurochemistry. Striatal DA is significantly reduced at 16 weeks in WT-Mn mice. However, we failed to detect morphological alterations in MSN dendrites of WT mice exposed to Mn at either time point. We identified the onset of alterations in striatal neurochemistry and MSN dendritic neuropathology at 16 weeks postnatal in YAC128 mice. The neurochemical changes that we identified may promote NMDAR excitotoxicity in the YAC128 mice. Finally, we identified *in vivo* correlates of a disease-toxicant interaction as anticipated by our previously reported *in vitro* interactions (Kwakye et al., 2011; Williams et al., 2010b). However, the finding of both restorative (Gly, Ser and DA neurochemistry) and degenerative effects (dendritic morphology changes) by Mn exposure on the early YAC128 mutant phenotypes suggests caution should be taken in determining the appropriate nutritional guidelines and environmental exposures to Mn for HD patients. Further investigation needs to be completed to determine the effect of the HD-Mn interaction on disease progression both at the neuroanatomical and behavioral level, as well as to gain insight into targets and mechanisms of disease modification.

CHAPTER VI

GENDER AND MANGANESE EXPOSURE INTERACTIONS ON MOUSE STRIATAL MEDIUM SPINY NEURON MORPHOLOGY

Abstract

Gender differences in sensitivity and toxicokinetics of multiple metals have been identified in humans. A recent study suggested that young girls performed worse on intellectual exams than young boys exposed to manganese (Mn) in the environment. Animal studies have shown that Mn exposure causes differential effects on behavior in male compared to female mice. We hypothesized that in response to Mn exposure striatal Mn accumulation and/or striatal medium spiny neuron (MSN) morphology show gender-dependent effects. We evaluated the contribution of gender to neuropathology by examining striatal MSN morphology in male and female mice exposed to Mn. We found that gender played a significant role in alterations of striatal MSN morphology in mice exposed to Mn. Gender-dependent changes were strongest when striatal Mn levels were elevated 24 hours following the final Mn exposure. Nevertheless, gender-dependent alterations in neuron morphology were still present 3 weeks after the final Mn exposure. Gender differences in neuron morphology were not due to differential striatal Mn accumulation between genders. We conclude that although gender does not affect striatal Mn accumulation, MSN morphology is differentially sensitive to elevated Mn levels.

Introduction

Gender differences in the toxicokinetics of xenobiotics have been previously reported (Clewell et al., 2002; Fletcher et al., 1994; Nicolson et al., 2010). These differences can be due to multiple factors; from differences in cytochrome P450 (CYP450) expression, transporter expression and influences of sex hormones on expression of these enzymes and transporters (Bonate, 1991; Harris et al., 1995). A limited number of studies have been conducted to examine gender differences in Mn toxicokinetics but none have examined morphological alterations as a function of gender.

Mn exposure typically occurs in occupational settings such as welding, smelting, Mn mining and working in a dry-cell battery factory (Bowler et al., 2006; Bowler et al., 2007a; Bowler et al., 2007b; Huang et al., 1989; Jiang et al., 2007; Ono et al., 2002; Wang et al., 1989; Zayed et al., 2003). Studies conducted in the general population, unexposed to high levels of Mn, have shown conflicting results. Men have been shown to have lower ferritin levels, reduced Mn absorption from the gastrointestinal tract and slower Mn clearance than women (Finley et al., 1994). Some studies indicate that in a healthy unexposed population, serum Mn levels are higher in men than women (Davis and Greger, 1992; Greger et al., 1990). However, more recent reports indicate that there is no gender difference in baseline serum Mn levels (Diaz et al., 2001; Rukgauer et al., 1997). One recent study explored intellectual function of children living in a Mexican Mn mining district. Children exposed to Mn had elevated levels (20x) of

Mn in hair and blood than children unexposed to high Mn levels. Young girls exposed to Mn performed worse on the revised Wechsler Intelligence Scale for Children than Mn exposed boys (Riojas-Rodriguez et al., 2010). Although there were no gender differences in Mn levels of exposed children, this suggests that cognitive performance may be differentially affected in boys and girls. Gender differences in response to metal exposure are not unique to Mn. Human studies have found gender differences in accumulation, storage and sensitivity to metals including cadmium (Cd), lead (Pb), Mn, mercury (Hg) and nickel (Ni) (Akesson et al., 2002; Akesson et al., 2005; Bjorkman et al., 2000; Grandjean et al., 1998; Gulson et al., 1998; Jin et al., 2004; Kobayashi et al., 2006; Manton et al., 2003; McKeown-Eyssen et al., 1983; Meding et al., 2001; Nielsen et al., 2002; Pounds et al., 1991; Uno et al., 2005; Vahter et al., 2007; Vahter et al., 2002). Animal studies also show gender differences in metal toxicokinetics and sensitivity. For example, male and female rats accumulated Mn differentially across body tissues following Mn exposure by inhalation; however, there was no difference in Mn accumulation in the striatum or other regions of the basal ganglia (Dorman et al., 2004). Gender differences in toxicokinetics following a single oral dose of the gasoline additive methylcyclopentadienyl manganese tricarbonyl (MMT) showed that female rats accumulated higher MMT levels than male rats due to slower clearance of MMT (Zheng et al., 2000). Erikson et al (2004a) exposed juvenile rats to airborne Mn for 13 weeks and found gender-specific changes in protein and mRNA expression of glutamine synthetase, metallothionein mRNA and glutathione levels in multiple regions of the brain. Gender differences in the

toxicokinetics of Mn are present regardless of route of administration and Mn speciation. As with humans, rodents show gender differences upon exposure to other metals such as Pb and Hg (Fortoul et al., 2005; Magos et al., 1981; Sager et al., 1984).

Mn overexposure results in motor symptoms that closely resemble Parkinson's disease (PD) (Calne et al., 1994; Lucchini et al., 2009). Acute high-level Mn exposure results in manganism, symptoms include cognitive, psychiatric and motor deficits. Motor symptoms of late-stage manganism are similar but distinct from idiopathic PD (Calne et al., 1994). Shared symptoms include rigidity and bradykinesia; however, manganism has a distinct cock-walk compared to the festinating gait observed in PD (Lucchini et al., 2009). Additionally, patients with manganism rarely show a sustained response to dopamine (DA) replacement therapy and fail to show reduced striatal DA uptake (Calne et al., 1994; Huang et al., 2003). More recently, studies have shown that chronic low level exposure to Mn is a risk factor for PD (Gorell et al., 1997; Gorell et al., 1999; Lucchini et al., 2009; Perl and Olanow, 2007). Mn accumulates preferentially in the basal ganglia, specifically the striatum, globus pallidus and substantia nigra (SN) (Aschner et al., 2005; Dobson et al., 2004; Dodd et al., 2005; Erikson et al., 2002; Erikson et al., 2004b; Fitsanakis et al., 2008; Olanow et al., 1996; Williams et al., 2010b). Rodent, non-human primate and human post-mortem research has found that the striatum shows damage following exposure to Mn (Aschner et al., 2007; Milatovic et al., 2009; Olanow, 2004; Perl and Olanow, 2007). Furthermore, the nigrostriatal DA system is impacted by Mn exposure (Guilarte et

al., 2008; Guilarte et al., 2006; Huang et al., 2003; Kessler et al., 2003; Kim et al., 2002; Stanwood et al., 2009). In PD, the pigmented DAergic neurons of the SN degenerate resulting in damage to striatal medium spiny neurons (MSN) (Day et al., 2006; Garcia et al., 2010; Wright et al., 2009; Zaja-Milatovic et al., 2005). Thus overlapping, but not identical brain regions are involved in Mn neurotoxicity and PD, with the striatal MSNs altered in both conditions.

Gender differences in prevalence, age of onset and progression have been described for PD (Haaxma et al., 2007; Miller and Cronin-Golomb, 2010; Shulman, 2007), however the influence of gender on behavior or neuropathology in Mn neurotoxicity has not been a major focus in the field of Mn toxicology. Females tend to have a later age of onset and less severe symptoms of PD. Gender studies in animal models of PD have also shown that estrogen plays a protective role in neuropathology and behavior. Survival of DA neurons following exposure to DA neurotoxicants, used in animal models of PD, is sensitive to gender (Richardson et al., 2008; Tamas et al., 2005). A study examining gender effects of 6-hydroxydopamine (6-OHDA) lesions on behavior and neuropathology showed that male rats are more sensitive to this toxicant than female rats. Male rats showed a greater loss of DA neurons in the SN and had greater deficits in locomotor activity than female rats (Tamas et al., 2005). This suggests that the nigrostriatal DA system is more sensitive to toxicants in male than female rodents. Animal models of manganism and PD share common features of neuropathology. Striatal neurodegeneration and damage to the nigrostriatal DA pathway is present in both diseases. A recent behavioral study suggests that

male mice are more susceptible to Mn exposure than female mice and that the behavioral deficit may be related to reduced striatal DA following Mn exposure (Moreno et al., 2009; Simon et al., 1994). A similar behavioral deficit has been found in a PD mouse model (George et al., 2008). Mn is known to cause damage to the nigrostriatal DA system and alter striatal MSN morphology (Guilarte et al., 2008; Guilarte et al., 2006; Milatovic et al., 2009; Stanwood et al., 2009), but gender specific changes in neuron morphology following Mn exposure have not been previously reported.

Previous studies carried out in our laboratory on female mice showed that their MSNs are vulnerable to Mn toxicity (Milatovic et al., 2009). Based on the literature of gender differences in Mn exposure, we hypothesized that gender may be a factor in Mn neuropathology. Therefore, we examined striatal MSN morphology and striatal Mn content 24 hours and 3 weeks following Mn exposure in mice of both genders to determine (1) if gender has an effect on MSN morphology in the presence or absence of Mn exposure, (2) if gender is a factor in striatal Mn accumulation and (3) if gender differences in MSN morphology are present when Mn levels return to baseline.

Results

Twelve-week-old mice were injected (s.c. hind limb) with Veh (water) or 50 mg/kg $MnCl_2$ (Mn) on experimental day 0, 3, and 6. MSN morphology was examined by Golgi silver impregnation on experimental day 7 (13 weeks old) and

day 28 (16 weeks old), which corresponds to 1 day and 3 weeks following the final Mn exposure, respectively.

Week 13

Total Neuron Measures

One day following the final Mn exposure, neuron morphology studies revealed a strong gender difference in neuron morphology. Total spine density was subject to a main effect of gender (Figure 28A, Table 7). Gender differences in total spine density were only present in Mn exposed mice. Female mice exposed to Mn (Mn-F) had MSNs with higher total spine density than Mn exposed male (Mn-M) mice ($p < 0.05$). There were no gender differences in total spine density of MSNs among Veh exposed mice. Additionally, we failed to detect a significant difference in total spine density between Veh and Mn exposed mice. A significant main effect of gender (Table 7) was found to affect total dendritic length one day post-exposure (Figure 28B). Gender differences in total dendritic length were only apparent in mice exposed to Mn. Mn-M mice had MSNs with significantly longer total dendritic length than Mn-F mice ($p = 0.001$). There was no significant difference in total dendritic length between genders of Veh exposed mice nor was there a significant difference between Veh and Mn exposed mice. Total spine number was also affected by gender (Table 7) one day post-exposure (Figure 28C). Mn-F mice had fewer total dendritic spines compared to Mn-M. This suggests that differences in total spine density were driven by differences in both total dendritic length and total spine number.

The total number of nodes, or dendritic branch points (Figure 28D), was subject to a main effect of gender (Table 7). Again, the only gender difference in total number of nodes was in Mn exposed mice. Mn-M mice had MSNs with more total nodes than Mn-F mice ($p = 0.005$). A main effect of gender (Table 7) was observed for the total number of dendrite endings (Figure 28E). Gender differences in total number of dendrite endings only occurred in Mn exposed mice. MSNs from Mn-M animals had more dendrite endings than Mn-F mice ($p < 0.01$). No significant difference in total nodes or total endings was found between Veh and Mn exposed mice. In general, at the 13 week time point gender differences were only present in Mn exposed mice. This held true for all total neuron measures. In most cases Mn exposure decreased measures of neuron morphology in female mice, except total spine density which was increased in female mice.

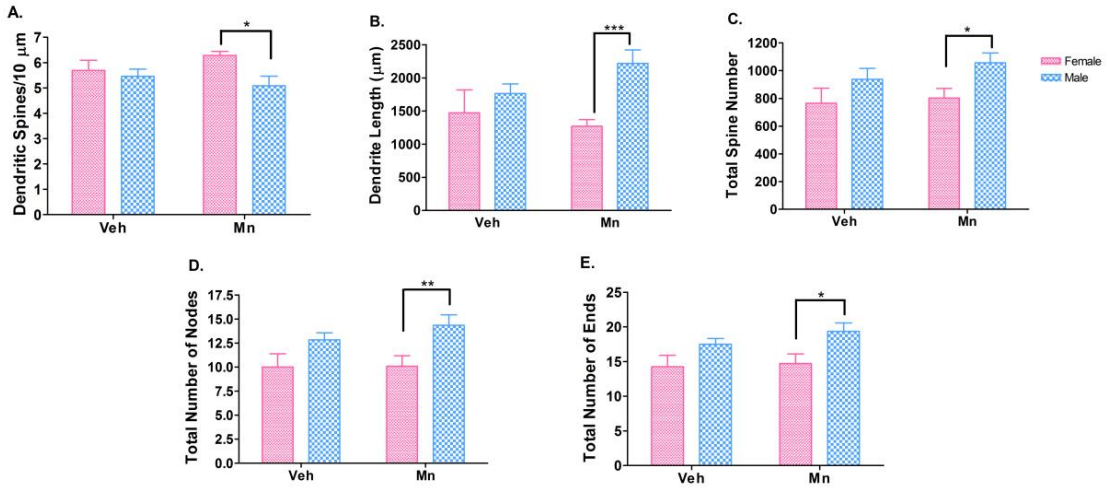

Figure 28. Mn exposed mice exhibit gender-specific changes in MSN morphology one day post-Mn exposure.

A) Total spine density was increased in female and decreased in male mice exposed to Mn ($p = 0.011$). **B)** Mn exposure increased total dendritic length in male mice but decreased total dendritic length in female mice ($p < 0.001$). **C)** Total number of spines were significantly different in male versus female Mn exposed mice ($p < 0.05$). **D)** Male mice exposed to Mn had a significantly higher number of total ends than Mn exposed female mice ($p < 0.011$). **E)** Mn exposed male mice had more total nodes than female Mn exposed mice ($p < 0.01$). Mean +/- SEM, * $p < 0.05$, # $p < 0.01$, *** $p < 0.001$.

Morphometric measures as a function of radius

Multiple measures of dendritic morphology were measured by Sholl analysis (Sholl, 1953). Briefly, concentric 10 μm circles were centered at the soma and dendrite measures were analyzed across these circles to give a more detailed view of neuron morphology. Repeated measures ANOVA were used to analyze neuron morphology as a function of distance from the soma. There was a significant main effect of distance x gender on dendritic branching complexity as a function of distance from the soma (Figure 29A, Table 7). Gender differences in branching complexity were present only in Mn exposed mice. There were no significant differences between Veh exposed MSNs or between Veh and Mn exposed MSNs. Branching complexity was significantly reduced in Mn-F mice compared to Mn-M mice ($p < 0.005$). Dendrite length as a function of distance from the soma was measured in concentric 10 μm shells (Figure 29B). There was a significant main effect of distance x gender on dendrite length as a function of distance from the soma (Table 7). Gender differences in dendrite length as a function of distance from the soma only occurred in Mn exposed mice. Mn-F mice had significantly shorter dendrite length per 10 μm shell than Mn-M mice ($p = 0.001$). There were no significant differences in dendrite length per shell in Veh exposed mice nor were there significant differences between Veh and Mn exposed mice. Distance x gender had an effect (Table 7) on spine number as a function of distance from the soma (Figure 29C). *Post hoc* analysis revealed that Mn-F mice had fewer dendritic spines per 10 μm shell than Mn-M mice ($p < 0.05$). Spine density as a function of distance from the soma (Figure

29D) was subject to a distance x gender effect (Table 7). *Post hoc* analysis failed to detect a statistically significant difference in spine density as a function of distance from the soma at one day post-exposure. In sum, main effects of gender were apparent for all measures of dendrite morphology one day post-exposure. Significant differences in neuron morphology across genders occurred only in mice exposed to Mn.

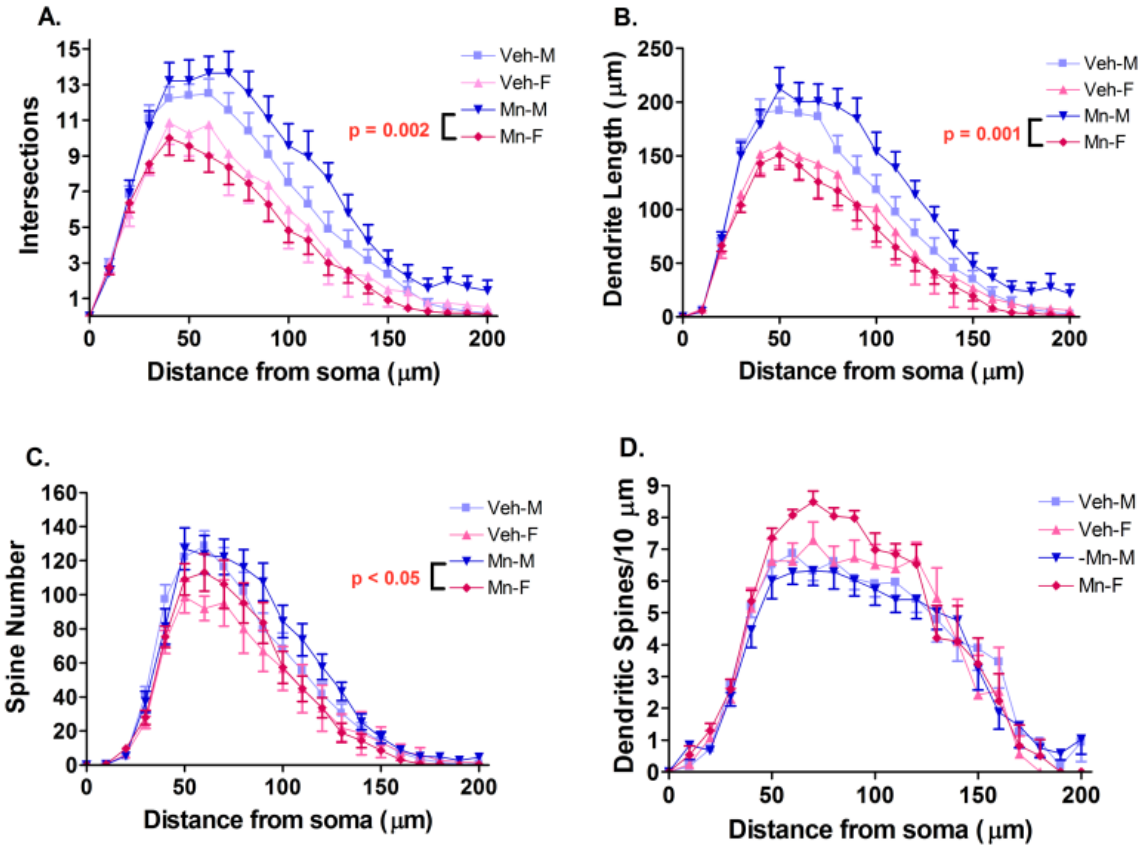

Figure 29. Mn exposure causes gender-dependent changes in neuron morphology as function of distance from soma at one day post-Mn exposure. **A)** Mn exposed mice showed gender differences in dendritic branching as a function of distance from the soma ($p < 0.005$). **B)** Gender differences in dendrite length as a function of distance from the soma were present in Mn exposed mice ($p < 0.001$). **C)** Mn exposure revealed significant gender differences in spine number as a function of distance from the soma ($p < 0.05$). **D)** There was no significant difference in spine density as a function of distance from the soma across groups at one day post-exposure. Mean +/- SEM, * $p < 0.05$, *** $p < 0.001$.

Table 7. ANOVA statistics for measures of neuron morphology one day post-exposure.

	Gender	Exposure	Gender x Exposure
Total Spine Density	**F(1,47)= 4.49, p < 0.05**	F(1,47)= 0.11, p > 0.70	F(1,47)= 2.09, p > 0.10
Total Dendritic Length	**F(1,47)= 9.71, p < 0.005**	F(1,47)= 0.41, p > 0.50	F(1,47)= 2.70, p > 0.10
Total Spine Number	**F(1,47)= 6.15, p < 0.05**	F(1,47)= 0.84, p > 0.30	F(1,47)= 0.23, p > 0.60
Total Nodes	**F(1,47)= 11.28, p < 0.005**	F(1,47)= 0.58, p > 0.40	F(1,47)= 0.46, p > 0.50
Total Ends	**F(1,47)= 10.21, p = 0.005**	F(1,47)= 0.90, p > 0.30	F(1,47)= 0.31, p > 0.50
Intersections by Radius	**F(30,1410)= 4.78, p < 0.001**	F(30,1410)= 0.34, p = 1.00	F(30,1410)= 0.94, p > 0.50
Dendrite Length by Radius	**F(30,1410)= 5.21, p < 0.001**	F(30,1410)= 0.56, p > 0.90	F(30,1410)= 0.94, p > 0.50
Spine Number by Radius	**F(30,1410)= 2.41, p < 0.001**	F(30,1410)= 0.98, p > 0.40	F(30,1410)= 0.661, p > 0.90
Spine Density by Radius	**F(17,799)= 1.67, p < 0.05**	F(17,799)= 0.68, p > 0.80	F(17,799)= 1.02, p > 0.40

Week 16

Total Neuron Morphology

Measures of MSN morphology three weeks post-exposure (age 16 weeks) were markedly different than at one day post-exposure (age 13 weeks). Only one metric of neuron morphology was affected by gender three weeks post-exposure. Total spine density (Figure 30A) was subject to a gender x exposure interaction (Table 8). The gender effect was only present in Mn exposed mice. Mn-F mice had significantly lower total spine density than Mn-M mice ($p < 0.05$). Mn exposure caused an increase in total spine density in male mice compared to Veh ($p < 0.05$); however, Mn exposure caused a decrease in total spine density in female mice compared to Veh ($p < 0.05$). Total dendritic length (Figure 30B), total spine number (Figure 30C), total number of nodes (Figure 30D) and total number of dendrite ends (Figure 30E) exhibited no significant effects of gender or Mn exposure. Most measures of neuron morphology do not show gender differences three weeks post-exposure, however Mn exposed mice showed gender differences in total spine density.

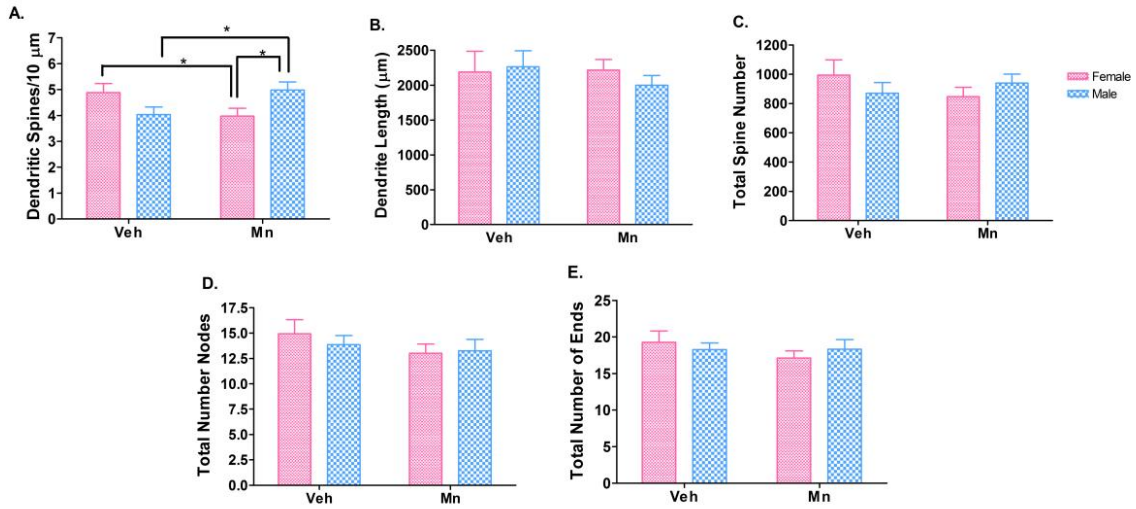

Figure 30. Gender specific changes in neuron morphology are present only in total spine density of Mn exposed mice three weeks post-Mn exposure.

A) Total spine density was the only measure of neuron morphology to have a significant gender difference three weeks post-exposure. Mn exposed male mice had a higher total spine density than Mn exposed female mice ($p < 0.05$). **B)** Total dendritic length, **C)** total number of spines, **D)** total nodes and **E)** total ends were not subject to gender effects three weeks after Mn exposure. Mean +/- SEM, * $p < 0.05$.

Morphometric measures as a function of radius

Dendrite measures as a function of distance from the soma three weeks post-exposure showed fewer changes in neuron morphology than one day post-exposure. Dendritic branching complexity (Figure 31A) and dendrite length (Figure 31B), measured by Sholl analysis, were not influenced by gender at three weeks post-exposure.

However, two measures of neuron morphology as a function of distance from the soma did show gender differences. Spine number as a function of distance from the soma (Figure 31C) was subject to an effect of distance x gender x exposure (Table 8). *Post hoc* tests did not reveal significant pairwise differences in spine number per 10 μm shell. Spine density as a function of distance from the soma (Figure 31D) was subject to main effects of distance x gender (Table 8), distance x exposure (Table 8) and a distance x gender x exposure interaction (Table 8). *Post hoc* analysis revealed that Mn exposure increased spine density as a function of distance from the soma in male mice compared to Veh exposure ($p < 0.05$). Veh-M mice had a decrease in spine density compared to Veh-F mice ($p < 0.05$).This is the only instance where a gender difference was observed in Veh exposed mice.

In summary, three weeks following Mn exposure there were few gender differences in neuron morphology. Spine number as a function of distance from the soma was subject to a distance x gender x exposure interaction. Spine density as a function of distance from the soma was subject to distance x gender, distance x exposure and distance x gender x exposure effects; however, this was

the only measure of neuron morphology to show gender differences in Veh exposed mice.

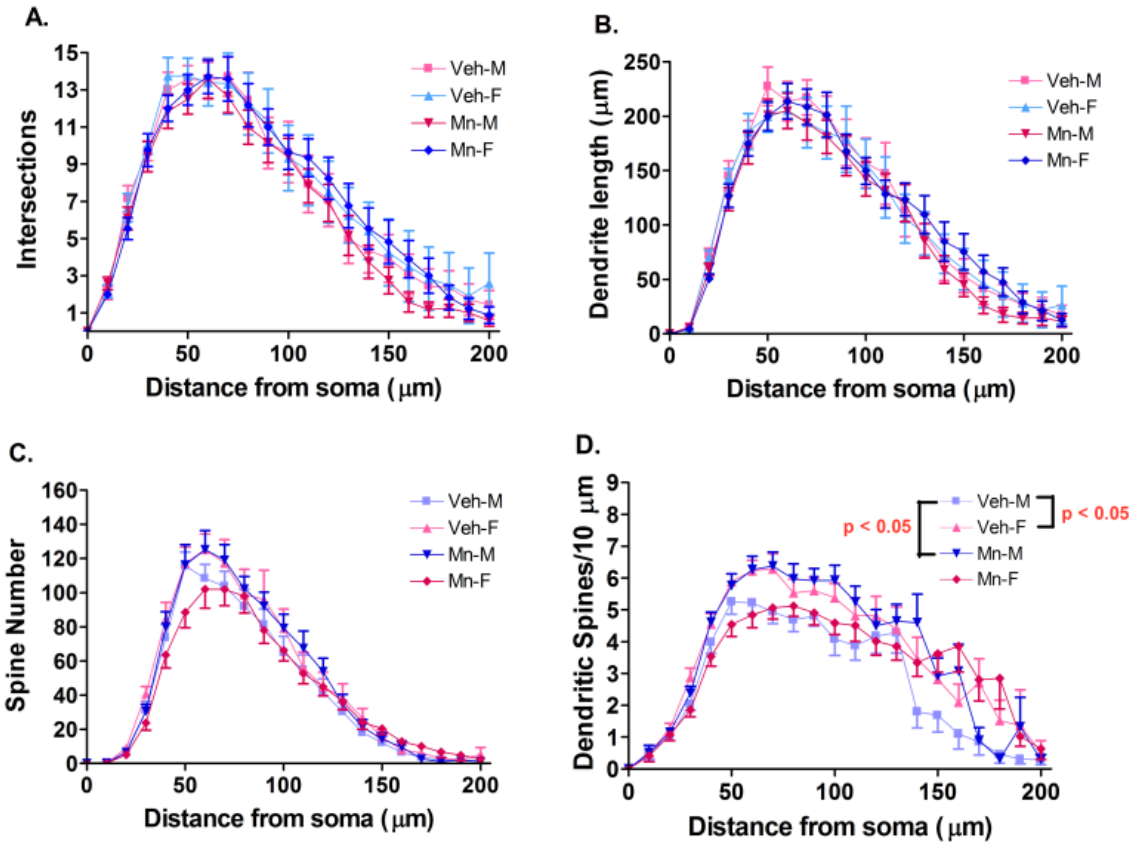

Figure 31. Few gender differences persist three weeks following Mn exposure. **A)** Dendritic branching as a function of distance from the soma and **B)** dendrite length as a function of distance from the soma exhibit no differences in neuron morphology across all groups. **C)** Spine number as a function of distance from the soma was subject to a distance x gender x exposure interaction ($F_{(30,2940)}$= 2.11, $p < 0.001$), but *post hoc* tests failed to find a significant difference. **D)** Mn exposure increased spine density as a function of distance from the soma in male mice vs Veh exposure ($p < 0.05$). A gender difference was present in Veh exposed mice ($p < 0.05$). Mean +/- SEM, * $p < 0.05$.

Table 8. ANOVA statistics for measures of neuron morphology three weeks post-exposure.

	Gender	Exposure	Gender x Exposure
Total Spine Density	F(1,55)= 0.60, p > 0.80	F(1,55)= 0.004, p > 0.90	**F(1,55)= 8.47, p = 0.005**
Total Dendritic Length	F(1,55)= 0.11, p > 0.70	F(1,55)= 0.32, p > 0.50	F(1,55)= 0.48, p > 0.40
Total Spine Number	F(1,55)= 0.02, p > 0.80	F(1,55)= 0.09, p > 0.70	F(1,55)= 2.72, p > 0.10
Total Nodes	F(1,55)= 0.14, p > 0.70	F(1,55)= 0.1.38, p > 0.20	F(1,55)= 0.37, p > 0.50
Total Ends	F(1,55)= 0.01, p > 0.90	F(1,55)= 0.78, p > 0.30	F(1,55)= 0.85, p > 0.30
Intersections by Radius	F(30,1530)= 0.58, p > 0.90	F(30,1530)= 0.53, p > 0.90	F(30,1530)= 0.43, p > 0.90
Dendrite Length by Radius	F(30,1530)= 0.46, p > 0.90	F(30,1530)= 0.40, p > 0.90	F(30,1530)= 0.20, p > 0.90
Spine Number by Radius	F(30,1530)= 0.55, p > 0.90	F(30,1530)= 0.66, p > 0.90	**F(30,1530)= 1.55, p < 0.05**
Spine Density by Radius	**F(17,867)= 2.10, p < 0.01**	**F(17,867)= 2.65, p < 0.001**	**F(17,867)= 1.73, p < 0.01**

Effects of gender on sensitivity to Mn across age

Mice at three weeks post-exposure did not show the same gender sensitivity to Mn exposure as mice one day post-exposure. We examined neuron morphology across time from exposure groups to gain a better understanding of factors important to this difference in susceptibility. Total spine density (Table 9) was subject to a main effect of time from exposure (Table 10) and a time from exposure x gender x exposure interaction (Table 10). Mn exposed mice had differential changes in total spine density across gender at both time points ($p < 0.05$). Time from exposure dependent changes in total spine density were observed in Veh exposed male mice and Mn exposed female mice ($p < 0.01$). Mn exposure had opposing effects on total spine density in male and female mice at three weeks post-exposure ($p < 0.05$) but no significant effect one day post-exposure. Total dendritic length (Table 9) was subject to a main effect of time from exposure (Table 10) and a time from exposure x gender interaction (Table 4). These effects were due to the fact that gender effects only occurred one day post-exposure in Mn exposed animals ($p < 0.005$). Time from exposure had a significant effect on total dendritic length in female mice only. Mn and Veh exposed female mice had an increase in total dendritic length three weeks post-exposure compared to one day post-exposure ($p < 0.05$).

Total number of nodes (Table 9) was subject to a main effect of gender (Table 10), time from exposure (Table 10) and a time from exposure x gender interaction (Table 10). A gender difference in total number of nodes was only present one day post-exposure in Mn exposed mice ($p < 0.01$). Total number of

nodes changed from one day to three weeks post-exposure in female mice only in both Mn and Veh exposed mice ($p < 0.05$) The total number of ends (Table 9) was subject to a main effect of gender (Table 10), time from exposure (Table 10) and a time from exposure x gender interaction (Table 10). Gender differences in total number of endings only occurred in Mn exposed mice one day post-exposure ($p <0.01$). A time from exposure effect was present only in Veh exposed female mice ($p < 0.05$).

Dendritic branching as a function of distance from the soma was subject to a distance x time from exposure effect (Table 10), a distance x gender effect (Table 10) and a distance x time from exposure x gender interaction (Table 10). Dendritic branching complexity in 13 but not 16 week old Mn exposed mice was subject to gender effects (Figure 29 and Figure 31). Gender differences in dendritic branching complexity were present in 13 week Mn exposed mice only ($p < 0.005$). The effect of time from exposure was present in both Mn and Veh exposed female mice ($p < 0.05$). Dendrite length as a function of distance from the soma (Figure 29 and Figure 31) was subject to a distance x time from exposure effect (Table 10), a distance x gender effect (Table 10) and a distance x time from exposure x gender interaction (Table 10). Similar to dendritic branching complexity, gender differences were only present in Mn exposed mice at one day but not three weeks after Mn exposure ($p < 0.005$). Also, time from exposure effects were found in both Mn and Veh exposed female mice ($p < 0.05$). Spine number as a function of distance from the soma (Figure 29 and Figure 31) was subject to a distance x gender effect (Table 10). However, *post*

hoc analysis failed to detect a significant difference between exposure groups. Spine density as a function of distance from the soma (Figure 29 and Figure 31) was subject to a distance x time from exposure (Table 10), distance x time from exposure x exposure (Table 10), a distance x time from exposure x gender effect (Table 10) and a distance x time from exposure x gender x exposure effect (Table 10). Mn exposure had an effect at three weeks post-exposure in male mice only ($p < 0.05$). A gender dependent difference in spine density as a function of distance from the soma was present only in Veh exposed female mice at three weeks ($p < 0.05$). An effect of time from exposure was present in Mn exposed female mice and Veh exposed male mice ($p < 0.001$).

In summary, mice one day post-exposure were more susceptible to gender differences in response to Mn exposure than at three weeks post-exposure. One day following Mn exposure all measures of neuron morphology were subject to gender based differences in response to Mn exposure. At three weeks post-exposure there were only two measures of neuron morphology that changed differently across gender following Mn exposure: total spine density and spine number as a function of distance from the soma. Spine density as a function of distance from the soma was the only characteristic of neuron morphology to show gender differences in Veh exposed mice. The only measure of neuron morphology subject to gender effects at both one day and three weeks post-exposure was total spine density.

Table 9. Mean values of MSN morphology characteristics.

	Total Spine Density	Total Dendritic Length	Total Spine Number	Total Nodes	Total Ends
13-Veh-F	5.686 ± 0.4028	1472 ± 345.2 [b]	765 ± 108.4	10 ± 1.389 [b]	14.25 ± 1.645
13-Veh-M	5.46 ± 0.2776	1765 ± 144.1	937.4 ± 80.17	12.83 ± 0.7242	17.5 ± 0.8135
13-Mn-F	6.282 ± 0.1624 [a,b]	1272 ± 98.42 [a,b]	802.7 ± 69.2	10.09 ± 1.083 [a,b]	14.73 ± 1.376 [a]
13-Mn-M	5.089 ± 0.3766 [a]	2218 ± 203.8 [a]	1057 ± 70.74	14.36 ± 1.087 [a]	19.36 ± 1.221 [a]
16-Veh-F	4.88 ± 0.3517	2187 ± 297.3 [b]	994.6 ± 105.1	14.92 ± 1.401 [b]	19.25 ± 1.577
16-Veh-M	4.032 ± 0.2898 [b]	2263 ± 228.2	870.9 ± 73.32	13.86 ± 0.8948	18.29 ± 0.9104
16-Mn-F	3.974 ± 0.3002 [a,b,c]	2214 ± 154.6 [b]	847.2 ± 63.95	13 ± 0.9034 [b]	17.12 ± 0.9847
16-Mn-M	4.978 ± 0.3188 [a,c]	1998 ± 141.4	940.5 ± 61.11	13.25 ± 1.122	18.33 ± 1.287

a $p < 0.05$ vs opposite gender

b $p < 0.05$ vs age counterpart

c $p < 0.05$ vs Veh exposure

[d] Groups named by age (weeks)-exposure group-gender. Data listed as mean ± SEM.

Table 10. ANOVA statistics for time from exposure analysis for measures of neuron morphology.

	Time from Exposure	Gender	Exposure	Gender x Exposure	Time from Exposure x Gender	Time from Exposure x Exposure	Time from Exposure x Gender x Exposure
Total Spine Density	**F(1,98)= 25.36, p < 0.001**	F(1,98)= 1.86, p > 0.10	F(1,98)= 0.08, p > 0.70	F(1,98)= 0.92, p > 0.30	F(1,98)= 2.89, p > 0.09	F(1,98)= 0.04, p > 0.80	**F(1,98)= 9.28, p < 0.005**
Total Dendritic Length	**F(1,98)= 11.06, p < 0.001**	F(1,98)= 3.56, p = 0.06	F(1,98)= 0.001, p > 0.90	F(1,98)= 0.39, p > 0.50	**F(1,98)= 11.06, p < 0.001**	F(1,98)= 0.71, p > 0.40	F(1,98)= 2.63, p > 0.10
Total Spine Number	F(1,98)= 0.19, p > 0.60	F(1,98)= 3.12, p > 0.08	F(1,98)= 0.24, p > 0.60	F(1,98)= 2.11, p > 0.10	F(1,98)= 3.86, p = 0.052	F(1,98)= 0.78, p > 0.30	F(1,98)= 0.54, p > 0.40
Total Nodes	**F(1,98)= 6.53, p < 0.05**	**F(1,98)= 4.31, p < 0.05**	F(1,98)= 0.09 , p > 0.70	F(1,98)= 0.82, p > 0.30	**F(1,98)= 6.82, p < 0.01**	F(1,98)= 1.87, p > 0.10	F(1,98)= 0.002, p > 0.90
Total Ends	**F(1,98)= 4.37, p < 0.05**	**F(1,98)= 5.64, p < 0.05**	F(1,98)= 0.01, p > 0.90	F(1,98)= 1.08, p > 0.30	**F(1,98)= 4.97, p < 0.05**	F(1,98)= 1.67, p > 0.20	F(1,98)= 0.06, p > 0.80
Intersections by Radius	**F(30,2940)= 1.49, p = 0.05**	**F(30,2940)= 4.53, p = 0.001**	F(30,2940)= 0.39, p > 0.90	F(30,2940)= 0.32, p > 0.90	**F(30,2940)= 2.80, p < 0.001**	F(30,2940)= 0.37, p > 0.90	F(30,2940)= 0.64, p > 0.90
Dendrite Length by Radius	**F(30,2940)= 2.40, p = 0.001**	**F(30,2940)= 5.15, p = 0.001**	F(30,2940)= 0.50, p > 0.90	F(30,2940)= 0.29, p > 0.90	**F(30,2940)= 2.12, p < 0.001**	F(30,2940)= 0.39, p > 0.90	F(30,2940)= 0.81, p > 0.70
Spine Number by Radius	F(30,2940)= 0.44, p > 0.90	**F(30,2940)= 2.11, p < 0.001**	F(30,2940)= 0.90, p > 0.60	F(30,2940)= 0.70, p > 0.80	F(30,2940)= 1.06, p > 0.30	F(30,2940)= 0.79, p > 0.70	F(30,2940)= 1.42, p = 0.07
Spine Density by Radius	**F(17,1666)= 5.24, p < 0.001**	F(17,1666)= 1.02, p > 0.40	F(17,1666)= 1.12, p > 0.30	F(17,1666)= 0.86, p > 0.60	**F(17,1666)= 2.71, p < 0.001**	**F(17,1666)= 1.75, p < 0.05**	**F(17,1666)= 1.75, p < 0.05**

Striatal Mn levels are insensitive to gender

Because there were gender differences in striatal MSN morphology in WT mice exposed to Mn, we analyzed striatal Mn levels by ICP-MS (Figure 32) to determine if gender plays a role in striatal Mn accumulation or if Mn levels can alter neuron morphology. At 24 hours following the last Mn exposure (Figure 32A), there was a significant effect of exposure ($F_{(1,10)}$= 405.89, $p < 0.001$). No significant effects of gender or a gender x exposure interaction were detected. Mn exposed mice of both genders had elevated striatal Mn levels compared to all Veh exposed mice ($p < 0.001$). There was no difference in striatal Mn between genders ($p > 0.7$). By three weeks Mn was almost completely cleared from the striatum (Figure 32B). There was only a trend towards statistical significance for the main effect of exposure ($F_{(1,6)}$= 4.50, $p = 0.078$) on striatal Mn levels. Again, there was no effect of gender and no gender x exposure interaction for striatal Mn at three weeks post-exposure. Our data show that gender plays no role in differential Mn accumulation in the striatum. Therefore, differential striatal Mn accumulation cannot account for gender differences in neuron morphology in Mn exposed mice.

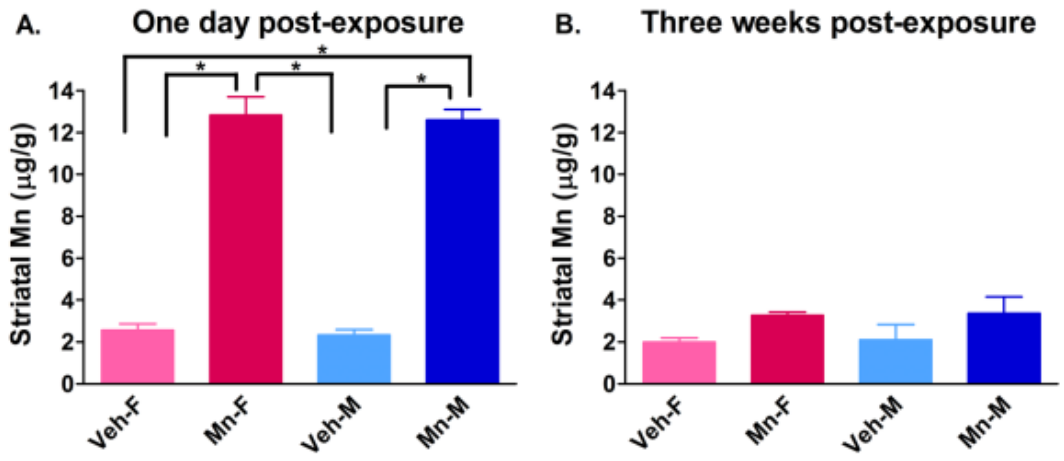

Figure 32. No gender difference in striatal Mn accumulation.

A) Mn exposure significantly elevated striatal Mn above Veh exposed mice ($p < 0.001$), but there was no difference in Mn accumulation between genders ($p > 0.70$). **B)** Striatal Mn was eliminated from the striatum by three weeks following exposure. No gender differences in striatal Mn were present. Mean +/- SEM, *** $p < 0.001$.

YAC128 mice show no gender differences

YAC128 mice exhibited no gender-dependent differences in neuron morphology. Veh exposed mice did not show gender differences in neuron morphology at 13 or 16 weeks. Unlike WT mice, Mn exposure of YAC128 mice did not result in gender-dependent differences in neuron morphology at either time point.

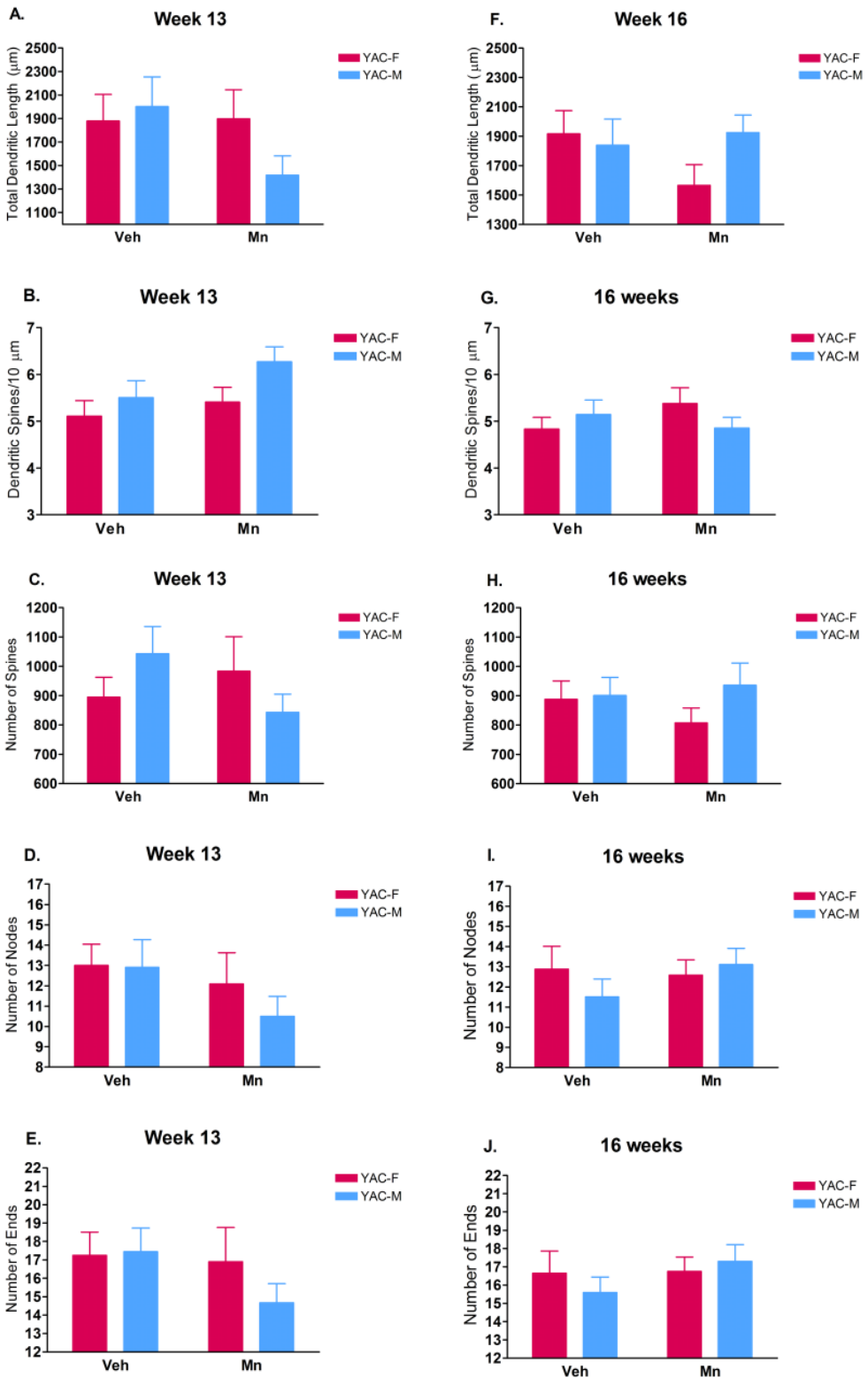

Figure 33. YAC128 neuron morphology is not affected by gender.

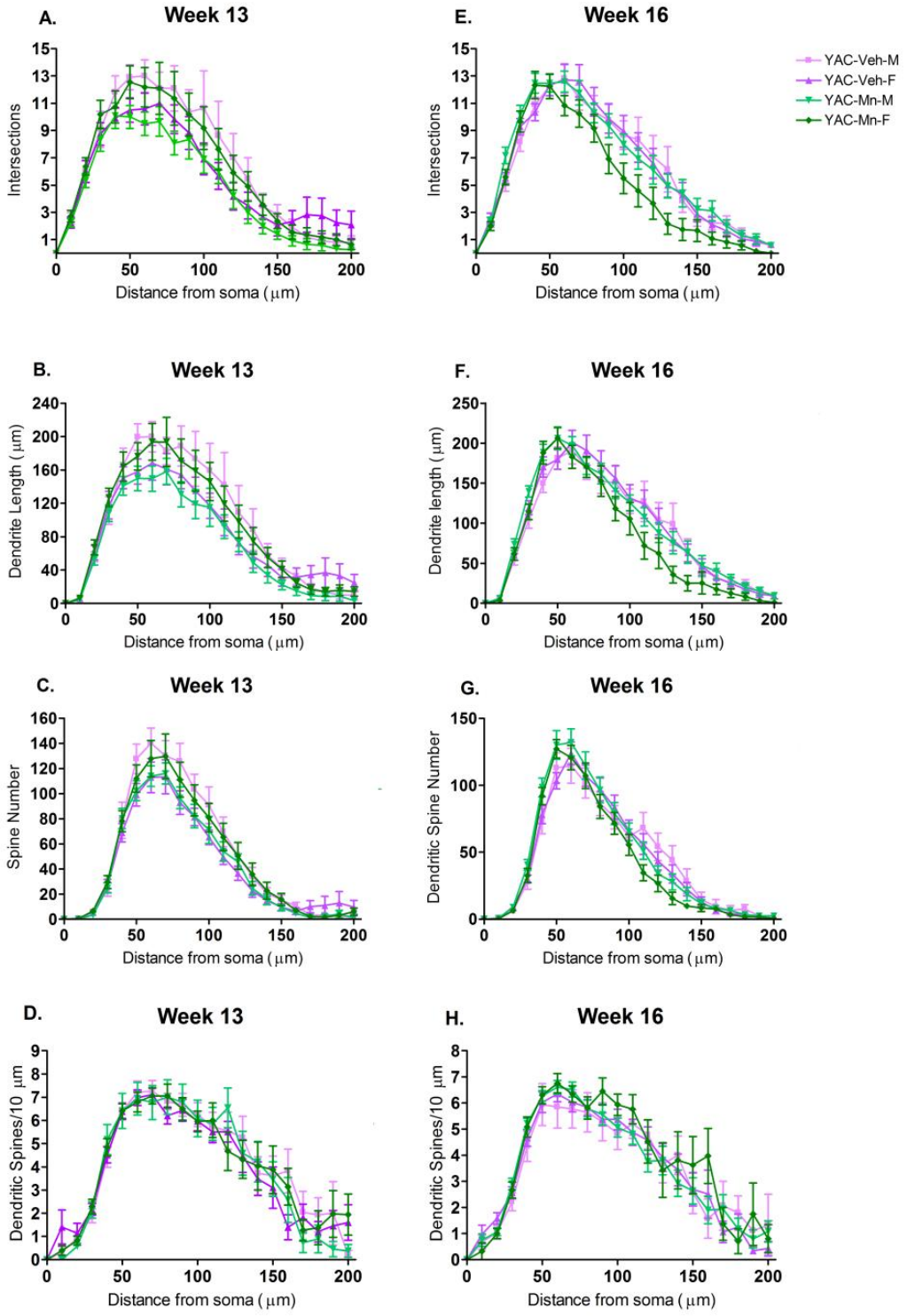

Figure 34. YAC128 MSN morphology as a function of distance from the soma is not affected by gender.

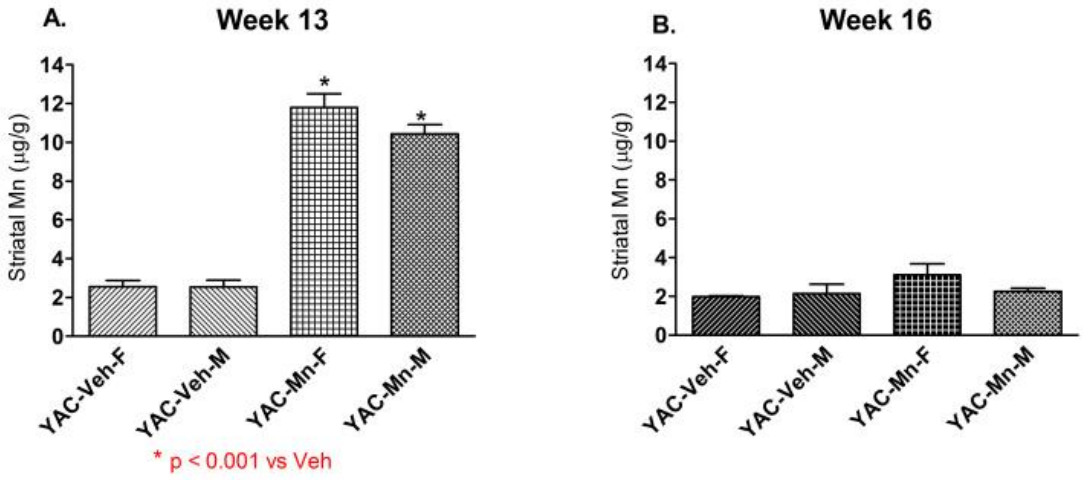

Figure 35. Mn accumulation in the striatum of YAC128 mice is not affected by gender.

Discussion

In this study we report gender-specific changes in striatal MSN morphology in mice exposed to Mn. We demonstrate that these gender-specific alterations in MSN morphology are not due to differential accumulation of Mn in the striatum of these mice. The gender effects were most pronounced one day post-exposure when Mn levels are elevated, but were also present at three weeks after Mn levels returned to baseline. To our knowledge, this is the first demonstration of gender-dependent differences in neuropathology following Mn exposure.

Gender differences parallel striatal Mn levels

Gender differences in neuron morphology parallel striatal Mn levels. Differences in neuron morphology between genders were more prevalent one day post-exposure when Mn levels were elevated (Figures 1 and 2). We detected no difference between genders in Mn accumulation in the striatum (Figure 5). This suggests that excess Mn may interact with gender-specific hormones to alter neuron morphology. When striatal Mn returns to baseline levels, most gender differences in neuron morphology disappear. However, there are long lasting gender-dependent changes in neuron morphology that remain, even when Mn levels have returned to baseline three weeks post-exposure (Figures 3 and 4). This suggests that these changes are not solely dependent on transient increases in Mn levels, but that neuron morphology has been altered long-term.

The results extend findings from a previous study from our laboratory examining MSN morphology in female mice only (Milatovic et al., 2009). The previous study used the same exposure schedule as ours; however C57Bl/6 mice were exposed to a higher dose of Mn (100 mg/kg $MnCl_2$) at a younger age (6-8 weeks old) than in our study. Only female mice were used in that experiment and were sacrificed 24 hours after the last exposure, which is equivalent in duration to our one day post-exposure time point. Milatovic et al. (2009) found a decrease in total dendritic length and total spine number in Mn exposed mice. Although our results do not show a statistically significant decrease in total dendritic length in Mn-F vs Veh-F mice (Figure 1), Mn-F MSNs do have shorter total dendritic length compared to Mn-M ($p < 0.001$). Similarly, we saw a significant difference in total spine number, total spine density, total number of nodes and total number of endings between Mn-F and Mn-M MSNs (Figure 1). Milatovic et al. (2009) showed that female mice experience changes in MSN morphology after Mn exposure and our findings add to this by demonstrating that these changes in MSN morphology are gender-specific.

Gender differences in neuron morphology in the literature

Few accounts of gender differences in environmental modulation of neuron morphology, regardless of brain region, have been reported in the literature. Two examples are chronic restraint stress and environmental enrichment (EE), both of which have been shown to have differential effects on neuron morphology depending on gender (Galea et al., 1997; Juraska, 1984;

Juraska et al., 1985; Juraska et al., 1989). In the case of chronic restraint, male rats had a decrease in CA3 pyramidal cell apical branching and dendritic length while the apical branches of female rats were unaffected. However, female rats did experience decreased branching complexity in the basilar dendritic arbor (Galea et al., 1997). EE affected pyramidal neurons in visual cortex differently than in the dentate gyrus and CA3 region of the hippocampus. In the visual cortex, EE caused an increase in dendrite length of layer III and layer IV pyramidal cells from male rats (Juraska, 1984). In the dentate gyrus, female rats with EE showed an increase in branching complexity compared to males (Juraska et al., 1985). EE caused differential changes in the apical arbor of CA3 pyramidal cells across gender and radius from the soma. Proximal to the soma, CA3 pyramidal cells from female rats with EE had a higher branching complexity than males with EE. Distal to the soma, male rats had CA3 pyramidal cells with a higher branching complexity than female rats with EE (Juraska et al., 1989). In each of these examples, the exposure had a different effect on neurons from each gender. There were differential effects on neurons in different brain regions from the same exposure. These studies provide evidence that neurons can respond differently to an environment based on the gender of the animal.

Interestingly, in our study several parameters of neuron morphology (Figure 1 and Figure 3) showed gender-specific changes in opposite directions upon exposure to Mn. Compared to females, male mice exposed to Mn showed larger changes in neuron morphology (Figure 1 and 2). Gender differences in MSN morphology in control animals have not been previously reported in the

literature. We found only one instance in which there was a gender difference in neuron morphology in Veh exposed mice (Figure 4D). However the majority of our data suggest that gender differences in MSN morphology are only revealed upon exposure to an insult (Figure 1-4). If gender is ignored, Mn exposure was not sufficient to cause significant changes in neuron morphology from control, one day following our 1-week exposure paradigm; however, Mn exposure did cause differential responses of MSNs between genders. Estrogen may be responsible for the gender specific changes in neuron morphology upon exposure to Mn (Lee et al., 2009a; Lee et al., 2009b).

Estrogen may be neuroprotective

Mn neuropathology shares similarities to PD neuropathology (Garcia et al., 2010; Milatovic et al., 2009; Stanwood et al., 2009; Zaja-Milatovic et al., 2005). Gender differences in PD have been frequently documented (Miller and Cronin-Golomb, 2010; Shulman, 2007). Men have a higher risk of PD (2:1), an earlier age of onset, and present with bradykinesia or rigidity. Females have an average age of onset 2 years later than males and present with resting tremor as their first sign of disease. Nigrostriatal dopamine (DA) uptake binding sites were quantified by single photon emission computed tomography (SPECT) using the radioligand [^{123}I]FP-CIT and women were found to have more binding sites for DA uptake than men (Haaxma et al., 2007). The later onset in PD, milder initial symptoms and a nigrostriatal DA system that is more intact in females has been hypothesized to be due to estrogen. Estrogen has been shown to play a role in

maintaining nigrostriatal DA neurons and in striatal MSN maturation (Leranth et al., 2000; Stroppolo et al., 2004). Female rodents are less sensitive to nigrostriatal damage due to DA toxicants (Richardson et al., 2008; Tamas et al., 2005). Estrogen has been shown to be protective in multiple neurotoxicant models of PD (Baraka et al., 2011; Miller et al., 1998; Morale et al., 2008; Ookubo et al., 2008; Smith et al., 2007). Similarly, primary cortical neurons and astrocytes are protected from Mn-induced toxicity by pre-treatment with estrogen or tamoxifen (Lee et al., 2009a; Lee et al., 2009b). Moreno et al. (2011) recently demonstrated that young male mice supplemented with estrogen do not exhibit decreased striatal DA levels. Additionally, protein nitrosylation in the SN and glial inflammatory signaling in the striatum and SN are decreased in estrogen supplemented male mice exposed to Mn. These data suggest that changes in MSN morphology in female mice exposed to Mn (Figure 1 and 2) may be less pronounced as a result of higher estrogen levels (compared to males).

Changes in total spine density similar to what we observed in our mouse model, may lead to parkinsonian-like symptoms in Mn-exposed humans. This is because MSN dendritic spines are the primary recipients of glutamatergic and DA input to the striatum. This input is critical to normal motor function. If the input to the striatum is altered, the ability of the striatum to integrate and relay information through the extrapyramidal motor system, and therefore motor function, may be impaired (Deutch et al., 2007). Alterations in total spine density are evident in MSNs from post-mortem human PD patients and animal models of

PD both of which show motor dysfunction similar to manganism associated motor symptoms (Garcia et al., 2010; Zaja-Milatovic et al., 2005).

YAC128 mice do not show gender difference

YAC128 mice did not show gender differences in neuron morphology following Veh or Mn exposure. This suggests that mHTT can interact with sex hormones or Mn in a way that blocks the gender specific differences in neuron morphology from occurring. Gender differences in YAC128 mice have been observed for various motor and behavior phenotypes (Bode et al., 2008; Dorner et al., 2007; Orr et al., 2008; Zajac et al., 2010). Male YAC128 mice had a reduced total distance traveled in an open field test compared to female mice at 16 weeks (Menalled 2009). The gender differences in total distance traveled are not due to gender specific differences in MSN morphology at this age since we detected no significant gender differences in YAC128 mice. However, the genotype effect of reduced motor activity may be related to changes in neuron morphology that we previously reported (Madison et al., 2011). Other gender differences in weight, rearing activity and light-dark preference occurred at older ages not relevant to this study (Menalled 2009).

Conclusions

In summary, we report gender differences in striatal MSN morphology in response to elevated Mn levels in WT but not YAC128 mice. These gender dependent changes in neuron morphology correlated with elevated Mn in the

striatum, however this was not due to differential Mn accumulation between genders. Although the gender effects were more prevalent at 13 weeks when Mn levels were elevated, we also observed gender effects at 16 weeks when Mn levels were back to baseline. These data raise three important points to consider in future studies of Mn toxicity. First, gender may play an important role in neuropathology following exposure to Mn. Second, gender-dependent changes may be transient and occur only when Mn levels are elevated. Finally, not all readouts of Mn toxicity may be dependent on gender. However, that does not mean that gender differences are meaningless, rather that gender should always be considered as an important factor in Mn toxicity.

CHAPTER VIII

DISCUSSION AND FUTURE DIRECTIONS

Discussion

The novel findings of these studies include (1) identification of the onset of striatal dendritic pathology and neurochemical changes in YAC128 HD mice between 13 and 16 weeks old, (2) identifying *in vivo* correlates of diseae-toxicant interaction between mutant *HTT* and Mn, (3) discovering gender specific Mn-induced changes in striatal MSN morphology that are most pronounced when striatal Mn is elevated and (4) determining that gender differences in MSN morphology are not present in YAC128 Veh or Mn exposed mice.

NMDAR excitotoxicity

The morphological changes that we identified in YAC128-Veh MSNs at 16 weeks may be due to alterations in striatal neurotransmitter content that promote glutamatergic excitotoxicity. Disruption of the nigrostriatal DA system, which occurs in Parkinson's disease (PD), is known to cause morphological alterations in MSNs of the striatum. 6-hydroxydopamine (6-OHDA) lesions of the SN, a rodent model of PD, have been shown to cause dopaminergic cell death in the SN, a decrease in striatal DA and a reduction in dendritic spine density of MSNs (Day et al., 2006; Ingham et al., 1989; Ingham et al., 1993; Ingham et al., 1998). DA release in the striatum decreases corticostriatal Glu release through

stimulation of the D2 autoreceptor on presynaptic glutamatergic terminals (Bamford et al., 2004). If DA levels are reduced, as is the case in the YAC128-Veh mice at 16 weeks, Glu release may become dysregulated and lead to excitotoxicity. Presynaptic dysfunction of the corticostriatal glutamatergic synapse is detectible before YAC128 mice become symptomatic (Milnerwood and Raymond, 2007). Additionally, the response of the glutamatergic corticostriatal terminal to DA changes as the YAC128 mice progress from a presymptomatic to a symptomatic state (Joshi et al., 2009). The decrease in striatal DA levels that we observed in YAC128-Veh mice at 16 weeks may further contribute to the dysfunction of the corticostriatal terminal.

In addition to changes in the nigrostriatal DA system, amino acids Gly and Ser were also elevated in the striatum. The amino acid L-Ser is converted into the NMDA co-agonist D-Ser by the enzyme serine racemase that is expressed in the MSNs of the striatum (Miya et al., 2008; Pollegioni and Sacchi, 2010). Elevation of these co-agonists may facilitate signaling through the NMDAR, which is consistent with the sensitivity to NMDAR exictotoxicity present in YAC128 mice. Increased levels of these neurotransmitters are also present in other neurodegenerative diseases. An increase in spinal cord Ser has been identified as a key factor in Glu toxicity in animal models of amyotrophic lateral sclerosis (ALS) (Sasabe et al., 2007) and PD patients have been shown to have an increase in plasma Gly (Iwasaki et al., 1992). Importantly, Gly levels were found to be elevated in HD patient platelets and CSF (Nicoli et al., 1993; Reilmann et al., 1997).

Not only do YAC128 mice have an increase in NMDAR co-agonists Ser and Gly, they also have an increase in NR2B expressing extrasynaptic NMDA receptors (Milnerwood et al., 2010). YAC128 mice are known to be sensitive to NMDAR excitotoxicity and signaling through extrasynaptic NMDARs has been shown to increase apoptosis of MSNs in these mice (Fernandes et al., 2007; Graham et al., 2009; Graham et al., 2006; Shehadeh et al., 2006; Tang et al., 2005; Zeron et al., 2004; Zeron et al., 2002). However, two groups have found that treatment of YAC128 mice with memantine to reduce signaling through extrasynaptic NMDARs is neuroprotective and improve motor function (Milnerwood et al., 2010; Okamoto et al., 2009).

We have found multiple factors that may contribute to NMDAR dependent excitotoxicity in YAC128 mice at the 16 week time point. First, we observed an increase in striatal MSN dendritic spine density. This increase in spine density could lead to excitotoxicity through the glutamatergic inputs that synapse primarily onto dendritic spine heads, where NMDARs are localized. Secondly, we found a reduction in striatal DA that may result in less modulation of glutamatergic signaling at dendritic spines. Finally, an increase in striatal levels of NMDAR co-agonists Ser and Gly may facilitate signaling through the NMDAR. The facilitation of NMDAR signaling in the context of increased dendritic spine density and dysregulation of Glu release likely contributes to an excitotoxic environment.

Reducing NMDAR excitotoxicity may have a positive effect on HD. Two recent studies in YAC128 mice support the hypothesis that reducing

extrasynaptic NMDAR signaling can reduce Glu excitotoxicity in HD mice (Milnerwood et al., 2010; Okamoto et al., 2009). Memantine is an uncompetitive open-channel NMDAR antagonist that has been shown to have selectivity for extrasynaptic NMDARs at low concentrations (Lipton, 2006; Lipton, 2007). YAC128 mice were administered memantine in water at 1 mg/kg/day or 30 mg/kg/day from the age of 2-12 months. Behavior and gross neuropathology were assessed at 12 months and compared to 12 month old untreated YAC128 at WT mice. Low dose memantine (1 mg/kg/day) improved motor function and prevented a loss of striatal volume at 12 months. However, high dose memantine (30 mg/kg/day) worsened striatal volume loss and failed to improve motor function (Okamoto et al., 2009). Although YAC128 mice show only subtle neuropathology at 2-4 months (Madison et al., 2011), they do show a procedural learning deficit (Van Raamsdonk et al., 2005b). A second independent study examined if the procedural learning deficit could be rectified by treatment with memantine. Two month old YAC128 mice were treated with 1 mg/kg/day memantine and tested at four months. Memantine treatment prevented the procedural learning deficit in YAC128 mice. These studies support the hypothesis that reducing NMDAR excitotoxicity can result in marked improvement in HD animal models.

There have been few clinical studies on the effectiveness of memantine in HD. The first published account of memantine clinical trials for HD was a multicenter open label prospective trial over two years (Beister et al., 2004). Subjects with HD were titrated up to 30 mg/day memantine and assessed prior to

starting treatment, at one year and two years. The authors detected no significant improvement or deterioration after treatment with memantine. Importantly, there was no significant increase in choreiform movements during the trial. The HD Study Group showed a 5.3% decrease in motor function over 6 months in untreated HD patients. This trial showed only a 4.3% decrease in motor function over 2 years. Data from this trial suggest that memantine appears to be promising in slowing the progression of HD. The only other published clinical trial of memantine in HD was a single center open label trial at Baylor College of Medicine Movement Disorders Center (Ondo et al., 2007). HD subjects were titrated to 20 mg/day of memantine over one month and continued at this dose for three months. There was no significant change in cognition, behavior, total functional capacity or independence; however a significant decrease in chorea was detected at the final examination. These clinical trials suggest that memantine may be beneficial in HD. A randomized, double-blind crossover study was initiated in 2008 (Trial NCT00652457), but there have been no reports on this trial since its posting (http://clinicaltrials.gov/ct2/show/NCT00652457).

Oxidative stress

Oxidative stress is severely damaging to cellular function and vitality. Oxidative damage can occur to DNA, proteins and lipids through reactive oxygen species (ROS). Mn exposure (Benedetto et al., 2010; dos Santos et al., 2010; Lee et al., 2009b; Li et al., 2011; Milatovic et al., 2007; Milatovic et al., 2009; Zhang et al., 2007) and expression of mutant *HTT* (Bogdanov et al., 2001;

Browne et al., 1997; Gu et al., 1996; Mann et al., 1990; Perez-Severiano et al., 2004; Perluigi et al., 2005; Tabrizi et al., 1999; Tabrizi et al., 2000; Wyttenbach et al., 2002; Zourlidou et al., 2007) have both been shown to increase ROS in the brain. Glu excitotoxicity is known to cause generation of ROS though stimulation of the NMDAR, increase intracellular Ca^{2+} that overwhelms the mitochondria and causes production of ROS (Choi et al., 1987; Rao et al., 2003; Reynolds and Hastings, 1995). Rao et al. (2003) showed that ROS generated in neurons could pass through the plasma membrane and impair astrocyte Glu transporter function, thus perpetuating the cycle of Glu excitotoxicity.

Contribution of astrocytes

Although astrocytes were not examined in these studies, they play an important role in both Mn exposure and HD. Astrocytes are important regulators of neuron function and cerebral blood flow. One of the most important metabolic functions of astrocytes is the glutamate-glutamine (Gln) shuttle. Astrocytes take up most of the extracellular Glu through the glutamate-aspartate transporter (GLAST or excitatory amino acid transporter 1, EAAT1 in humans) or glutamate transporter-1 (GLT-1, or EAAT2 in humans) and convert it into Gln through the Mn-containing enzyme glutamine synthetase (GS). Gln is then shuttled to neurons to serve as precursors to Glu and GABA. Through this amino acid shuttle, astrocytes protect neurons from Glu excitotoxicity by rapidly taking up excess Glu in the synaptic cleft. GLT-1 knock-out mice show phenotypes consistent with excitotoxicity; namely hyperexcitability and lethal spontaneous

seizures (Tanaka et al., 1997). This shows the important role of astrocytes in regulating extracellular Glu to prevent excitotoxicity.

Astrocytes are a reservoir for Mn because as much as 80% of Mn in the brain is associated with the astrocytic enzyme GS (Tiffany-Castiglion and Qian, 2001; Wedler et al., 1989). Exposure of cultured astrocytes to elevated levels of Mn causes a decrease in expression of Glu and Gln transporters (Lee et al., 2009a; Sidoryk-Wegrzynowicz et al., 2009; Sidoryk-Wegrzynowicz et al., 2010). Similarly, exposure to CHO cells expressing GLAST and GLT-1 shows a significant decrease in Glu uptake following Mn exposure (Mutkus et al., 2005). This can result in higher extracellular Glu levels and lead to excitotoxicity, similar to the GLT-1 knock-out animals. Mn exposure in rats confirms the decrease in striatal GLT-1 and GLAST expression *in vivo* (Deng et al., 2009). In the studies discussed herein, we found no significant effect of Mn exposure on striatal Glu; however we measured the amount of Glu in whole tissue and were not able to determine extracellular Glu levels. Perhaps if microdialysis studies were conducted, one could determine if this Mn exposure paradigm did indeed result in increased striatal extracellular Glu.

As previously mentioned, MSNs in the YAC128 mice are more sensitive to NMDAR induced excitotoxicity than WT mice (Fernandes et al., 2007; Graham et al., 2009; Milnerwood et al., 2010). Thus, dysfunction in astrocyte function in these mice may lead to an inability to correctly regulate Glu levels in the striatum and lead to excitotoxicity. Post-mortem studies of HD patients have shown a decrease in mRNA and protein expression of GLT-1 that is correlated with

disease severity (Arzberger et al., 1997; Faideau et al., 2010). Additionally, cortical Glu uptake in severely reduced in HD patients in a grade dependent manner (Hassel et al., 2008). Studies in R6/2 mice have also shown a decrease in GLT-1 expression in the striatum and cortex at 12 weeks (Behrens et al., 2002; Faideau et al., 2010; Lievens et al., 2001). A transgenic mouse model expressing mutant *HTT* in astrocytes only showed symptoms similar to mice that express mutant *HTT* ubiquitously. These mice also show a reduction in GLT-1 expression that is due to increased binding of mutant *HTT* with the transcription factor Sp1 that decreases binding of Sp1 to the GLT-1 promoter (Bradford et al., 2009). Treatment of R6/2 mice with ceftriaxone, a beta-lactam antibiotic that has been shown to increase Glu transporter expression, improves motor symptoms, decreases extracellular Glu and increases protein expression of GLT-1 (Miller et al., 2008; Sari et al., 2010).

Dysfunction of astrocytes has not been thoroughly studied in YAC128 mice thus far. The few studies that have examined astrocytes have not found significant changes in YAC128 astrocytes (Battaglia et al., 2011; Ellrichmann et al., 2011). Our studies are consistent with Glu excitotoxicity in 16 week old YAC128 mice. Astrocyte dysfunction may contribute to the Glu excitotoxicity through downregulation of Glu transporter expression and function like in the R6/2 mouse model and human HD patients. If in fact, there is a reduction in GLAST and/or GLT-1 expression or function, this would result in an increase in extracellular Glu. This, in combination with elevated striatal Gly and Ser levels

would certainly be able to potentiate signaling through extrasynaptic NR2B containing NMDARs and initiate apoptosis in MSNs.

Together, these data also suggest that the gene-environment interaction between mutant *HTT* and Mn may be detrimental to astrocyte and ultimately neuron function. In both Mn overexposure and mutant *HTT* expression, there is a reduction in expression and/or function of astrocytic Glu transporters that can lead to excitotoxicity. However, it is also possible for an antagonistic relationship to occur between Mn and mutant *HTT* like in the case of striatal DA levels. In both WT-Mn and YAC128-Veh mice, DA levels were reduced compared to WT-Veh. One might expect that the combination of mutant *HTT* expression and Mn exposure might further reduce DA levels. However, we observed an antagonistic effect between Mn and mutant *HTT*, where DA levels were not reduced further than the single insults of Mn exposure or mutant *HTT* expression. It is possible that a similar antagonistic relationship may occur for astrocyte function or that the disease-toxicant interaction may be additive or synergistic and damage astrocytes further that either insult individually.

Direct vs indirect pathway

The indirect pathway in the basal ganglia has been shown to be more affected in human patients with HD. A post-mortem study of DA receptors in the striatum of HD subjects showed a decrease in the number of cells expressing D1 and D2 receptor mRNA. There was a significant reduction in D2R mRNA per cell that correlated with disease progression, but no decrease in D1R mRNA per cell

(Augood et al., 1997). Positron emission tomography (PET) imaging over time shows a progressive loss of D2Rs in the striatum (Brandt et al., 1990; Feigin et al., 2007; Ginovart et al., 1997; Pavese et al., 2010). One study carried out over more than three years showed a greater loss of D2Rs over time in asymptomatic subjects, but a greater loss of D1Rs over time in symptomatic HD subjects (Andrews et al., 1999). Animal studies have shown mixed results as to which pathway is more affected in HD. Some studies show a greater or earlier dysfunction of the D1R, and therefore the direct pathway (Andre et al., 2011; Cha et al., 1998; Kung et al., 2007; Tang et al., 2007), while others show a greater dysfunction of the D2R, indirect pathway (Cummings et al., 2007; Joshi et al., 2009; Spektor et al., 2002; Vetter et al., 2003; Xie et al., 2010).

Andre et al., (2011) crossed YAC128 mice with mice that express enhanced green fluorescent protein under the control of either the D1R promoter or the D2R promoter to be able to distinguish between these subpopulations of MSNs. Electrophysiology studies were carried out on these distinct subpopulations of MSNs from 1.5 months to 12 months old. Andre et al. (2011) found that D1R expressing MSNs were affected to a greater extent than D2R expressing MSNs at pre-symptomatic and symptomatic stages. Andre et al. (2011) found that there was an increase in Glu release onto D1R expressing MSNs at 1.5 months that may result in the hyperkinetic phenotype. Additionally, studies implicating the indirect pathway generally show a decrease in signaling through or expression of the D2R. This would result in an increase in motor behavior as the indirect pathway is responsible for decreasing motor activity.

Together these data show the hyperactivity exhibited by YAC128 mice at 12 weeks may be due to a decrease in D2R signaling and an increase in D1R signaling. Unfortunately, our studies are not able to shed light onto whether there are changes in MSN morphology of one or both subtypes due to the limitations of Golgi impregnation.

Gender contribution

Gender dependent differences in MSN morphology were only observed in Mn exposed WT mice and were more prominent when Mn levels were elevated. The fact that YAC128 mice showed no gender differences upon exposure to Veh or Mn suggests that mutant *HTT* interacts with sex hormones or Mn to prevent their interaction or mutant *HTT* may act downstream of the interaction between Mn and sex hormones to block the gender effect. Unfortunately there is very little known about gender differences in neuron morphology under normal conditions, let alone following exposure to a toxicant or in a disease state. As previously stated, the vast majority (40-60%) of *in vivo* neuroscience or pharmacology experiments use only male animals (Wald and Wu, 2010). Both genders are used only 10-20% of the time in neuroscience or pharmacology experiments. Animals of unspecified gender are used approximately 5-20% of the time and a very small percentage, less than 20%, use female animals only. Furthermore, even when both genders are included in experiments, only two-thirds of those manuscripts included gender as a factor in data analysis (Wald, 2010). This

severely limits the knowledge we have about gender differences in response to disease or toxicant exposure.

Implications

These studies may provide some insight into whether Mn exposure can alter the onset or progression of HD. We show that Mn exposure altered the neurochemical environment of the striatum and affected MSN morphology in YAC128 mice. Previous work has demonstrated that survival of striatal cells expressing mutant *HTT* was bolstered by low concentrations of Mn (Williams et al., 2010b). Several potential scenarios may occur with HD patients exposed to Mn. First, HD patients may be protected from Mn toxicity due to reduced accumulation of Mn in the neostriatum. A second scenario is that HD patients may accumulate less Mn in the striatum, but may be rendered more sensitive to fluctuations in Mn levels due to mutant *HTT*. This is exemplified by the morphological changes as a function of distance from the soma observed in YAC128-Mn treated mice compared to WT-Mn mice. Although not reaching statistical significance, there are trends towards a greater effect of Mn on MSN morphology in YAC128 mice (Figures 4 and 5). These HD mutant mice at 3-4 months old have been shown to be more sensitive to NMDAR induced excitotoxicity (Graham et al., 2009) and Mn exposure results in an increase in NMDAR co-agonists Ser and Gly. Although, Mn rescues the elevated amino acids by 16 weeks in YAC128 mice, the facilitation of NMDAR signaling at 13 weeks may have initiated events leading to morphological changes in MSNs. In

this scenario mutant *HTT* may interact with Mn transport resulting in less Mn accumulation in the striatum. These mice may not have the ability to correctly modulate excess Mn following exposure. This means that even though less Mn is getting into the striatum of YAC128 mice, they are not able to effectively handle this increase of Mn, thus rendering them more sensitive to changes in Mn levels.

Another scenario that may increase Mn toxicity is development of Fe deficiency anemia in HD subjects. Fe-deficient humans and mice have been shown to accumulate higher levels of Mn compared to non-Fe deficient subjects (Fitsanakis et al., 2008; Kim et al., 2005). We recently reported that defects in the Fe transport system are not responsible for the reduced Mn accumulation in striatal cells expressing mutant *HTT* (Williams et al., 2010a). Furthermore, the Fe:Mn ratio may be an important consideration in neurotoxicity of these metals since an imbalance in their pro-oxidant and anti-oxidant roles may result in production of reactive oxygen species (Dobson et al., 2004). Other considerations are the duration, route and level of Mn exposure encountered by HD patients. Manganism is typically observed after very high levels of Mn exposure after a relatively short time whereas Mn-induced parkinsonian symptoms are usually present after a continuous exposure to low level Mn (Lucchini et al., 2009). Based on this, we would expect radically different effects of Mn on the onset and progression of HD depending on the route and duration of Mn exposure encountered.

Although our *in vitro* and *in vivo* models of HD have shown a disease-toxicant interaction between mutant *HTT* and Mn, it remains to be seen whether

human patients share the phenotype. Our research, thus far, is not conclusive as to whether Mn exposure has a beneficial or detrimental effect on HD onset and progression. In some instances, Mn exposure normalized amino acids that were elevated by mutant *HTT*, such as Gly and Ser, back to WT-Veh levels at week 16. On the other hand, Mn exposure also causes acute neurochemical changes that may result in morphological alterations in MSNs. At this point, we do not know precisely how the morphometric changes we observe affect neuron function, or how they continue to change with time.

The research described in Chapter VI demonstrates that male and female MSNs respond differently to Mn exposure. Gender differences in response to Mn exposure have rarely been examined. A recent study of cognition in children exposed to environmental Mn suggests that although children of both genders accumulate similar levels of Mn, it affects their cognitive function differently (Riojas-Rodriguez et al., 2010). These studies provide compelling evidence for further study of gender differences in response to toxicant exposure and disease. The use of both genders in preclinical research may elucidate data early on that would allow for targeted therapies that would benefit patients of both genders.

Future Directions

Continued efforts must be made to understand the disease-toxicant interaction between HD and Mn to determine if this interaction is beneficial or detrimental to disease onset and progression. Studies should be carried out to examine the contribution of astrocyte dysfunction in the HD-Mn disease-toxicant

interaction. As of yet, no studies have been undertaken to examine astrocytes in YAC128 mice. Two studies reported no changes in protein expression in astrocytes from YAC128 mice, but an in depth examination of astrocytes of these animals has not been done (Battaglia et al., 2011; Ellrichmann et al., 2011). Future experiments should be carried out to determine astrocyte function in YAC128 mice and how Mn exposure alters YAC128 astrocytes. The rate and amount of Mn uptake in astrocytes of WT and YAC128 mice should be examined. Glu uptake by astrocytes in the absence and presence of Mn should also be examined to determine if astrocyte dysfunction adds to the Glu excitotoxicity that has been described in the YAC128 mice. Measurement of oxidative stress and response to oxidative stress through signaling pathways can also give insight into the health and function of YAC128 astrocytes.

While it appears that the D1R expressing MSNs in YAC128 mice are affected earlier than D2R expressing MSNs, the evidence in humans shows that D2R expressing MSNs are more affected (Andre et al., 2011; Augood et al., 1997; Brandt et al., 1990). Morphological studies should be carried out using the mice generated by Andre et al (2011) to determine the time course of changes in morphology among D1R and D2R expressing MSNs. Intracellular fills of D1R or D2R expressing MSNs throughout the lifespan of YAC128 mice, can allow insight into how the direct and indirect pathways are affected at each stage of symptomatology. Additionally, the MSNs can be examined following Mn exposure to determine how changed in morphology are affected by exposure to Mn.

Studies should be carried out using mice of both genders to continue to elucidate gender differences in HD symptom progression or retardation due to Mn exposure. Behavioral studies should be undertaken to determine how the disease-toxicant interaction affects symptom onset and progression. The current Mn exposure paradigm can be used to examine how the HD-Mn interaction affects the procedural learning deficit that appears at 2 months. It would also be beneficial to examine how Mn exposure modifies the onset and progression of motor symptoms in YAC128 mice. These studies are crucial to understanding if the HD-Mn interaction is beneficial or detrimental to disease progression. Electrophysiological studies may be able to shed insight into how Mn perturbs MSN morphology and function in YAC128 mice. Understanding how the HD-Mn interaction alters MSN function can give more mechanistic insight into the behavioral effects of the disease-toxicant interaction. Electrophysiological studies and behavioral studies examining motor function should be carried to determine how Mn exposure affects the progression of HD associated motor dysfunction in these mice to definitively answer whether Mn exposure is beneficial or detrimental to motor symptom onset and progression.

A time course of behavioral and electrophysiological experiments should be performed to determine if the HD-Mn interaction has long lasting effects or is only transient while Mn levels are elevated. Other Mn exposure paradigms should also be considered. A chronic low dose Mn exposure paradigm may be more beneficial than a subchronic high dose exposure. If the HD-Mn interaction is truly beneficial to slowing disease progression, then the proper level of Mn

exposure must be determined. However, if the HD-Mn interaction is detrimental to disease onset and progression, then the molecular mechanism of this interaction will be able to give insight into new targets of disease modifying therapy.

REFERENCES

AC, L., et al., 1992. 3-Nitropropionic acid decreases cellular energy levels and causes neuronal degeneration in cortical explants. Neurodegeneration. 1**,** 151–161.

Akesson, A., et al., 2002. Cadmium exposure in pregnancy and lactation in relation to iron status. Am J Public Health. 92**,** 284-7.

Akesson, A., et al., 2005. Tubular and glomerular kidney effects in Swedish women with low environmental cadmium exposure. Environ Health Perspect. 113**,** 1627-31.

Alcantara-Gonzalez, F., et al., 2010. Enhanced dendritic spine number of neurons of the prefrontal cortex, hippocampus and nucleus accumbens in old rats after chronic donepezil administration. Synapse.

Alfarez, D. N., et al., 2009. Corticosterone reduces dendritic complexity in developing hippocampal CA1 neurons. Hippocampus.

Alvarez, V. A., Sabatini, B. L., 2007. Anatomical and physiological plasticity of dendritic spines. Annu Rev Neurosci. 30**,** 79-97.

Anca, M. H., et al., 2004. Different phenotypic expression in monozygotic twins with Huntington disease. Am J Med Genet A. 124A**,** 89-91.

Anderson, J. G., et al., 2007. Inhibition of DAT function attenuates manganese accumulation in the globus pallidus. Environ Toxicol Pharmacol. 23**,** 179–184.

Andre, V. M., et al., 2011. Differential electrophysiological changes in striatal output neurons in Huntington's disease. J Neurosci. 31**,** 1170-82.

Andre, V. M., et al., 2010. Dopamine and glutamate in Huntington's disease: A balancing act. CNS Neurosci Ther. 16**,** 163-78.

Andrew, S. E., et al., 1993. The relationship between trinucleotide (CAG) repeat length and clinical features of Huntington's disease. Nat Genet. 4**,** 398-403.

Andrews, T. C., et al., 1999. Huntington's disease progression. PET and clinical observations. Brain. 122 (Pt 12)**,** 2353-63.

Angulo, A., et al., 1996. A reliable method for Golgi staining of retina and brain slices. J Neurosci Methods. 66**,** 55-9.

Angulo, A., et al., 1994. Golgi-Colonnier method: correlation of the degree of chromium reduction and pH change with quality of staining. J Histochem Cytochem. 42**,** 393-403.

Archibald, F. S., Tyree, C., 1987. Manganese poisoning and the attack of trivalent manganese upon catecholamines. Arch Biochem Biophys. 256**,** 638-50.

Arzberger, T., et al., 1997. Changes of NMDA receptor subunit (NR1, NR2B) and glutamate transporter (GLT1) mRNA expression in Huntington's disease--an in situ hybridization study. J Neuropathol Exp Neurol. 56**,** 440-54.

Aschner, J. L., Aschner, M., 2005. Nutritional aspects of manganese homeostasis. Mol Aspects Med. 26**,** 353-62.

Aschner, M., 2000. Manganese: brain transport and emerging research needs. Environmental Health Perspectives. 103**,** 429-432.

Aschner, M., et al., 2005. Manganese dosimetry: species differences and implications for neurotoxicity. Crit Rev Toxicol. 35**,** 1-32.

Aschner, M., Gannon, M., 1994. Manganese (Mn) transport across the rat blood-brain barrier: saturable and transferrin-dependent transport mechanisms. Brain Res Bull. 33**,** 345-9.

Aschner, M., et al., 2007. Manganese: recent advances in understanding its transport and neurotoxicity. Toxicol Appl Pharmacol. 221**,** 131-47.

Augood, S. J., et al., 1997. Dopamine D1 and D2 receptor gene expression in the striatum in Huntington's disease. Ann Neurol. 42**,** 215-21.

Autissier, N., et al., 1982. Dopamine and norepinephrine turnover in various regions of the rat brain after chronic manganese chloride administration. Toxicology. 24**,** 175-82.

Aylward, E. H., et al., 2000. Rate of caudate atrophy in presymptomatic and symptomatic stages of Huntington's disease. Mov Disord. 15**,** 552-60.

Aylward, E. H., et al., 2011. Longitudinal change in regional brain volumes in prodromal Huntington disease. J Neurol Neurosurg Psychiatry. 82**,** 405-10.

Aylward, E. H., et al., 2004. Onset and rate of striatal atrophy in preclinical Huntington disease. Neurology. 63**,** 66-72.

Bader, M., et al., 1999. Biomonitoring of manganese in blood, urine and axillary hair following low-dose exposure during the manufacture of dry cell batteries. Int Arch Occup Environ Health. 72**,** 521-7.

Balleine, B. W., et al., 2009. The integrative function of the basal ganglia in instrumental conditioning. Behav Brain Res. 199**,** 43-52.

Bamford, N. S., et al., 2004. Dopamine modulates release from corticostriatal terminals. J Neurosci. 24**,** 9541-52.

Baraka, A. M., et al., 2011. The possible role of estrogen and selective estrogen receptor modulators in a rat model of Parkinson's disease. Life Sci.

Battaglia, G., et al., 2011. Early defect of transforming growth factor beta1 formation in Huntington's disease. J Cell Mol Med. 15**,** 555-71.

Beal, M. F., et al., 1993. Neurochemical and histologic characterization of striatal excitotoxic lesions produced by the mitochondrial toxin 3-nitropropionic acid. J Neurosci. 13**,** 4181-92.

Beal, M. F., et al., 1991. Neurochemical characterization of excitotoxin lesions in the cerebral cortex. J Neurosci. 11**,** 147-58.

Behrens, P. F., et al., 2002. Impaired glutamate transport and glutamate-glutamine cycling: downstream effects of the Huntington mutation. Brain. 125**,** 1908-22.

Beister, A., et al., 2004. The N-methyl-D-aspartate antagonist memantine retards progression of Huntington's disease. J Neural Transm Suppl. 117-22.

Benedetto, A., et al., 2010. Extracellular dopamine potentiates mn-induced oxidative stress, lifespan reduction, and dopaminergic neurodegeneration in a BLI-3-dependent manner in Caenorhabditis elegans. PLoS Genet. 6.

Bernheimer, H., et al., 1973. Brain dopamine and the syndromes of Parkinson and Huntington. Clinical, morphological and neurochemical correlations. J Neurol Sci. 20**,** 415-55.

Bibb, J. A., et al., 2000. Severe deficiencies in dopamine signaling in presymptomatic Huntington's disease mice. Proceedings of the National Academy of Sciences of the United States of America. 97**,** 6809-6814.

Bindu, B., et al., 2007. Short-term exposure to an enriched environment enhances dendritic branching but not brain-derived neurotrophic factor expression in the hippocampus of rats with ventral subicular lesions. Neuroscience. 144**,** 412-23.

Bjorkman, L., et al., 2000. Both the environment and genes are important for concentrations of cadmium and lead in blood. Environ Health Perspect. 108**,** 719-22.

Blanpied, T. A., Ehlers, M. D., 2004. Microanatomy of dendritic spines: emerging principles of synaptic pathology in psychiatric and neurological disease. Biol Psychiatry. 55**,** 1121-7.

Bock, N. A., et al., 2008. Cerebrospinal fluid to brain transport of manganese in a non-human primate revealed by MRI. Brain Res. 1198**,** 160-70.

Bode, F. J., et al., 2008. Sex differences in a transgenic rat model of Huntington's disease: decreased 17beta-estradiol levels correlate with reduced numbers of DARPP32+ neurons in males. Hum Mol Genet. 17**,** 2595-609.

Bogdanov, M. B., et al., 2001. Increased oxidative damage to DNA in a transgenic mouse model of Huntington's disease. J Neurochem. 79**,** 1246-9.

Bolte, S., et al., 2004. Human exposure to respirable manganese in outdoor and indoor air in urban and rural areas. J Toxicol Environ Health A. 67**,** 459-67.

Bonate, P. L., 1991. Gender-related differences in xenobiotic metabolism. J Clin Pharmacol. 31**,** 684-90.

Bonilla, E., et al., 1988. Huntington's disease: studies on brain free amino acids. Life Sci. 42**,** 1153-8.

Boudia, N., et al., 2006. Manganese concentrations in the air of the Montreal (Canada) subway in relation to surface automobile traffic density. Sci Total Environ. 366**,** 143-7.

Bowler, R. M., et al., 2006. Manganese exposure: neuropsychological and neurological symptoms and effects in welders. Neurotoxicology. 27**,** 315-26.

Bowler, R. M., et al., 2007a. Sequelae of fume exposure in confined space welding: a neurological and neuropsychological case series. Neurotoxicology. 28**,** 298-311.

Bowler, R. M., et al., 2007b. Dose-effect relationships between manganese exposure and neurological, neuropsychological and pulmonary function in confined space bridge welders. Occup Environ Med. 64**,** 167-77.

Bradford, J., et al., 2009. Expression of mutant huntingtin in mouse brain astrocytes causes age-dependent neurological symptoms. Proc Natl Acad Sci U S A. 106**,** 22480-5.

Brandt, J., et al., 1990. D2 receptors in Huntington's disease: positron emission tomography findings and clinical correlates. J Neuropsychiatry Clin Neurosci. 2**,** 20-7.

Brennan, W. A., Jr., et al., 1985. Regional mitochondrial respiratory activity in Huntington's disease brain. J Neurochem. 44**,** 1948-50.

Brinkman, R. R., et al., 1997. The likelihood of being affected with Huntington disease by a particular age, for a specific CAG size. Am J Hum Genet. 60**,** 1202-10.

Brouillet, E., et al., 1993. Age-dependent vulnerability of the striatum to the mitochondrial toxin 3-nitropropionic acid. J Neurochem. 60**,** 356-9.

Browne, S., et al., 1997. Oxidative damage and metabolic dysfunction in Huntington's disease: selective vulnerability of the basal ganglia. Ann Neurol. 41**,** 646-653.

Browne, S. E., Beal, M. F., 1994. Oxidative damage and mitochondrial dysfunction in neurodegenerative diseases. Biochem Soc Trans. 22**,** 1002-6.

Buell, S. J., 1982. Golgi-Cox and rapid golgi methods as applied to autopsied human brain tissue: widely disparate results. J Neuropathol Exp Neurol. 41**,** 500-7.

Burton, N. C., Guilarte, T. R., 2009. Manganese neurotoxicity: lessons learned from longitudinal studies in nonhuman primates. Environ Health Perspect. 117**,** 325-32.

Burton, N. C., et al., 2009. Effects of chronic manganese exposure on glutamatergic and GABAergic neurotransmitter markers in the nonhuman primate brain. Toxicol Sci. 111**,** 131-9.

Butterworth, R. F., 2010. Metal toxicity, liver disease and neurodegeneration. Neurotox Res. 18**,** 100-5.

Butterworth, R. F., et al., 1995. Manganese toxicity, dopaminergic dysfunction and hepatic encephalopathy. Metab Brain Dis. 10**,** 259-67.

Calne, D. B., et al., 1994. Manganism and idiopathic parkinsonism: similarities and differences. Neurology. 44**,** 1583-6.

Carroll, J. B., et al., 2011. Natural history of disease in the YAC128 mouse reveals a discrete signature of pathology in Huntington disease. Neurobiol Dis.

Cha, J. H., et al., 1998. Altered brain neurotransmitter receptors in transgenic mice expressing a portion of an abnormal human huntington disease gene. Proc Natl Acad Sci U S A. 95**,** 6480-5.

Chakravarthy, V. S., et al., 2010. What do the basal ganglia do? A modeling perspective. Biol Cybern. 103**,** 237-53.

Chen, J. R., et al., 2009. Gonadal Hormones Modulate the Dendritic Spine Densities of Primary Cortical Pyramidal Neurons in Adult Female Rat. Cereb Cortex.

Chen, J. Y., et al., 2001. Differential cytotoxicity of Mn(II) and Mn(III): special reference to mitochondrial [Fe-S] containing enzymes. Toxicol Appl Pharmacol. 175**,** 160-8.

Chia, K. S., 2008. Gene-environment interactions in breast cancer. Novartis Found Symp. 293**,** 143-50; discussion 150-5, 181-3.

Choi, D. W., et al., 1987. Glutamate neurotoxicity in cortical cell culture. J Neurosci. 7**,** 357-68.

Clewell, H. J., et al., 2002. Review and evaluation of the potential impact of age- and gender-specific pharmacokinetic differences on tissue dosimetry. Crit Rev Toxicol. 32**,** 329-89.

Clifford, J. J., et al., 2002. Essential fatty acids given from conception prevent topographies of motor deficit in a transgenic model of Huntington's disease. Neuroscience. 109**,** 81-8.

Colonnier, M., 1964. THE TANGENTIAL ORGANIZATION OF THE VISUAL CORTEX. J Anat. 98**,** 327-44.

Cooper, W. C., 1984. The health implications of increased manganese in the environment resulting from the combustion of fuel additives: a review of the literature. J Toxicol Environ Health. 14**,** 23-46.

Couper, J., 1837. On the effects of black oxide of manganese when inhaled into the lungs. Br Ann Med Pharm Vital Stat Gen Sci. 41-42.

Coyle, J. T., Schwarcz, R., 1976. Lesion of striatal neurones with kainic acid provides a model for Huntington's chorea. Nature. 263**,** 244-6.

Cummings, D. M., et al., 2007. Abnormal cortical synaptic plasticity in a mouse model of Huntington's disease. Brain Res Bull. 72**,** 103-7.

D'Amelio, F. E., 1983. The Golgi-Hortega-Lavilla technique, with a useful additional step for application to brain tissue after prolonged fixation. Stain Technol. 58**,** 79-84.

Davis, C. D., Greger, J. L., 1992. Longitudinal changes of manganese-dependent superoxide dismutase and other indexes of manganese and iron status in women. Am J Clin Nutr. 55**,** 747-52.

Davis, C. D., et al., 1993. Manganese metabolism in rats: an improved methodology for assessing gut endogenous losses. Proc Soc Exp Biol Med. 202**,** 103-8.

Day, M., et al., 2006. Selective elimination of glutamatergic synapses on striatopallidal neurons in Parkinson disease models. Nat Neurosci. 9**,** 251-9.

de Bie, R. M., et al., 2007. Manganese-induced Parkinsonism associated with methcathinone (Ephedrone) abuse. Arch Neurol. 64**,** 886-9.

de la Monte, S. M., et al., 1988. Morphometric demonstration of atrophic changes in the cerebral cortex, white matter, and neostriatum in Huntington's disease. J Neuropathol Exp Neurol. 47**,** 516-25.

Deng, Y., et al., 2009. The protective effect of riluzole on manganese caused disruption of glutamate-glutamine cycle in rats. Brain Res. 1289**,** 106-17.

Deutch, A. Y., et al., 2007. Striatal plasticity and medium spiny neuron dendritic remodeling in parkinsonism. Parkinsonism Relat Disord. 13 Suppl 3**,** S251-8.

Diaz, C., et al., 2001. Serum manganese concentrations in a representative sample of the Canarian population. Biol Trace Elem Res. 80**,** 43-51.

Dobson, A. W., et al., 2004. Manganese neurotoxicity. Ann N Y Acad Sci. 1012**,** 115-28.

Dodd, C. A., et al., 2005. Basal Ganglia accumulation and motor assessment following manganese chloride exposure in the C57BL/6 mouse. Int J Toxicol. 24**,** 389-97.

Donovan, J., Brown, P., 1998. Anesthesia. Current Protocols in Immunology. 27**,** 1.4.1-1.4.5.

Donovan, J., Brown, P., 2006. Euthanasia. Current Protocols in Immunology. 73**,** 1.8.1-1.8.4.

Dorman, D. C., et al., 2004. Old age and gender influence the pharmacokinetics of inhaled manganese sulfate and manganese phosphate in rats. Toxicol Appl Pharmacol. 197**,** 113-24.

Dorman, D. C., et al., 2006a. Tissue manganese concentrations in young male rhesus monkeys following subchronic manganese sulfate inhalation. Toxicol Sci. 92**,** 201-10.

Dorman, D. C., et al., 2006b. Correlation of brain magnetic resonance imaging changes with pallidal manganese concentrations in rhesus monkeys following subchronic manganese inhalation. Toxicol Sci. 92**,** 219-27.

Dorner, J. L., et al., 2007. Sex differences in behavior and striatal ascorbate release in the 140 CAG knock-in mouse model of Huntington's disease. Behav Brain Res. 178**,** 90-7.

dos Santos, A. P., et al., 2010. Rat brain endothelial cells are a target of manganese toxicity. Brain Res. 1326**,** 152-61.

Duan, W., et al., 2003. Dietary restriction normalizes glucose metabolism and BDNF levels, slows disease progression, and increases survival in huntingtin mutant mice. Proc Natl Acad Sci U S A. 100**,** 2911-6.

Dumas, E. M., et al., 2011. Early changes in white matter pathways of the sensorimotor cortex in premanifest Huntington's disease. Hum Brain Mapp.

Duyao, M. P., et al., 1995. Inactivation of the mouse Huntington's disease gene homolog Hdh. Science. 269**,** 407 - 410.

Eadie, B. D., et al., 2005. Voluntary exercise alters the cytoarchitecture of the adult dentate gyrus by increasing cellular proliferation, dendritic complexity, and spine density. J Comp Neurol. 486**,** 39-47.

Ellrichmann, G., et al., 2011. Efficacy of fumaric acid esters in the R6/2 and YAC128 models of Huntington's disease. PLoS One. 6**,** e16172.

Erikson, K. M., Aschner, M., 2006. Increased manganese uptake by primary astrocyte cultures with altered iron status is mediated primarily by divalent metal transporter. Neurotoxicology. 27**,** 125-30.

Erikson, K. M., et al., 2004a. Airborne manganese exposure differentially affects end points of oxidative stress in an age- and sex-dependent manner. Biol Trace Elem Res. 100**,** 49-62.

Erikson, K. M., et al., 2005. Manganese accumulation in striatum of mice exposed to toxic doses is dependent upon a functional dopamine transporter. Environmental Toxicology and Pharmacology. 20**,** 390-394.

Erikson, K. M., et al., 2002. Manganese accumulates in iron-deficient rat brain regions in a heterogeneous fashion and is associated with neurochemical alterations. Biol Trace Elem Res. 87**,** 143-56.

Erikson, K. M., et al., 2004b. Globus pallidus: a target brain region for divalent metal accumulation associated with dietary iron deficiency. J Nutr Biochem. 15**,** 335-41.

Faideau, M., et al., 2010. In vivo expression of polyglutamine-expanded huntingtin by mouse striatal astrocytes impairs glutamate transport: a correlation with Huntington's disease subjects. Hum Mol Genet. 19**,** 3053-67.

Feigin, A., et al., 2007. Thalamic metabolism and symptom onset in preclinical Huntington's disease. Brain. 130**,** 2858-67.

Fernandes, H. B., et al., 2007. Mitochondrial Sensitivity and Altered Calcium Handling Underlie Enhanced NMDA-Induced Apoptosis in YAC128 Model of Huntington's Disease. J. Neurosci. 27**,** 13614-13623.

Ferrante, R. J., 2009. Mouse models of Huntington's disease and methodological considerations for therapeutic trials. Biochim Biophys Acta. 1792**,** 506-20.

Ferrante, R. J., et al., 1993. Excitotoxin lesions in primates as a model for Huntington's disease: histopathologic and neurochemical characterization. Exp Neurol. 119**,** 46-71.

Ferrante, R. J., et al., 1991. Proliferative and degenerative changes in striatal spiny neurons in Huntington's disease: a combined study using the section-Golgi method and calbindin D28k immunocytochemistry. J Neurosci. 11**,** 3877-87.

Fiala, J. C., et al., 2002. Dendritic spine pathology: cause or consequence of neurological disorders? Brain Res Brain Res Rev. 39**,** 29-54.

Finley, J. W., et al., 1994. Sex affects manganese absorption and retention by humans from a diet adequate in manganese. Am J Clin Nutr. 60**,** 949-55.

Fischer, M., et al., 2000. Glutamate receptors regulate actin-based plasticity in dendritic spines. Nat Neurosci. 3**,** 887-94.

Fitsanakis, V. A., et al., 2008. Measuring Brain Manganese and Iron Accumulation in Rats following 14 Weeks of Low-Dose Manganese Treatment Using Atomic Absorption Spectroscopy and Magnetic Resonance Imaging. Toxicol. Sci. 103**,** 116-124.

Fletcher, C. V., et al., 1994. Gender differences in human pharmacokinetics and pharmacodynamics. J Adolesc Health. 15**,** 619-29.

Florence, T. M., Stauber, J. L., 1989. Manganese catalysis of dopamine oxidation. Sci Total Environ. 78**,** 233-40.

Folstein, S. E., 1989. Huntington's Disease: A Disorder of Families.

Fortoul, T. I., et al., 2005. Sex differences in bronchiolar epithelium response after the inhalation of lead acetate (Pb). Toxicology. 207**,** 323-30.

Friedman, J. H., et al., 2005. Monozygotic twins discordant for Huntington disease after 7 years. Arch Neurol. 62**,** 995-7.

Fuchs, E., et al., 2006. Remodeling of neuronal networks by stress. Front Biosci. 11**,** 2746-58.

Gabbott, P. L., Somogyi, J., 1984. The 'single' section Golgi-impregnation procedure: methodological description. J Neurosci Methods. 11**,** 221-30.

Galea, L. A., et al., 1997. Sex differences in dendritic atrophy of CA3 pyramidal neurons in response to chronic restraint stress. Neuroscience. 81**,** 689-97.

Garcia, B. G., et al., 2010. Cortical Regulation of Striatal Medium Spiny Neuron Dendritic Remodeling in Parkinsonism: Modulation of Glutamate Release Reverses Dopamine Depletion-Induced Dendritic Spine Loss. Cereb. Cortex. 20**,** 2423-2432.

Garey, L. J., et al., 1998. Reduced dendritic spine density on cerebral cortical pyramidal neurons in schizophrenia. J Neurol Neurosurg Psychiatry. 65**,** 446-453.

Garthwaite, J., 2008. Concepts of neural nitric oxide-mediated transmission. Eur J Neurosci. 27**,** 2783-802.

Gavin, C. E., et al., 1999. Manganese and calcium transport in mitochondria: implications for manganese toxicity. Neurotoxicology. 20**,** 445-53.

George, S., et al., 2008. Alpha-synuclein transgenic mice exhibit reduced anxiety-like behaviour. Exp Neurol. 210**,** 788-92.

Georgiou, N., et al., 1999. Differential clinical and motor control function in a pair of monozygotic twins with Huntington's disease. Mov Disord. 14**,** 320-5.

Gerfen, C. R., et al., 1990. D1 and D2 dopamine receptor-regulated gene expression of striatonigral and striatopallidal neurons. Science. 250**,** 1429-32.

Gianutsos, G., Murray, M. T., 1982. Alterations in brain dopamine and GABA following inorganic or organic manganese administration. Neurotoxicology. 3**,** 75-81.

Gibb, R., Kolb, B., 1998. A method for vibratome sectioning of Golgi-Cox stained whole rat brain. J Neurosci Methods. 79**,** 1-4.

Ginovart, N., et al., 1997. PET study of the pre- and post-synaptic dopaminergic markers for the neurodegenerative process in Huntington's disease. Brain. 120 (Pt 3)**,** 503-14.

Glantz, L. A., Lewis, D. A., 2000. Decreased Dendritic Spine Density on Prefrontal Cortical Pyramidal Neurons in Schizophrenia. Arch Gen Psychiatry. 57**,** 65-73.

Glaser, E. M., Van der Loos, H., 1981. Analysis of thick brain sections by obverse-reverse computer microscopy: application of a new, high clarity Golgi-Nissl stain. J Neurosci Methods. 4**,** 117-25.

Golgi, C., 1873. Sulla struttura della sostanza grigia del cervello (Communicazione preventiva). Gazetta Medica Italiana, Lombardia. 33**,** 244-246.

Golub, M. S., et al., 2005. Neurobehavioral evaluation of rhesus monkey infants fed cow's milk formula, soy formula, or soy formula with added manganese. Neurotoxicol Teratol. 27**,** 615-27.

Gomez-Esteban, J. C., et al., 2007. Monozygotic twins suffering from Huntington's disease show different cognitive and behavioural symptoms. Eur Neurol. 57**,** 26-30.

Gorell, J. M., et al., 1997. Occupational exposures to metals as risk factors for Parkinson's disease. Neurology. 48**,** 650-8.

Gorell, J. M., et al., Occupational metal exposures and the risk of Parkinson's disease. Neuroepidemiology, Switzerland, 1999, pp. 303-8.

Gourfinkel-An, I., et al., 2003. Changes in GAD67 mRNA expression evidenced by in situ hybridization in the brain of R6/2 transgenic mice. J Neurochem. 86**,** 1369-78.

Graham, R. K., et al., 2009. Differential Susceptibility to Excitotoxic Stress in YAC128 Mouse Models of Huntington Disease between Initiation and Progression of Disease. J. Neurosci. 29**,** 2193-2204.

Graham, R. K., et al., 2006. Levels of mutant huntingtin influence the phenotypic severity of Huntington disease in YAC128 mouse models. Neurobiology of Disease. 21**,** 444-455.

Grandjean, P., et al., Cognitive performance of children prenatally exposed to "safe" levels of methylmercury. Environ Res. 1998 Academic Press., United States, 1998, pp. 165-72.

Graveland, G., et al., 1985a. Evidence for degenerative and regenerative changes in neostriatal spiny neurons in Huntington's disease. Science. 227**,** 770-773.

Graveland, G., et al., 1985b. Evidence for degenerative and regenerative changes in neostriatal spiny neurons in Huntington's disease. Science. 227**,** 770-773.

Graveland, G. A., et al., 1985c. A Golgi study of the human neostriatum: neurons and afferent fibers. J Comp Neurol. 234**,** 317-33.

Gray, M., et al., 2008. Full-length human mutant huntingtin with a stable polyglutamine repeat can elicit progressive and selective neuropathogenesis in BACHD mice. J Neurosci. 28**,** 6182-95.

Greger, J. L., et al., 1990. Intake, serum concentrations, and urinary excretion of manganese by adult males. Am J Clin Nutr. 51**,** 457-61.

Gu, M., et al., 1996. Mitochondrial defect in Huntington's disease caudate nucleus. Ann Neurol. 39**,** 385-9.

Gualtierotti, R., et al., 2010. Updating on the pathogenesis of systemic lupus erythematosus. Autoimmun Rev. 10**,** 3-7.

Guevara-Guzman, R., et al., 1994. Modulation of in vivo striatal transmitter release by nitric oxide and cyclic GMP. J Neurochem. 62**,** 807-10.

Guidetti, P., et al., 2001. Early Degenerative Changes in Transgenic Mice Expressing Mutant Huntingtin Involve Dendritic Abnormalities but No

Impairment of Mitochondrial Energy Production. Experimental Neurology. 169, 340-350.

Guilarte, T. R., et al., 2008. Impairment of nigrostriatal dopamine neurotransmission by manganese is mediated by pre-synaptic mechanism(s): implications to manganese-induced parkinsonism. J Neurochem. 107, 1236-47.

Guilarte, T. R., et al., 2006. Nigrostriatal dopamine system dysfunction and subtle motor deficits in manganese-exposed non-human primates. Exp Neurol. 202, 381-90.

Gulson, B. L., et al., 1998. Mobilization of lead from the skeleton during the postnatal period is larger than during pregnancy. J Lab Clin Med. 131, 324-9.

Gupta, R. C., et al., 2007. Neuronal oxidative injury and dendritic damage induced by carbofuran: protection by memantine. Toxicol Appl Pharmacol. 219, 97-105.

Gwiazda, R. H., et al., 2002. Low cumulative manganese exposure affects striatal GABA but not dopamine. Neurotoxicology. 23, 69-76.

Haaxma, C. A., et al., 2007. Gender differences in Parkinson's disease. J Neurol Neurosurg Psychiatry. 78, 819-24.

Halpain, S., et al., 2005. Dynamics and pathology of dendritic spines. Prog Brain Res. 147, 29-37.

Hancock, D. B., et al., 2006. NOS2A and the modulating effect of cigarette smoking in Parkinson's disease. Ann Neurol. 60, 366-73.

Hancock, D. B., et al., 2008. Nitric oxide synthase genes and their interactions with environmental factors in Parkinson's disease. Neurogenetics. 9, 249-62.

Hannan, A. J., 2004. Molecular mediators, environmental modulators and experience-dependent synaptic dysfunction in Huntington's disease. Acta Biochim Pol. 51, 415-30.

Harjes, P., Wanker, E. E., 2003. The hunt for huntingtin function: interaction partners tell many different stories. Trends Biochem Sci. 28, 425 - 33.

Harper, P. S., 1992. The epidemiology of Huntington's disease. Hum Genet. 89, 365-76.

Harris, R. Z., et al., 1995. Gender effects in pharmacokinetics and pharmacodynamics. Drugs. 50**,** 222-39.

Hassel, B., et al., 2008. Glutamate uptake is reduced in prefrontal cortex in Huntington's disease. Neurochem Res. 33**,** 232-7.

Hayden, M. R., et al., 1981. Huntington's chorea on the island of Mauritius. S Afr Med J. 60**,** 1001-2.

Heinsen, H., et al., 1999. Nerve cell loss in the thalamic mediodorsal nucleus in Huntington's disease. Acta Neuropathol. 97**,** 613-22.

Hobbs, N. Z., et al., 2010. The progression of regional atrophy in premanifest and early Huntington's disease: a longitudinal voxel-based morphometry study. J Neurol Neurosurg Psychiatry. 81**,** 756-63.

Hockly, E., et al., 2002. Environmental enrichment slows disease progression in R6/2 Huntington's disease mice. Ann Neurol. 51**,** 235-42.

Hockly, E., et al., 2003. Standardization and statistical approaches to therapeutic trials in the R6/2 mouse. Brain Res Bull. 61**,** 469-79.

Horowitz, M. P., Greenamyre, J. T., 2010. Gene-environment interactions in Parkinson's disease: the importance of animal modeling. Clin Pharmacol Ther. 88**,** 467-74.

Huang, C. C., et al., 1989. Chronic manganese intoxication. Arch Neurol. 46**,** 1104-6.

Huang, C. C., et al., 2003. Dopamine transporter binding in chronic manganese intoxication. Journal of Neurology. 250**,** 1335-1339.

Hunter, D. J., 2005. Gene-environment interactions in human diseases. Nat Rev Genet. 6**,** 287-98.

Huntington's Disease Collaborative Research, G., 1993. A novel gene containing a trinucleotide repeat that is expanded and unstable on Huntington's Disease chromosomes. Cell. 72**,** 971-083.

Ikeda, S., et al., 2000. Manganese deposition in the globus pallidus in patients with biliary atresia. Transplantation. 69**,** 2339-43.

Ingham, C. A., et al., 1989. Spine density on neostriatal neurones changes with 6-hydroxydopamine lesions and with age. Brain Res. 503**,** 334-8.

Ingham, C. A., et al., 1993. Morphological changes in the rat neostriatum after unilateral 6-hydroxydopamine injections into the nigrostriatal pathway. Experimental Brain Research. 93**,** 17-27.

Ingham, C. A., et al., 1998. Plasticity of synapses in the rat neostriatum after unilateral lesion of the nigrostriatal dopaminergic pathway. J Neurosci. 18**,** 4732-43.

Investigators, H. S. G. T.-H., 2008. Randomized controlled trial of ethyl-eicosapentaenoic acid in Huntington disease: the TREND-HD study. Arch Neurol. 65**,** 1582-9.

Irwin, S. A., et al., 2000. Dendritic Spine Structural Anomalies in Fragile-X Mental Retardation Syndrome. Cereb. Cortex. 10**,** 1038-1044.

Iwasaki, Y., et al., 1992. Increased plasma concentrations of aspartate, glutamate and glycine in Parkinson's disease. Neuroscience Letters. 145**,** 175-177.

Izzo, P. N., et al., 1987. Characterization of substance P- and [Met]enkephalin-immunoreactive neurons in the caudate nucleus of cat and ferret by a single section Golgi procedure. Neuroscience. 20**,** 577-87.

Jiang, Y., et al., 2007. Brain magnetic resonance imaging and manganese concentrations in red blood cells of smelting workers: search for biomarkers of manganese exposure. Neurotoxicology. 28**,** 126-35.

Jin, T., et al., 2004. Environmental epidemiological study and estimation of benchmark dose for renal dysfunction in a cadmium-polluted area in China. Biometals. 17**,** 525-30.

Johansson, B. B., Belichenko, P. V., 2002. Neuronal plasticity and dendritic spines: effect of environmental enrichment on intact and postischemic rat brain. J Cereb Blood Flow Metab. 22**,** 89-96.

Johnson, J. W., Ascher, P., 1987. Glycine potentiates the NMDA response in cultured mouse brain neurons. Nature. 325**,** 529-31.

Johnson, M. A., et al., 2006. Dopamine release is severely compromised in the R6/2 mouse model of Huntington's disease. Journal of Neurochemistry. 97**,** 737-746.

Jones, E. G., History of cortical cytology. In: A. Peters, E. G. Jones, Eds.), Cerebral Cortex. Plenum Press, New York, 1988, pp. 1-32.

Joshi, P. R., et al., 2009. Age-Dependent Alterations of Corticostriatal Activity in the YAC128 Mouse Model of Huntington Disease. J. Neurosci. 29**,** 2414-2427.

Juraska, J. M., 1984. Sex differences in dendritic response to differential experience in the rat visual cortex. Brain Res. 295**,** 27-34.

Juraska, J. M., et al., 1985. Sex differences in the dendritic branching of dentate granule cells following differential experience. Brain Res. 333**,** 73-80.

Juraska, J. M., et al., 1989. The dendritic morphology of pyramidal neurons in the rat hippocampal CA3 area. II. Effects of gender and the environment. Brain Res. 479**,** 115-9.

Kalia, K., et al., 2008. Manganese accumulates primarily in nuclei of cultured brain cells. Neurotoxicology. 29**,** 466-70.

Kartvelishvily, E., et al., 2006. Neuron-derived D-serine release provides a novel means to activate N-methyl-D-aspartate receptors. J Biol Chem. 281**,** 14151-62.

Kassubek, J., et al., 2005. Thalamic atrophy in Huntington's disease co-varies with cognitive performance: a morphometric MRI analysis. Cereb Cortex. 15**,** 846-53.

Kaufmann, W. E., Moser, H. W., 2000. Dendritic anomalies in disorders associated with mental retardation. Cereb Cortex. 10**,** 981-91.

Kessler, K. R., et al., 2003. Secondary progressive chronic manganism associated with markedly decreased striatal D2 receptor density. Mov Disord. 18**,** 217-8.

Kim, Y., et al., 2002. Dopamine transporter density is decreased in parkinsonian patients with a history of manganese exposure: what does it mean? Mov Disord. 17**,** 568-75.

Kim, Y., et al., 2005. Blood manganese concentration is elevated in iron deficiency anemia patients, whereas globus pallidus signal intensity is minimally affected. Neurotoxicology. 26**,** 107-11.

Kipps, C. M., et al., 2005. Progression of structural neuropathology in preclinical Huntington's disease: a tensor based morphometry study. J Neurol Neurosurg Psychiatry. 76**,** 650-5.

Kish, S. J., et al., 1987. Elevated serotonin and reduced dopamine in subregionally divided Huntington's disease striatum. Ann Neurol. 22**,** 386-9.

Klapstein, G. J., et al., 2001. Electrophysiological and Morphological Changes in Striatal Spiny Neurons in R6/2 Huntington's Disease Transgenic Mice. J Neurophysiol. 86**,** 2667-2677.

Klomp, L. W., et al., 2000. Molecular characterization of 3-phosphoglycerate dehydrogenase deficiency--a neurometabolic disorder associated with reduced L-serine biosynthesis. Am J Hum Genet. 67**,** 1389-99.

Kloppel, S., et al., 2009. Magnetic resonance imaging of Huntington's disease: preparing for clinical trials. Neuroscience. 164**,** 205-19.

Knobloch, M., Mansuy, I. M., 2008. Dendritic spine loss and synaptic alterations in Alzheimer's disease. Mol Neurobiol. 37**,** 73-82.

Kobayashi, E., et al., 2006. Estimation of benchmark dose for renal dysfunction in a cadmium non-polluted area in Japan. J Appl Toxicol. 26**,** 351-5.

Kontur, P. J., Fechter, L. D., 1988. Brain regional manganese levels and monoamine metabolism in manganese-treated neonatal rats. Neurotoxicol Teratol. 10**,** 295-303.

Kopsch, F., 1896. Erfahrungen uber die Verwendung des Formaldehyds bei der Chromsilber-Impragnation. Anat An. 11**,** 727.

Krieger, D., et al., 1995. Manganese and chronic hepatic encephalopathy. Lancet. 346**,** 270-4.

Kung, V. W., et al., 2007. Dopamine-dependent long term potentiation in the dorsal striatum is reduced in the R6/2 mouse model of Huntington's disease. Neuroscience. 146**,** 1571-80.

Kusnoor, S. V., et al., 2010. Extracerebellar role for Cerebellin1: Modulation of dendritic spine density and synapses in striatal medium spiny neurons. The Journal of Comparative Neurology. 518**,** 2525-2537.

Kwakye, G. F., et al., 2011. Novel high-throughput assay to assess cellular manganese levels in a striatal cell line model of Huntington's disease confirms a deficit in manganese accumulation. Neurotoxicology.

Laviola, G., et al., 2008. Effects of enriched environment on animal models of neurodegenerative diseases and psychiatric disorders. Neurobiol Dis. 31**,** 159-68.

Lee, E. S., et al., 2009a. Estrogen and tamoxifen reverse manganese-induced glutamate transporter impairment in astrocytes. J Neurochem. 110**,** 530-44.

Lee, E. S., et al., 2009b. Estrogen and tamoxifen protect against Mn-induced toxicity in rat cortical primary cultures of neurons and astrocytes. Toxicol Sci. 110**,** 156-67.

Lee, K. W., et al., 2006. Cocaine-induced dendritic spine formation in D1 and D2 dopamine receptor-containing medium spiny neurons in nucleus accumbens. Proc Natl Acad Sci U S A. 103**,** 3399-404.

Leggio, M. G., et al., 2005. Environmental enrichment promotes improved spatial abilities and enhanced dendritic growth in the rat. Behav Brain Res. 163**,** 78-90.

Leranth, C., et al., 2000. Estrogen is essential for maintaining nigrostriatal dopamine neurons in primates: implications for Parkinson's disease and memory. J Neurosci. 20**,** 8604-9.

Li, H., et al., 2011. Nrf2/HO-1 pathway activation by manganese is associated with reactive oxygen species and ubiquitin-proteasome pathway, not MAPKs signaling. J Appl Toxicol.

Lievens, J. C., et al., 2001. Impaired glutamate uptake in the R6 Huntington's disease transgenic mice. Neurobiol Dis. 8**,** 807-21.

Lipe, G. W., et al., 1999. Effect of manganese on the concentration of amino acids in different regions of the rat brain. J Environ Sci Health B. 34**,** 119-32.

Lipton, S., 2006. Paradigm shift in neuroprotection by NMDA receptor blockade: Memantine and beyond. Nat Rev Drug Disc. 5**,** 160-170.

Lipton, S., 2007. Pathologically activated therapeutics for neuroprotection. Nat Rev Neurosci. 8**,** 803-808.

Lonart, G., Johnson, K. M., 1994. Inhibitory effects of nitric oxide on the uptake of [3H]dopamine and [3H]glutamate by striatal synaptosomes. J Neurochem. 63**,** 2108-17.

Lucchini, R. G., et al., 2007. High prevalence of Parkinsonian disorders associated to manganese exposure in the vicinities of ferroalloy industries. Am J Ind Med. 50**,** 788-800.

Lucchini, R. G., et al., 2009. From manganism to manganese-induced parkinsonism: a conceptual model based on the evolution of exposure. Neuromolecular Med. 11**,** 311-21.

Magos, L., et al., 1981. Comparative study of the sensitivity of male and female rats to methylmercury. Arch Toxicol. 48**,** 11-20.

Majid, D. S., et al., 2011. Automated structural imaging analysis detects premanifest Huntington's disease neurodegeneration within 1 year. Mov Disord.

Mangiarini, L., et al., 1996. Exon 1 of the HD gene with an expanded CAG repeat is sufficient to cause a progressive neurological phenotype in transgenic mice. Cell. 87**,** 493-506.

Mann, V. M., et al., 1990. Mitochondrial function and parental sex effect in Huntington's disease. Lancet. 336**,** 749.

Manton, W. I., et al., 2003. Release of lead from bone in pregnancy and lactation. Environ Res. 92**,** 139-51.

Margolis, R. L., et al., 2005. Huntington's disease like-2: review and update. Acta Neurol Taiwan. 14**,** 1-8.

Marin-Padilla, M., 1995. Prenatal development of fibrous (white matter), protoplasmic (gray matter), and layer I astrocytes in the human cerebral cortex: a Golgi study. J Comp Neurol. 357**,** 554-72.

McGeer, E. G., McGeer, P. L., 1976. Duplication of biochemical changes of Huntington's chorea by intrastriatal injections of glutamic and kainic acids. Nature. 263**,** 517-9.

McKeown-Eyssen, G. E., et al., 1983. Methyl mercury exposure in northern Quebec. II. Neurologic findings in children. Am J Epidemiol. 118**,** 470-9.

McMillan, D. E., 1999. A brief history of the neurobehavioral toxicity of manganese: some unanswered questions. Neurotoxicology. 20**,** 499-507.

Meding, B., et al., 2001. Self-diagnosed dermatitis in adults. Results from a population survey in Stockholm. Contact Dermatitis. 45**,** 341-5.

Melendez-Ferro, M., et al., 2009. A new use for long-term frozen brain tissue: golgi impregnation. J Neurosci Methods. 176**,** 72-7.

Menalled, L., et al., 2009. Systematic behavioral evaluation of Huntington's disease transgenic and knock-in mouse models. Neurobiol Dis. 35**,** 319-36.

Menalled, L. B., Chesselet, M. F., 2002. Mouse models of Huntington's disease. Trends Pharmacol Sci. 23**,** 32-9.

Mervis, R. F., et al., 1991. Exogenous nerve growth factor reverses age-related structural changes in neocortical neurons in the aging rat. A quantitative Golgi study. Ann N Y Acad Sci. 640**,** 95-101.

Milatovic, D., et al., 2010. Morphometric analysis in neurodegenerative disorders. Current Protocols in Toxicology. 43**,** 12.16.1-12.16.14.

Milatovic, D., et al., 2007. Manganese induces oxidative impairment in cultured rat astrocytes. Toxicol Sci. 98**,** 198-205.

Milatovic, D., et al., 2009. Oxidative damage and neurodegeneration in manganese-induced neurotoxicity. Toxicol Appl Pharmacol. 240**,** 219-25.

Milatovic, D., et al., 2003. Pharmacologic suppression of neuronal oxidative damage and dendritic degeneration following direct activation of glial innate immunity in mouse cerebrum. J Neurochem. 87**,** 1518-26.

Milatovic, D., et al., 2004. Neuronal oxidative damage and dendritic degeneration following activation of CD14-dependent innate immune response in vivo. J Neuroinflammation. 1**,** 20.

Miller, B. R., et al., 2008. Up-regulation of GLT1 expression increases glutamate uptake and attenuates the Huntington's disease phenotype in the R6/2 mouse. Neuroscience. 153**,** 329-37.

Miller, D. B., et al., 1998. The impact of gender and estrogen on striatal dopaminergic neurotoxicity. Ann N Y Acad Sci. 844**,** 153-65.

Miller, I. N., Cronin-Golomb, A., 2010. Gender differences in Parkinson's disease: clinical characteristics and cognition. Mov Disord. 25**,** 2695-703.

Millhouse, O. E., The Golgi methods. In: L. Heiner, M. J. Robards, Eds.), Neuroanatomical Tract-Tracing Methods. Plenum Press, New York, 1981, pp. 311-343.

Milnerwood, A. J., et al., 2010. Early increase in extrasynaptic NMDA receptor signaling and expression contributes to phenotype onset in Huntington's disease mice. Neuron. 65**,** 178-90.

Milnerwood, A. J., Raymond, L. A., 2007. Corticostriatal synaptic function in mouse models of Huntington's disease: early effects of huntingtin repeat length and protein load. The Journal of Physiology. 585**,** 817-831.

Miya, K., et al., 2008. Serine racemase is predominantly localized in neurons in mouse brain. Journal of Comparative Neurology. 510**,** 641-654.

Montine, T. J., et al., 2002. Neuronal oxidative damage from activated innate immunity is EP2 receptor-dependent. J Neurochem. 83**,** 463-70.

Morale, M. C., et al., 2008. Loss of aromatase cytochrome P450 function as a risk factor for Parkinson's disease? Brain Res Rev. 57**,** 431-43.

Moreno, J. A., et al., 2011. Manganese-induced NF-{kappa}B activation and nitrosative stress is decreased by estrogen in juvenile mice. Toxicol Sci.

Moreno, J. A., et al., 2008. Manganese potentiates nuclear factor-kappaB-dependent expression of nitric oxide synthase 2 in astrocytes by activating soluble guanylate cyclase and extracellular responsive kinase signaling pathways. J Neurosci Res. 86**,** 2028-38.

Moreno, J. A., et al., 2009. Age-dependent susceptibility to manganese-induced neurological dysfunction. Toxicol Sci. 112**,** 394-404.

Mutkus, L., et al., 2005. The in vitro uptake of glutamate in GLAST and GLT-1 transfected mutant CHO-K1 cells is inhibited by manganese. Biol Trace Elem Res. 107**,** 221-30.

Nabholz, C. E., von Overbeck, J., 2004. Gene-environment interactions and the complexity of human genetic diseases. J Insur Med. 36**,** 47-53.

Naver, B., et al., 2003. Molecular and behavioral analysis of the R6/1 Huntington's disease transgenic mouse. Neuroscience. 122**,** 1049-57.

Nicniocaill, B., et al., 2001. Altered striatal amino acid neurotransmitter release monitored using microdialysis in R6/1 Huntington transgenic mice. Eur J Neurosci. 13**,** 206-10.

Nicoli, F., et al., 1993. CSF and serum metabolic profile of patients with Huntington's chorea: a study by high resolution proton NMR spectroscopy and HPLC. Neurosci Lett. 154**,** 47-51.

Nicolson, T. J., et al., 2010. Gender differences in drug toxicity. Trends Pharmacol Sci. 31**,** 108-14.

Nielsen, N. H., et al., 2002. Incidence of allergic contact sensitization in Danish adults between 1990 and 1998; the Copenhagen Allergy Study, Denmark. Br J Dermatol. 147**,** 487-92.

Nimchinsky, E. A., et al., 2002. Structure and function of dendritic spines. Annual Review of Physiology. 64**,** 313-353.

Nithianantharajah, J., et al., 2009. Modeling brain reserve: experience-dependent neuronal plasticity in healthy and Huntington's disease transgenic mice. Am J Geriatr Psychiatry. 17**,** 196-209.

Okamoto, S., et al., 2009. Balance between synaptic versus extrasynaptic NMDA receptor activity influences inclusions and neurotoxicity of mutant huntingtin. Nat Med. 15**,** 1407-13.

Olanow, C. W., 2004. Manganese-Induced Parkinsonism and Parkinson's Disease. Annals of the New York Academy of Sciences. 1012**,** 209-223.

Olanow, C. W., et al., 1996. Manganese intoxication in the rhesus monkey: a clinical, imaging, pathologic, and biochemical study. Neurology. 46**,** 492-8.

Ondo, W. G., et al., 2007. A pilot study of the clinical efficacy and safety of memantine for Huntington's disease. Parkinsonism Relat Disord. 13**,** 453-4.

Ono, K., et al., 2002. Myoclonic involuntary movement associated with chronic manganese poisoning. J Neurol Sci. 199**,** 93-6.

Ookubo, M., et al., 2008. Effects of estrogens on striatal damage after 1-methyl-4-phenyl-1,2,3,6-tetrahydropyridine (MPTP) neurotoxicity in male and female mice. Mol Cell Endocrinol. 296**,** 87-93.

Orr, A. L., et al., 2008. Sex-dependent effect of BAG1 in ameliorating motor deficits of Huntington disease transgenic mice. J Biol Chem. 283**,** 16027-36.

Ortiz, A. N., et al., 2010. Dysregulation of intracellular dopamine stores revealed in the R6/2 mouse striatum. J Neurochem. 112**,** 755-61.

Ortiz, A. N., et al., 2011. Impaired dopamine release and uptake in R6/1 Huntington's disease model mice. Neurosci Lett. 492**,** 11-4.

Pal, P. K., et al., 1999. Manganese neurotoxicity: a review of clinical features, imaging and pathology. Neurotoxicology. 20**,** 227-38.

Panas, M., et al., 2008. Phenotypic discordance in a pair of monozygotic twins with Huntington's disease. Clin Genet. 74**,** 291-2.

Paulsen, J. S., et al., 2005. Depression and stages of Huntington's disease. J Neuropsychiatry Clin Neurosci. 17**,** 496-502.

Pavese, N., et al., 2010. Cortical dopamine dysfunction in symptomatic and premanifest Huntington's disease gene carriers. Neurobiol Dis. 37**,** 356-61.

Pennington, J. A., Young, B. E., 1991. Total diet study nutritional elements, 1982-1989. J Am Diet Assoc. 91**,** 179-83.

Perez-Severiano, F., et al., 2004. Increased formation of reactive oxygen species, but no changes in glutathione peroxidase activity, in striata of mice transgenic for the Huntington's disease mutation. Neurochem Res. 29**,** 729-33.

Perl, D. P., Olanow, C. W., 2007. The neuropathology of manganese-induced Parkinsonism. J Neuropathol Exp Neurol. 66**,** 675-82.

Perluigi, M., et al., 2005. Proteomic analysis of protein expression and oxidative modification in r6/2 transgenic mice: a model of Huntington disease. Mol Cell Proteomics. 4**,** 1849-61.

Petersen, A., Bjorkqvist, M., 2006. Hypothalamic-endocrine aspects in Huntington's disease. Eur J Neurosci. 24**,** 961-7.

Pfeifer, G. D., et al., 2004. Health and environmental testing of manganese exhaust products from use of methylcyclopentadienyl manganese tricarbonyl in gasoline. Sci Total Environ. 334-335**,** 397-408.

Pfeiffer, R. F., 2007. Wilson's Disease. Semin Neurol. 27**,** 123-32.

Pizer, L. I., 1964. ENZYMOLOGY AND REGULATION OF SERINE BIOSYNTHESIS IN CULTURED HUMAN CELLS. J Biol Chem. 239**,** 4219-26.

Pogun, S., et al., 1994. Nitric oxide inhibits 3H-glutamate transport in synaptosomes. Synapse. 18**,** 21-6.

Politis, M., et al., 2008. Hypothalamic involvement in Huntington's disease: an in vivo PET study. Brain. 131**,** 2860-9.

Pollegioni, L., Sacchi, S., 2010. Metabolism of the neuromodulator D-serine. Cell Mol Life Sci. 67**,** 2387-404.

Pounds, J. G., et al., 1991. Cellular and molecular toxicity of lead in bone. Environ Health Perspect. 91**,** 17-32.

Puri, B. K., et al., 2005. Ethyl-EPA in Huntington disease: a double-blind, randomized, placebo-controlled trial. Neurology. 65**,** 286-92.

Ramon y Cajal, S., 1888. Estructura de los centros nervisos de las aves. Rev. Trim. Histol. Norm. Patol. 1**,** 1-10.

Ramón-Moliner, E., 1970. The Golgi-Cox technique. Springer, New York.

Rao, S. D., et al., 2003. Disruption of glial glutamate transport by reactive oxygen species produced in motor neurons. J Neurosci. 23**,** 2627-33.

Reaney, S. H., et al., 2006. Brain accumulation and toxicity of Mn(II) and Mn(III) exposures. Toxicol Sci. 93**,** 114-24.

Reilmann, R., et al., 1997. Huntington's disease: N-methyl-D-aspartate receptor coagonist glycine is increased in platelets. Exp Neurol. 144**,** 416-9.

Reynolds, I. J., Hastings, T. G., 1995. Glutamate induces the production of reactive oxygen species in cultured forebrain neurons following NMDA receptor activation. J Neurosci. 15**,** 3318-27.

Richardson, J. R., et al., 2008. Developmental heptachlor exposure increases susceptibility of dopamine neurons to N-methyl-4-phenyl-1,2,3,6-tetrahydropyridine (MPTP)in a gender-specific manner. Neurotoxicology. 29**,** 855-63.

Riley, J. N., 1979. A reliable Golgi-Kopsch modification. Brain Res Bull. 4**,** 127-9.

Riojas-Rodriguez, H., et al., 2010. Intellectual function in Mexican children living in a mining area and environmentally exposed to manganese. Environ Health Perspect. 118**,** 1465-70.

Rosoklija, G., et al., 2003. Optimization of Golgi methods for impregnation of brain tissue from humans and monkeys. J Neurosci Methods. 131**,** 1-7.

Roth, J. A., 2009. Are there common biochemical and molecular mechanisms controlling manganism and parkisonism. Neuromolecular Med. 11**,** 281-96.

Roth, J. A., Garrick, M. D., 2003. Iron interactions and other biological reactions mediating the physiological and toxic actions of manganese. Biochem Pharmacol. 66**,** 1-13.

Rukgauer, M., et al., 1997. Reference values for the trace elements copper, manganese, selenium, and zinc in the serum/plasma of children, adolescents, and adults. J Trace Elem Med Biol. 11**,** 92-8.

Rymar, V. V., et al., 2004. Neurogenesis and stereological morphometry of calretinin-immunoreactive GABAergic interneurons of the neostriatum. J Comp Neurol. 469**,** 325-39.

Sager, P. R., et al., 1984. Persistent, differential alterations in developing cerebellar cortex of male and female mice after methylmercury exposure. Brain Res. 314**,** 1-11.

Sanotsky, Y., et al., 2007. Manganic encephalopathy due to "ephedrone" abuse. Mov Disord. 22**,** 1337-43.

Sari, Y., et al., 2010. Ceftriaxone-induced up-regulation of cortical and striatal GLT1 in the R6/2 model of Huntington's disease. J Biomed Sci. 17**,** 62.

Sasabe, J., et al., 2007. D-serine is a key determinant of glutamate toxicity in amyotrophic lateral sclerosis. EMBO J. 26**,** 4149-59.

Schwartz, D. A., 2010. Epigenetics and environmental lung disease. Proc Am Thorac Soc. 7**,** 123-5.

Selikhova, M., et al., 2008. Parkinsonism and dystonia caused by the illicit use of ephedrone--a longitudinal study. Mov Disord. 23**,** 2224-31.

Shansky, R. M., et al., 2009. Stress-Induced Dendritic Remodeling in the Prefrontal Cortex is Circuit Specific. Cereb Cortex.

Shehadeh, J., et al., 2006. Striatal neuronal apoptosis is preferentially enhanced by NMDA receptor activation in YAC transgenic mouse model of Huntington disease. Neurobiol Dis. 21**,** 392-403.

Sholl, D. A., 1953. Dendritic organization in the neurons of the visual and motor cortices of the cat. J Anat. 87**,** 387-406.

Shulman, L. M., 2007. Gender differences in Parkinson's disease. Gend Med. 4**,** 8-18.

Sidoryk-Wegrzynowicz, M., et al., 2009. Manganese disrupts astrocyte glutamine transporter expression and function. J Neurochem. 110**,** 822-30.

Sidoryk-Wegrzynowicz, M., et al., 2010. Manganese-induced downregulation of astroglial glutamine transporter SNAT3 involves ubiquitin-mediated proteolytic system. Glia. 58**,** 1905-12.

Sikk, K., et al., 2011. Manganese-Induced Parkinsonism due to Ephedrone Abuse. Parkinsons Dis. 2011**,** 865319.

Sikk, K., et al., 2010. Clinical, neuroimaging and neurophysiological features in addicts with manganese-ephedrone exposure. Acta Neurol Scand. 121**,** 237-43.

Sikk, K., et al., 2007. Irreversible motor impairment in young addicts--ephedrone, manganism or both? Acta Neurol Scand. 115**,** 385-9.

Simon, P., et al., 1994. Thigmotaxis as an index of anxiety in mice. Influence of dopaminergic transmissions. Behav Brain Res. 61**,** 59-64.

Slow, E. J., et al., 2003. Selective striatal neuronal loss in a YAC128 mouse model of Huntington disease. Hum. Mol. Genet. 12**,** 1555-1567.

Smith, C. P., et al., 2007. Tamoxifen effect on L-DOPA induced response complications in parkinsonian rats and primates. Neuropharmacology. 52**,** 515-26.

Solis, O., et al., 2009. Decreased dendritic spine density of neurons of the prefrontal cortex and nucleus accumbens and enhanced amphetamine sensitivity in postpubertal rats after a neonatal amygdala lesion. Synapse. 63**,** 1143-53.

Somogyi, P., et al., 1981. Monosynaptic cortical input and local axon collaterals of identified striatonigral neurons. A light and electron microscopic study using the Golgi-peroxidase transport-degeneration procedure. J Comp Neurol. 195**,** 567-84.

Spacek, J., 1989. Dynamics of the Golgi method: a time-lapse study of the early stages of impregnation in single sections. J Neurocytol. 18**,** 27-38.

Spacek, J., 1992. Dynamics of Golgi impregnation in neurons. Microsc Res Tech. 23**,** 264-74.

Spektor, B. S., et al., 2002. Differential D1 and D2 receptor-mediated effects on immediate early gene induction in a transgenic mouse model of Huntington's disease. Brain Res Mol Brain Res. 102**,** 118-28.

Spires, T. L., et al., 2004. Dendritic spine pathology and deficits in experience-dependent dendritic plasticity in R6/1 Huntington's disease transgenic mice. Eur J Neurosci. 19**,** 2799-807.

Spokes, E. G., et al., 1980. Distribution of GABA in post-mortem brain tissue from control, psychotic and Huntington's chorea subjects. J Neurol Sci. 48**,** 303-13.

Squitti, R., et al., 2009. Implications of metal exposure and liver function in Parkinsonian patients resident in the vicinities of ferroalloy plants. J Neural Transm. 116**,** 1281-7.

Srivastava, A. K., et al., 1991. An investigation of metal concentrations in blood of industrial workers. Vet Hum Toxicol. 33**,** 280-2.

Stanwood, G. D., et al., 2009. Manganese exposure is cytotoxic and alters dopaminergic and GABAergic neurons within the basal ganglia. J Neurochem. 110**,** 378-389.

Stepens, A., et al., 2008. A Parkinsonian syndrome in methcathinone users and the role of manganese. N Engl J Med. 358**,** 1009-17.

Stephens, B., et al., 2005. Evidence of a breakdown of corticostriatal connections in Parkinson's disease. Neuroscience. 132**,** 741-54.

Stine, O. C., et al., 1993. Correlation between the onset age of Huntington's disease and length of the trinucleotide repeat in IT-15. Hum. Mol. Genet. 2**,** 1547-1549.

Stocco, A., et al., 2010. Conditional routing of information to the cortex: a model of the basal ganglia's role in cognitive coordination. Psychol Rev. 117**,** 541-74.

Stranahan, A. M., et al., 2007. Running induces widespread structural alterations in the hippocampus and entorhinal cortex. Hippocampus. 17**,** 1017-22.

Stroppolo, A., et al., 2004. 17beta-Estradiol promotes striatal medium size spiny neuronal maturation in vitro. Neuroendocrinology. 79**,** 259-67.

Struve, M. F., et al., 2007. Basal ganglia neurotransmitter concentrations in rhesus monkeys following subchronic manganese sulfate inhalation. Am J Ind Med. 50**,** 772-8.

Sun, Z., et al., 2003. Enkephalinergic striatal projection neurons become less affected by quinolinic acid than substance P-containing striatal projection neurons as rats age. Exp Neurol. 184**,** 1034-42.

Sun, Z., et al., 2002. The differential vulnerability of striatal projection neurons in 3-nitropropionic acid-treated rats does not match that typical of adult-onset Huntington's disease. Exp Neurol. 176**,** 55-65.

Surmeier, D. J., et al., 2007. D1 and D2 dopamine-receptor modulation of striatal glutamatergic signaling in striatal medium spiny neurons. Trends Neurosci. 30**,** 228-35.

Tabrizi, S. J., et al., 1999. Biochemical abnormalities and excitotoxicity in Huntington's disease brain. Ann Neurol. 45**,** 25-32.

Tabrizi, S. J., et al., 2011. Biological and clinical changes in premanifest and early stage Huntington's disease in the TRACK-HD study: the 12-month longitudinal analysis. Lancet Neurol. 10**,** 31-42.

Tabrizi, S. J., et al., 2000. Mitochondrial dysfunction and free radical damage in the Huntington R6/2 transgenic mouse. Ann Neurol. 47**,** 80-6.

Takeda, A., et al., 2002. Manganese influences the levels of neurotransmitters in synapses in rat brain. Neuroscience. 114**,** 669-74.

Takeda, A., et al., 2003. Influence of manganese on the release of neurotransmitters in rat striatum. Brain Res. 965**,** 279-82.

Tamas, A., et al., 2005. Age and gender differences in behavioral and morphological outcome after 6-hydroxydopamine-induced lesion of the substantia nigra in rats. Behav Brain Res. 158**,** 221-9.

Tanaka, K., et al., 1997. Epilepsy and exacerbation of brain injury in mice lacking the glutamate transporter GLT-1. Science. 276**,** 1699-702.

Tang, T. S., et al., 2007. Dopaminergic Signaling and Striatal Neurodegeneration in Huntington's Disease. J. Neurosci. 27**,** 7899-7910.

Tang, T. S., et al., 2005. Disturbed Ca2+ signaling and apoptosis of medium spiny neurons in Huntington's disease. Proceedings of the National Academy of Sciences of the United States of America. 102**,** 2602-2607.

Taskiran, D., et al., 2003. Effect of carbon monoxide on dopamine and glutamate uptake and cGMP levels in rat brain. Neuropsychopharmacology. 28**,** 1176-81.

Thu, D. C., et al., 2010. Cell loss in the motor and cingulate cortex correlates with symptomatology in Huntington's disease. Brain. 133**,** 1094-110.

Tiffany-Castiglion, E., Qian, Y., 2001. Astroglia as metal depots: molecular mechanisms for metal accumulation, storage and release. Neurotoxicology. 22**,** 577-92.

Tjalkens, R. B., et al., 2006. Manganese suppresses ATP-dependent intercellular calcium waves in astrocyte networks through alteration of mitochondrial and endoplasmic reticulum calcium dynamics. Brain Res. 1113**,** 210-9.

Uno, T., et al., 2005. Health effects of cadmium exposure in the general environment in Japan with special reference to the lower limit of the benchmark dose as the threshold level of urinary cadmium. Scand J Work Environ Health. 31**,** 307-15.

Urquhart, N., et al., 1975. GABA content and glutamic acid decarboxylase activity in brain of Huntington's chorea patients and control subjects. J Neurochem. 24**,** 1071-5.

Vaddadi, K. S., et al., 2002. A randomised, placebo-controlled, double blind study of treatment of Huntington's disease with unsaturated fatty acids. Neuroreport. 13**,** 29-33.

Vahter, M., et al., 2007. Gender differences in the disposition and toxicity of metals. Environ Res. 104**,** 85-95.

Vahter, M., et al., 2002. Metals and women's health. Environ Res. 88**,** 145-55.

van Dellen, A., et al., 2000. Delaying the onset of Huntington's in mice. Nature. 404**,** 721-2.

van Dellen, A., et al., 2005. Gene-environment interactions, neuronal dysfunction and pathological plasticity in Huntington's disease. Clin Exp Pharmacol Physiol. 32**,** 1007-19.

van Dellen, A., Hannan, A. J., 2004. Genetic and environmental factors in the pathogenesis of Huntington's disease. Neurogenetics. 5**,** 9-17.

van den Bogaard, S. J., et al., 2011. Early atrophy of pallidum and accumbens nucleus in Huntington's disease. J Neurol. 258**,** 412-20.

Van Raamsdonk, J. M., et al., 2005a. Ethyl-EPA treatment improves motor dysfunction, but not neurodegeneration in the YAC128 mouse model of Huntington disease. Experimental Neurology. 196**,** 266-272.

Van Raamsdonk, J. M., et al., 2005b. Cognitive Dysfunction Precedes Neuropathology and Motor Abnormalities in the YAC128 Mouse Model of Huntington's Disease. J. Neurosci. 25**,** 4169-4180.

Vance, J. M., et al., 2010. Gene-environment interactions in Parkinson's disease and other forms of parkinsonism. Neurotoxicology. 31**,** 598-602.

Vetter, J. M., et al., 2003. Mice transgenic for exon 1 of Huntington's disease: properties of cholinergic and dopaminergic pre-synaptic function in the striatum. J Neurochem. 85**,** 1054-63.

Vezer, T., et al., 2007. Behavioral effects of subchronic inorganic manganese exposure in rats. Am J Ind Med. 50**,** 841-52.

Vezer, T., et al., 2005. Behavioral and neurotoxicological effects of subchronic manganese exposure in rats. Environmental Toxicology and Pharmacology. 19**,** 797-810.

Vidal, L., et al., 2005. Effects of manganese on extracellular levels of dopamine in rat striatum: an analysis in vivo by brain microdialysis. Neurochem Res. 30**,** 1147-54.

Vonsattel, J. P., 2008. Huntington disease models and human neuropathology: similarities and differences. Acta Neuropathol. 115**,** 55-69.

Vonsattel, J. P., DiFiglia, M., 1998. Huntington disease. J Neuropathol Exp Neurol. 57**,** 369 - 84.

Vonsattel, J. P., et al., 1985. Neuropathological classification of Huntington's disease. J Neuropathol Exp Neurol. 44**,** 559-577.

Voorn, P., et al., 2004. Putting a spin on the dorsal-ventral divide of the striatum. Trends in Neurosciences. 27**,** 468-474.

Wald, C., Wu, C., 2010. Biomedical research. Of mice and women: the bias in animal models. Science. 327**,** 1571-2.

Walker, F. O., 2007. Huntington's disease. Lancet. 369**,** 218-28.

Wang, J. D., et al., 1989. Manganese induced parkinsonism: an outbreak due to an unrepaired ventilation control system in a ferromanganese smelter. Br J Ind Med. 46**,** 856-9.

Wedler, F. C., et al., 1989. Manganese(II) dynamics and distribution in glial cells cultured from chick cerebral cortex. Neurochem Res. 14**,** 1129-35.

West, A. R., Galloway, M. P., 1997. Inhibition of glutamate reuptake potentiates endogenous nitric oxide-facilitated dopamine efflux in the rat striatum: an in vivo microdialysis study. Neurosci Lett. 230**,** 21-4.

Wexler, N. S., et al., 2004a. Venezuelan kindreds reveal that genetic and environmental factors modulate Huntington's disease age of onset. Proc Natl Acad Sci U S A. 101**,** 3498-503.

Wexler, N. S., et al., 2004b. Venezuelan kindreds reveal that genetic and environmental factors modulate Huntington's disease age of onset. Proc Natl Acad Sci U S A. 101**,** 3498-503.

Wild, E. J., et al., 2010. Rate and acceleration of whole-brain atrophy in premanifest and early Huntington's disease. Mov Disord. 25**,** 888-95.

Wild, E. J., et al., 2008. Huntington's disease phenocopies are clinically and genetically heterogeneous. Mov Disord. 23**,** 716-20.

Wild, E. J., Tabrizi, S. J., 2007. Huntington's disease phenocopy syndromes. Curr Opin Neurol. 20**,** 681-7.

Williams, B. B., et al., 2010a. Altered manganese homeostasis and manganese toxicity in a Huntington's disease striatal cell model are not explained by defects in the iron transport system. Toxicol Sci. 117**,** 169-79.

Williams, B. B., et al., 2010b. Disease-toxicant screen reveals a neuroprotective interaction between Huntington's disease and manganese exposure. J Neurochem. 112**,** 227-37.

Wilson, S., 1914. An experimental research into the anatomy and physiology of the corpus striatum. Brain. 36**,** 427-492.

Wirdefeldt, K., et al., 2011. Heritability of Parkinson disease in Swedish twins: a longitudinal study. Neurobiol Aging.

Wright, A. K., et al., 2009. Slowly progressive dopamine cell loss--a model on which to test neuroprotective strategies for Parkinson's disease? Rev Neurosci. 20**,** 85-94.

Wu, J. Y., et al., 1979. Abnormalities of neurotransmitter enzymes in Huntington's chorea. Neurochem Res. 4**,** 575-86.

Wyttenbach, A., et al., 2002. Heat shock protein 27 prevents cellular polyglutamine toxicity and suppresses the increase of reactive oxygen species caused by huntingtin. Hum Mol Genet. 11**,** 1137-51.

Xie, Y., et al., 2010. BDNF overexpression in the forebrain rescues Huntington's disease phenotypes in YAC128 mice. J Neurosci. 30**,** 14708-18.

Yang, J. H., et al., 2010. Brain-specific Phgdh deletion reveals a pivotal role for L-serine biosynthesis in controlling the level of D-serine, an N-methyl-D-aspartate receptor co-agonist, in adult brain. J Biol Chem. 285**,** 41380-90.

Yelnik, J., et al., 1991. Morphological taxonomy of the neurons of the primate striatum. J Comp Neurol. 313**,** 273-94.

Yokel, R. A., 2006. Blood-brain barrier flux of aluminum, manganese, iron and other metals suspected to contribute to metal-induced neurodegeneration. J Alzheimers Dis. 10**,** 223-53.

Yuste, R., Bonhoeffer, T., 2001. Morphological changes in dendritic spines associated with long-term synaptic plasticity. Annu Rev Neurosci. 24**,** 1071-89.

Zaja-Milatovic, S., et al., 2009. Protection of DFP-induced oxidative damage and neurodegeneration by antioxidants and NMDA receptor antagonist. Toxicol Appl Pharmacol. 240**,** 124-31.

Zaja-Milatovic, S., et al., 2008. Pharmacologic suppression of oxidative damage and dendritic degeneration following kainic acid-induced excitotoxicity in mouse cerebrum. Neurotoxicology. 29**,** 621-7.

Zaja-Milatovic, S., et al., 2005. Dendritic degeneration in neostriatal medium spiny neurons in Parkinson disease. Neurology. 64**,** 545-7.

Zajac, M. S., et al., 2010. Wheel running and environmental enrichment differentially modify exon-specific BDNF expression in the hippocampus of wild-type and pre-motor symptomatic male and female Huntington's disease mice. Hippocampus. 20**,** 621-36.

Zayed, J., et al., 2003. Estimation of annual Mn emissions from MMT source in the Canadian environment and the Mn pollution index in each province. Sci Total Environ. 312**,** 147-54.

Zeron, M. M., et al., 2004. Potentiation of NMDA receptor-mediated excitotoxicity linked with intrinsic apoptotic pathway in YAC transgenic mouse model of Huntington's disease. Mol Cell Neurosci. 25**,** 469-79.

Zeron, M. M., et al., 2002. Increased sensitivity to N-methyl-D-aspartate receptor-mediated excitotoxicity in a mouse model of Huntington's disease. Neuron. 33**,** 849-60.

Zhang, P., et al., 2007. Manganese chloride stimulates rat microglia to release hydrogen peroxide. Toxicol Lett. 173**,** 88-100.

Zheng, W., et al., 2000. Comparative toxicokinetics of manganese chloride and methylcyclopentadienyl manganese tricarbonyl (MMT) in Sprague-Dawley rats. Toxicol Sci. 54**,** 295-301.

Zourlidou, A., et al., 2007. Hsp27 overexpression in the R6/2 mouse model of Huntington's disease: chronic neurodegeneration does not induce Hsp27 activation. Hum Mol Genet. 16**,** 1078-90.